Modelling the Development of Tissues In Vitro from Pluripotent Stem Cells

DOMINIC DAVID GREGORY OWENS

Modelling the Development of Tissues *In Vitro* from Pluripotent Stem Cells

Dominic D. G. Owens BSc
School of Biological and Biomedical Sciences, Durham University

Abstract

Using the classical embryoid body approach, 3D aggregate cultures facilitate enhanced multi-lineage differentiation of pluripotent stem cells compared to 2D culture. However, such cellular aggregates can become necrotic over prolonged culture in suspension reducing their ability to form complex tissues. We have developed a two-stage 3D culture system whereby stem cells are grown first as aggregates in suspension and then maintained as 3D constructs for extended periods on porous polystyrene scaffolds. Combining 3D culture strategies in this way enhances the formation of complex tissues by providing a suitable microenvironment and sufficient time for developmental processes to occur. Differentiating pluripotent stem cells forming complex tissues *in vitro* may provide an alternative to the current gold standard teratoma formation pluripotency assay. Additionally, the role that morphogens and small molecules play in development can be investigated using this unique culture system, providing a novel approach to study aspects of human embryonic development.

This thesis is dedicated to the memory of Dr. S. M. Owens

Scientist, Teacher, and Mother.

Acknowledgements

First I must thank my supervisor Prof. Stefan Przyborski for providing me with the opportunity to carry out this project and for his enthusiasm throughout.

I am extremely grateful to all members of the Przyborski group and especially Rebecca Quelch, Kirsty Klarke, Hesham Haffez, Ally Chaatwal, Neil Robinson, Dr. Mathilde Roger, Dr. Nichola Fullard, and Dr. Steven OReilly for their interesting conversations and invaluable guidance throughout the year.

I would also like to thank all of my friends and family for their support. Dr. Benjamin Owens provided expert assistance with flow cytometry and useful guidance throughout the project.

Finally, I am indebted to The Grevillea Trust who through providing funding made this opportunity a reality.

Contents

List of Figures

List of Tables

1 Introduction

Pluripotent stem cells (PSCs) are defined by their ability to: (1) self-replicate indefinitely in culture, and (2) produce differentiated derivatives of all three embryonic germ layers (ectoderm, mesoderm, and endoderm) that are formed during development as a result of gastrulation (Tam and Behringer, 1997; Smith, 2001). The first pluripotent cell type to be identified, known as an embryonal carcinoma (EC) cell, was isolated from murine teratocarcinomas—solid tumours containing differentiated tissues and undifferentiated EC cells—in 1964 and shown to exhibit the two determining characteristics of pluripotency (Kleinsmith and Pierce, 1964). Pioneering research with EC cells led the way to the isolation of the iconic embryonic stem cell (ESC).

Murine ESCs (mESCs) were isolated in 1981 by explanting the inner cell mass (ICM) of pre-implantation blastocysts. mESCs could be maintained in an undifferentiated state in culture and produce differentiated derivatives of all three embryonic germ layers and certain extraembryonic lineages (Evans et al., 1981; Martin, 1981). In 1998, human ESCs (hESCs) that shared many similarities with mESCs were derived from human blastocysts (Thomson et al., 1998).

Induced PSCs (iPSCs) were generated in 2006 by retroviral transduction of murine embryonic or adult fribroblasts with factors known to be required for pluripotency maintenance during early embryonic development (Takahashi and Yamanaka, 2006). Expression of exogenous Oct4, Klf-4, Sox2, and c-Myc successfully generated murine iPSCs that could be maintained in culture for extended periods and produced differentiated tissues representative of all three germ layers. Shortly afterward, human iPSCs (hiPSCs) were generated using similar methods (Takahashi et al., 2007).

Recent advances have provided a deeper understanding of PSCs and their developmental origins. Epiblast stem cells (EpiSCs) and region-specific EpiSCs (rsEpiSCs) have been isolated from post-implantation epiblast stage murine embryos and shown to be equivalent to cells of the pluripotent ICM-derived epiblast that contributes to somatic lineages but not extraembryonic structures (Brons et al., 2007; Tesar et al., 2007; Wu et al., 2015). Both of these primed PSC types differ from naive mESCs and reflect biologically distinct pluripotent states occurring in development (**Figure 1**).

PSCs—especially hiPSCs—have huge potential for regenerative medicine due to their capacity to generate an array of differentiated cells and tissues that may be used for transplantation therapies or for disease modelling and drug discovery (Murry and Keller, 2008). It will be interesting to see what advances in regenerative medicine result from the increasing understanding of the biology of pluripotency.

Extensive characterisation of newly derived cell lines is vital in order to validate their differentiation potential. Various methodologies for assessing cellular pluripotency have been reported, including; *in vitro* characterisation, embryoid body (EB) formation, chimaera contribution, and teratoma formation (Martí et al., 2013). Each of these methods has applications and limitations which will now be discussed.

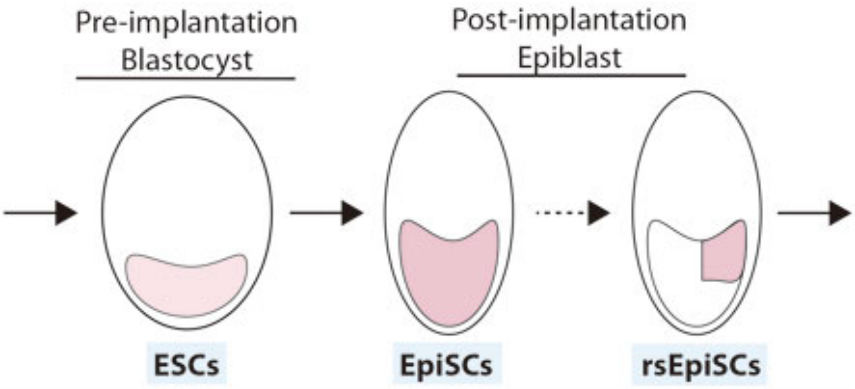

Growth conditions	2i, LIF	FGF2, Activin-A	FGF2, WNTi
Clonogenicity	High	Low	High
Tumorigenicity	High	High	Low

Figure 1: A schematic representation of distinct pluripotent stem cell populations.

Distinct pluripotent states occur during murine embryonic development and pluripotent stem cells can be isolated at different stages. Embryonic stem cells (ESCs) are isolated from the inner cell mass of pre-implantation blastocysts and can differentiate to embryonic and extraembryonic lineages. Epiblast stem cells (EpiSCs) are derived from explanted epiblast cultures and differentiate to epiblast-derived somatic lineages. Region-specific EpiSCs (rsEpiSCs) correspond to a distinct posterior-proximal epiblast population that can also differentiate to epiblast-derived somatic lineages. Figure taken from Weissbein and Benvenisty (2015).

1.1 *In Vitro* Culture

1.1.1 Assessing pluripotency

The first step in the characterisation of a newly derived cell line occurs *in vitro*. Morphological characteristics such as small size and high nuclear:cytoplasmic ratio are typical of PSCs (Brons et al., 2007). Placental alkaline phosphatase (AP) is an enzyme expressed in ESCs that can be detected through a colorimetric assay or immunohistochemical techniques (Martí et al., 2013).

Immunocytochemical staining is routinely used for the further characterisation of PSCs *in vitro* via fluorescence microscopy and flow cytometry. Several markers specific for pluripotency maintenance and ESC physiology are known and their expression in a given cell is indicative of pluripotency (Martí et al., 2013). Transcription factors including Nanog (Chambers et al., 2003), Oct4 (Scholer et al., 1989), and Sox2 (Yuan et al., 1995) are expressed in both mESCs and hESCs, while surface antigens including TRA-1-60, TRA-1-80, SSEA-3, and SSEA-4 are associated with hESCs, and SSEA-1 is expressed only on mESCs (Solter and Knowles, 1978; Martí et al., 2013).

1.1.2 Pluripotency maintenance

A key facet of PSCs is that they replicate indefinitely in culture. There is considerable cell type variation, however, in the conditions that are required to maintain stem cells in an undifferentiated state.

EC cells have comparably low requirements in order to maintain their undifferentiated state. Some EC lines, such as the human EC (hEC) line TERA2.cl.SP12, only needs to be grown at high confluence using standard cell culture reagents in order to prevent differentiation (Przyborski et al., 2004). ESCs are considerably more challenging to culture than EC cells and traditionally required feeder layers of mitotically inactivated cells or conditioned media (Martin, 1981; Thomson et al., 1998).

Modern techniques allow mESCs to be cultured without feeder layers if supplied with exogenous leukaemia inhibitory factor (LIF) and active bone morphogenetic protein (BMP) signalling that can be provided by the addition of serum or recombinant BMP4 to the media (Williams et al., 1988; Ying et al., 2003). Later it was shown that culturing mESCs with chemical inhibitors of mitogen-activated protein kinase (to inhibit fibroblast growth factor signalling) and glycogen synthase kinase 3β (to activate Wnt/β-catenin signalling)—known as 2i conditions—was sufficient to derive and maintain germ-line competent mESCs serum-free without the addition of LIF or BMP (Ying et al., 2008). This shed light on the ground state of mESC self renewal, indicating that pluripotency maintenance required a block to differentiation rather than inductive signals.

hESCs on the other hand differ in their pluripotency mechanisms and require supplementation with basic fibroblast growth factor (bFGF) and activin/nodal signalling—known as F/A conditions—to maintain their undifferentiated state (Levenstein et al., 2006; Brons et al., 2007). EpiSCs were derived from murine post-implantation epiblasts under F/A conditions—demonstrating their equivalence to hESCs—and undergo rapid and effiecient spontaneous differentiation to all three embryonic germ layers that

is indicative of their primed pluripotent state and has led to interest in their use as a source for cell transplantation therapies (Brons et al., 2007; Wu et al., 2015; Najm et al., 2011). EpiSCs are disctinct from mESCs in terms of genomic, epigenomic, and metabolic profiles, clonogenicity, differentiation capacity, growth characteristics, and culture conditions.

rsEpiSCs, however, were derived from explanted post-implantation epiblast exposed to bFGF and IWR1 (an inhibitor of Wnt signalling)—known as F/R1 conditions—and are generated from epiblast with a much higher efficiency than EpiSCs (Wu et al., 2015). rsEpiSCs differ are distinct from EpiSCs in terms of their transcriptomic, epigenomic, and metabolic profiles, their clonogenicity, tumorigenicity and chimaera contribution; occupying a stabilised primed pluripotent state that corresponds specifically to the posterior-proximal epiblast *in vivo* (**Figure 1**). It has been suggested that epiblast patterning may demarcate cell populations corresponding to distinct regions in adult organisms, although this remains to be determined (Wu et al., 2015).

Recent advances allow PSCs to be cultured feeder-free and in defined media. Defined medium without the use of animal derived products such as serum is essential for differentiation protocols to be reproducible and for the therapeutic potential of PSCs to be realised (Murry and Keller, 2008).

1.1.3 Karyotypic stability

An important step in the *in vitro* characterisation of pluripotent stem cell lines is to investigate their karyotypic stability over prolonged culture. Andrews *et al.* showed that accumulated chromosome translocations acquired during hESC culture reduced the requirements for maintaining pluripotency to a level more similar to hEC cells (Andrews et al., 2005). Interestingly, the aneuploidy seen in long-term cultured hESCs reflected chromosomal translocations seen in EC cells. EC cells will have been placed under considerable selective pressure towards a self-maintenance phenotype during tumour growth and similarly, faster growing ES cells will be selected for if cultured for extended periods under suboptimal conditions (Andrews et al., 2005).

The karyotypic stability of a PSC line must be demonstrated in order for any therapeutic applications to be realised. One study found that mESCs cultured beyond passage 14 were developmentally compromised (Nagy et al., 1993), highlighting the special care required during PSC culture and the importance of this characterisation step.

1.2 *In Vivo* Differentiation

In vivo techniques have traditionally been widely relied on to characterise the development potential of newly derived stem cell lines because expression of pluripotency markers alone *in vitro* is not sufficient confirmation of true pluripotency. Differentiation *in vivo* supports cellular development through interactions with host tissues and PSCs readily form complex tissues when cultured *in vivo* (Przyborski, 2005).

1.2.1 Chimaera contribution

Soon after the initial isolation of mESCs they were shown to produce functional germline competent chimaeras (Bradley et al., 1984). Chimaera formation was assayed by injecting mESCs into the ICM of a murine blastocyst which was then implanted into the uterus of a pseudo-pregnant mouse. Implanted cells incorporated into all tissues in the adult, including the germ cells, and therefore the pluripotency of mESCs could be demonstrated unequivocally (**Figure 2**)(Bradley et al., 1984). Genetically labelled cells or more simply, cells from a different pigmentation background have been used in order to assess chimaera contribution phenotypically (Hall et al., 2009).

Functional germ-line chimaeras derived from cultured mESCs allowed knockout mice to be generated meaning that gene modifications made to mESCs *in vitro* could be incorporated into an entire animal (Hall et al., 2009). Knockout mice are extremely powerful research tools for disease modelling and drug discovery as well as for studying gene function in mammalian development.

Murine EC cells have also been shown to be able to contribute to normal development in the embryo in certain cases (Andrews, 2002). Germ line transmission has never been seen, however, indicative of the reduced developmental potential and malignant origins of EC cells.

EpiSCs incorporate into the post-implantation epiblast and contribute to all three germ layers but fail to incorporate into the pre-implantation ICM (Wu et al., 2015). rsEpiSCs, however, only incorporate efficiently and contribute to all three germ layers when implanted into the posterior epiblast. EpiSCs and rsEpiSCs differ to mESCs in their ability to proliferate rapidly and generate large numbers of differentiated cells when incorporated into the post-implantation epiblast that is indicative of their primed pluripotent state (Wu et al., 2015).

Strikingly, human region-specific PSCs (rsPSCs) derived from hESCs cultured under F/R1 conditions were able to form heterospecific chimaeras when implanted into the posterior epiblast of murine post-implantation embryos (Wu et al., 2015). This could allow unprecedented access to early human embryonic developmental processes and their study *in vitro*.

1.2.2 Tetraploid complementation

Tetraploid complementation is a more stringent pluripotency assay than chimaera contribution and the pluripotency of mESCs has been further validated using this method. Fusion of mouse morulae at the 2-cell stage generates a tetraploid embryo which is developmentally compromised (Nagy et al., 1993). When mESCs are fused with tetraploid

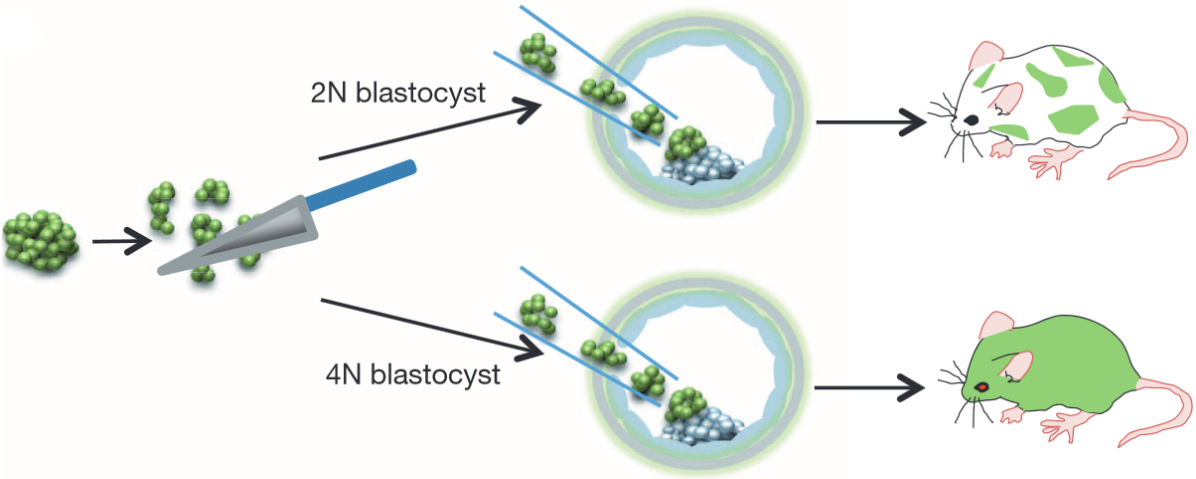

Figure 2: Chimaera formation from diploid (2N) and tetraploid (4N) blastocysts.

A schematic representation of chimaera formation from diploid 2N blastocysts and tetraploid (4N) blastocysts. To generate chimaeras, cultured mESCs are implanted into the inner cell mass (ICM) of 2N murine blastocysts which are then implanted into the uterus of a pseudo-pregnant mouse. Analysis of the chimaera that results can be used to determine which tissues of the animal were derived from the implanted cells. If the implanted cells were pluripotent then derivatives of all three embryonic germ layers and germ cells will be able to be derived from them. Figure taken from (Obokata et al., 2014).

embryos, diploid cells outcompete the tetraploid component and the entire neonate produced is derived entirely from the injected diploid cells (**Figure 2**)(Nagy et al., 1993). Tetraploid complementation has been used to confirm the pluripotency of both mESCs and iPSCs of murine origin (Zhao et al., 2009).

Chimaera formation and tetraploid complementation are considered the gold standard for assessing the potency of murine cells. In humans and non-human primates, however, chimaera formation is not possible for ethical reasons and the gold standard is teratoma formation.

1.2.3 Teratoma formation

A qualifying criterion for the pluripotency of a stem cell line to be established is that upon xenografting into immunocompromised animals a teratoma will form—a solid tumour containing differentiating tissues representative of all three embryonic germ layers (Andrews et al., 2001). It is well established that ESCs consistently form teratomas containing differentiated tissues representative of all three germ layers when grown as a xenograft in immunocompromised animals (**Figure 3**) (Martin, 1981; Thomson et al., 1998; Przyborski, 2005).

Early xenograft experiments showed that isolated murine EC cells were capable of regenerating an entire teratocarcinoma, confirming the notion that EC cells are the cancer stem cell origin of the tumours (Kleinsmith and Pierce, 1964). While some EC lines do possess the ability to form teratomas containing derivatives of all three germ layers, lineage-dependent differences exist.

Certain EC lineages, such as the hEC line TERA2.cl.SP12 display a propensity to form teratomas containing primarily neural and non-neural epithelial tissues (Przyborski et al., 2004). Moreover, some EC cell lines are incapable of differentiation without exogenous factors and thus considered nullipotent (Andrews, 2002). The limited differentiation capacity of EC cells *in vivo* is further evidence of their malignant origin and reduced developmental capacity in comparison to ESCs.

Particular clonal lineages of the first iPSCs failed to produce teratomas containing derivatives of all three germ layers, likely the result of incomplete reprogramming (Takahashi and Yamanaka, 2006). Since then, considerable research effort has refined the reprogramming process and, more recently, iPSCs consistently produce teratomas containing an array of differentiated tissues representative of all three germ layers (Takahashi et al., 2007; Kimbrel and Lanza, 2015).

EpiSCs and rsEpiSCs both form teratomas containing an array of differentiated tissues representative of all three embryonic germ layers, casting doubt on the hypothesis that epiblast patterning could account for distinct body regions (Brons et al., 2007; Tesar et al., 2007; Wu et al., 2015). Teratoma formation is slower and tumour volume smaller in rsEpiSC teratomas, however, leading to interest in their use as a source for cell transplantation therapies due to their reduced tumorigenicity (Weissbein and Benvenisty, 2015).

Teratoma formation is the gold standard pluripotency assay for newly derived human stem cell lines and is an informative way to investigate the development potential of a

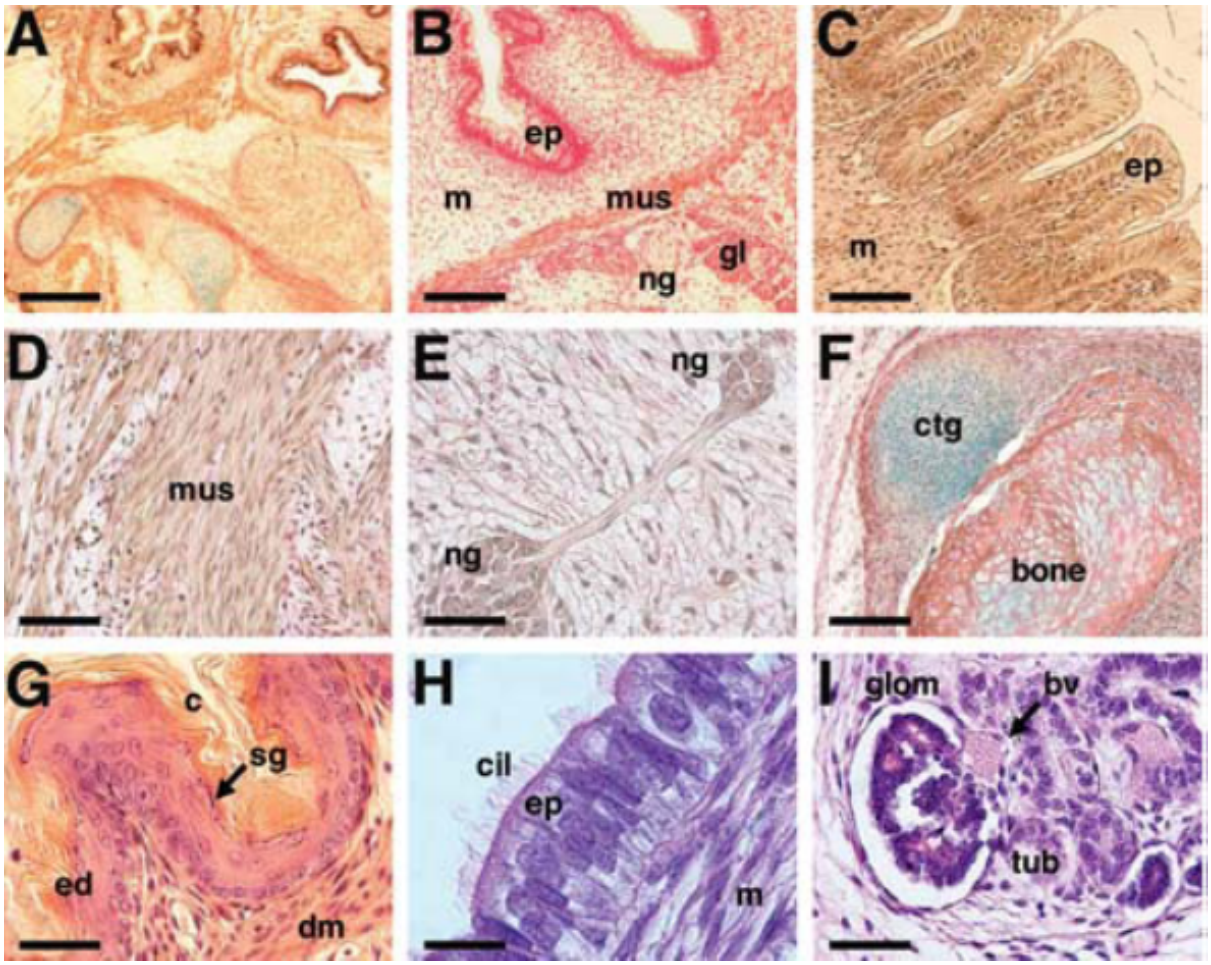

Figure 3: Histological analysis of teratomas derived from hESCs.

The heterogeneous teratoma structure is shown in (**A**) and differentiated tissues shown are intestinal wall (**B**), intestinal epithelial mucosa (**C**), smooth muscle (**D**), neural ganglia (**E**), cartilage and bone (**F**), skin (**G**), respiratory tract epithelium (**H**), and kidney tissue (**I**). Scale bars represent (**A**) 450 μm, (**B**,**F**) 150 μm, (**C**) 75 μm, (**D**, **E**, **I**) 50 μm, (**G**) 40 μm, and (**H**) 15 μm. Figure taken from Przyborski (2005).

given cell type. The technique has been criticised, however, due its lack of reliability and high animal usage (Gropp et al., 2012). In depth histological analysis of teratomas is required, as teratoma formation on its own does not confirm pluripotency. Although locally organised tissues are able to form, the overall tissue architecture of teratomas develop in a disorganised fashion due to uncoordinated developmental signals and a failure to allow proper developmental morphogenetic processes to occur (Przyborski, 2005). In addition, care must be taken for considerations such as the site of cell implantation and cell number implanted as both influence teratoma growth (Cooke et al., 2006). One meta-analysis called into question the gold standard status of the teratoma assay due to failure to report teratoma formation data in many newly derived hESC and hiPSC lines—with half of hESC lines and over a third of hiPSC lines not including any teratoma data in the primary literature reporting their derivation (Muller et al., 2010).

With the increasing number of PSC lines being established it will be necessary to develop new *in vitro* pluripotency testing methodologies that will reduce the need for *in vivo* differentiation techniques such as the teratoma assay. Differentiation *in vitro* can be more tightly controlled and studied than *in vivo* differentiation. *In vitro* differentiation techniques offer alternative pluripotency tests and allow greater opportunities for the generation of purified cell populations for cell transplantation and disease modelling.

1.3 *In Vitro* Differentiation

1.3.1 Differentiation in two-dimensions (2D)

The spontaneous differentiation of PSCs in 2D culture is disorganised and results in the formation of a variety of somatic and extra-embryonic cell types, predominantly endodermal lineages (Weitzer, 2006). Although purification of a desired cell type from complex mixtures is possible, in order for the clinical applications of PSCs to be realised directed differentiation to defined cell types is more desirable.

1.3.2 Directed differentiation

Taking a developmental biology approach to differentiation *in vitro* allows information gained from studying embryonic development in model systems to be applied to the directed differentiation of human PSCs for therapeutic purposes (Murry and Keller, 2008). Differentiation can be directed towards specific lineages by exogenous manipulation of pathways that are active and required during embryonic fate specification. Pathways such as Wnt/β -catenin, bone morphogenetic protein (BMP), FGF, sonic hedgehog (Shh), and nodal/activin are associated with patterning the early embryo and are frequently manipulated *in vitro* by using small molecules or recombinant proteins to achieve desired differentiation outcomes (Murry and Keller, 2008).

A developmental biology approach to directed differentiation has been successful in yielding pure populations of many somatic lineages from PSCs that may be useful for therapeutic cell transplantation. For example, Najm *et al.* described an elegant process that involved first specifying neuroepithelium (by inhibition of BMP and nodal/activin signalling) followed by exposure to retinoic acid and Shh at levels that are present in the ventral ventricular zone in the neural tube: the seat of oligodendrocytogenesis *in vivo* (Najm et al., 2011). Oligodendrocyte progenitor cells (OPCs) that are widely accepted as having potential to treat demyelinating diseases such as multiple sclerosis were robustly generated from EpiSCs with high efficiency and within a short space of time.

hiPSCs are the most desirable PSC type for directed differentiation to somatic lineages by minimising rejection risk (allowing autograft cell transplants) and facilitating the study of disease mechanisms. OPCs (Wang et al., 2013), cardiomyocytes (Myers et al., 2013), pancreatic islet cells (Thatava et al., 2011), hepatocytes (Roelandt et al., 2013), and dopaminergic neurons (Cai et al., 2010) have all been generated from hiPSCs *in vitro* and each of these breakthroughs may lead to regenerative medicine strategies for currently incurable human diseases.

However, not all somatic lineages can be generated. Haematopoietic stem cells (HSCs) can only be generated using inefficient EB cultures or teratomas (Chen, 2014; Amabile et al., 2013), but could offer a significant source for autologous transplantation to treat haematological diseases if an efficient and reproducible *in vitro* protocol existed. Studying human embryonic development *in vitro* through the use of hiPSCs/hESCs may lead to advances in directed differentiation that could result in improvements in generating certain cell types with clinical applications such as HSCs.

1.4 Developmental pathways

Development is a fascinating and tightly regulated process that requires coordinated signals to generate functioning tissues and eventually whole organisms from tiny groups of cells. Many signalling pathways have been studied with regards to their role in development; some of which will be discussed with relevance to *in vitro* stem cell differentiation.

1.4.1 Retinoic Acid Pathway

The vitamin A (retinol) derivative retinoic acid (RA) is essential for proper vertebrate development (Rhinn and Dolle, 2012). RA exhibits pleiotropic effects and is implicated in the development of the branchial apparatus, lung, pancreas, limbs, and somites, and in hindbrain and forebrain patterning, and neural tube differentiation (Rhinn and Dolle, 2012). Retinoids exhibit gene regulatory effects through binding to nuclear receptors (RARs/RXRs) to act as transcriptional activators of target retinoid-responsive genes (Mark et al., 2009). RA morphogen gradients are tightly regulated during development through the activities of synthesising and metabolising enzymes, and developmental abnormalities occur if these enzymes are non-functional (Mic et al., 2004). RA also acts as a teratogen at high concentrations when administered to embryos exogenously (Durston et al., 1989). The role of RA in development has been studied extensively *in vivo* and one isomer, all-*trans*-RA (ATRA), is also commonly used as an *in vitro* inducer of stem cell differentiation.

ATRA was first shown to induce differentiation in murine EC cultures, producing neural and glial cell types (Jones-Villeneuve et al., 1982). ATRA treatment of mESCs grown as EBs in suspension *in vitro* has been shown to direct differentiation to both neural and endodermal lineages, indicating the diverse roles of ATRA in regulating development (Bibel et al., 2004; Micallef et al., 2005). One of the limitations in studying the role of ATRA in cell specification is its instability and propensity to isomersise to any one of several different biologically active retinoids (that may have subtly distinct effects) upon heat or light exposure (Christie et al., 2010). This instability makes the active concentration of ATRA difficult to tightly regulate, which is of critical importance for accurately directing stem cell fate *in vitro* and generating reproducible differentiation protocols. One solution is to use the synthetic retinoid ec23 that was designed to be highly stable and to mimic ATRA activity (Christie et al., 2008). ATRA and ec23 have both been shown to induce robust neural differentiation in hEC line TERA2.cl.SP12 and induce formation of motor neurons in H9 hESCs (Christie et al., 2010).

1.4.2 Bone morphogenetic protein pathway

Bone morphogenetic proteins (BMPs) are a related group of signalling molecules that are members of the transforming growth factor β (TGF-β) superfamily. BMPs are ligands that bind to serine/threonine kinase membrane receptors including type I (BMPR-1A/ALK3, BMPR-1B/ALK6, ActR-1A/ALK2) and type II receptors (BMPR-2, ActR-2A, ActR-2B) (Wang et al., 2014). Type II receptors transphosphorylate type I receptors that phosphorylate and activate receptor regulated-Smads (R-Smads 1/5/8). R-Smads form a complex with co-mediator Smad4 and this complex translocates to the

nucleus where it exhibits gene regulatory effects through coactivators and corepressors (Wang et al., 2013).

BMPs were first identified as potent inducers of ectopic bone growth but have wide ranging roles in adult tissue homeostasis as well as being critical embryonic morphogens (Urist and Strates, 1971; Li and Chen, 2013). The default model of neural plate specification postulates that neurogenesis is under inhibitory control: that BMP inhibitors secreted by the organiser induce neural development in the embryonic ectoderm by inhibiting endogenous BMP activity that would result in epidermis formation (Spemann and Mangold, 1924; Ozair et al., 2013).

BMP4 was the first BMP identified that was capable of blocking neural induction in mammalian embryos (Wilson and Hemmati-Brivanlou, 1995). More recently, BMPs have been used to promote the development of endoderm and mesoderm in ESC cultures while inhibiting neurectodermal differentiation (Finley et al., 1999). BMP inhibition is frequently used to induce neural differentiation *in vitro* from ESCs including the small molecule dorsomorphin or the protein noggin (Groppe et al., 2002; Yu et al., 2008; Najm et al., 2011). However, other pathways likely play a role in neural specification and the absolute requirement for BMP inhibition has been challenged (Linker and Stern, 2004).

1.4.3 Wnt/β-catenin pathway

The Wnt signalling cascade is a ubiquitous cell signalling pathway with diverse roles in development and in the functioning of adult organisms (Arkell et al., 2013). β-catenin plays a central role in the canonical Wnt pathway.

In the absence of Wnt ligand a destruction complex comprising of Axin, adenomatosis polyposis coli (APC), protein phosphatase 2A (PP2A), glycogen synthase kinase 3β (GSK3β) and casein kinase 1α (CK1α) phosphorylates cytoplasmic β-catenin and it is subsequently ubiquitnylated and degraded by the proteasome (MacDonald et al., 2009). Nuclear T cell factor/lymphoid enhancer factor (TCF/LEF) transcription factors inhibit the expression of Wnt target genes. Wnt ligand binding to Frizzled-family receptors and low-density lipoprotein receptor related protein 5/6 (LRP5/6) coreceptors at the responding cell surface disrupts the destruction complex, allowing β-catenin to translocate to the nucleus where it forms complexes with TCF/LEF factors and activate Wnt target genes (MacDonald et al., 2009).

In the embryo, Wnt signalling is essential for primitive streak formation and maintenance and favours mesodermal differentiation at the expense of ectoderm (Gadue et al., 2006; Murry and Keller, 2008; Arkell et al., 2013). Wnt3 signals along with activin/nodal signalling specify the primitive streak population and in turn the anterior-posterior embryonic axis that generates different mesodermal derivatives (Funa et al., 2015).

Chiron99021 is a small molecule GSK3β inhibitor that is commonly used as an activator of Wnt signalling *in vitro*. Chi has been used to demonstrate that β-catenin induces expression of primitive streak genes and primitive streak-like motile behaviours through collaborative interactions with Oct4 and brachyury, respectively, in ESC *in vitro* models of primitive streak formation (Funa et al., 2015; Turner et al., 2014). Chi has also

been used to generate gastruloids—mEBs that undergo gastrulation-like morphogenetic proceses in response to Chi and activin A (van den Brink et al., 2014).

1.5 Differentiation in Three-Dimensions (3D)

Differentiation in 2D culture allows development potential to be examined *in vitro* without the use of animals. However, in terms of pluripotency testing it would be time consuming and costly to follow multiple directed differentiation protocols. Moreover, the limitations of 2D culture methods are slowly becoming more widely accepted, indicating the use of 3D cultures (Knight and Przyborski, 2014). For example; cell and nuclear flattening, cytoskeletal changes, and changes in gene expression and protein synthesis have all been reported in 2D culture (Vergani et al., 2004, Thomas et al., 2002). Fundamentally, 2D culture represents an artificial environment for cell growth and therefore the recapitulation of normal developmental processes in 2D cultures is limited.

1.5.1 Aggregate Cultures

Early research identified the ability of mESCs to spontaneously aggregate in suspension and form aggregates termed embryoid bodies (EBs). Myriad methodologies have since been developed for generating EBs from PSCs including liquid suspension culture, stirred flask culture, rotary cell culture systems, hanging drop cultures, ultra-low adhesion U-bottom multiwell plates, and indented solid microsurfaces (Aggrewell™) (Sheridan et al., 2012).

Aggregate cultures allow cells to produce their own extracellular matrix and provide enhanced cell interactions compared to 2D culture (Knight and Przyborski, 2014). Aggregation cultures of TERA2.cl.SP12 cells have been shown to substantially increase the efficiency of neural induction in response to retinoic acid compared to 2D cultures, higlighting the ability of this 3D culture technique to improve differentiation outomes (Horrocks et al., 2003). Tisses representative of all three embryonic germ layers including neuroepithelium, epidermis (ectoderm), connective tissues (mesoderm), and intestinal/respiratory epithelium (endoderm) spontaneously develop in EBs concomitant with tissue-specific marker expression (Sheridan et al., 2012). EBs derived from ESCs as well as iPSCs of murine or human origins undergo differentiation to all three germ layers (Doetschman et al., 1985; Itskovitz-Eldor et al., 2000; Takahashi and Yamanaka, 2006; Takahashi et al., 2007).

For this reason EB formation has been used as an *in vitro* pluripotency assay that is an animal-free alternative to teratoma formation (Sheridan et al., 2012). Moreover, human EBs facilitate the study of early human embryonic development that is inaccessible *in vitro* and may lead to advances in the clinical applications of PSCs. Marker expression and local small-scale tissue morphology that is frequently observed in EBs, however, does not mean that a functioning, *in vivo*-like tissue has been produced. Teratoma formation produces more highly complex tissues than in EBs meaning that *in vivo* differentiation techniques represent a more stringent test of developmental capacity (Buta et al., 2013).

EB development has been shown to be equivalent to early embryonic development up to 7 - 8 days (Weitzer, 2006) and more recent findings indicate their ability to undergo

gastrulation-like processes *in vitro* (ten Berge et al., 2008; van den Brink et al., 2014). Despite the resemblance of EB development to early embryogenesis, the later stages of development are not accurately recapitulated in EBs (Weitzer, 2006). Over prolonged periods in suspension culture differentiation in EBs is often disordered with abnormal structures and cystic EBs frequently observed (Amit and Itskovitz-Eldor, 2002; Murry and Keller, 2008). Ultimately, diffusion limits the ability of oxygen to reach the centre of cell aggregates since they are avascular structures (Buta et al., 2013). A recent study found that the oxygen concentration at the centre of large EBs (400 μm radius) was 50% lower than at the center of small EBs (200 μm radius) (Van Winkle et al., 2012). While differences in oxygen concentrations may be useful for developing cellular diversity within EBs, reduced nutrient availability can lead to the development of a hypoxic core and cell death (Van Winkle et al., 2012; Knight and Przyborski, 2014).

Attachment is frequently used in the culture and differentiation of EBs and can provide a more accurate recapitulation of the *in utero* environment through mimicking endometrial implantation (Weitzer, 2006). Moreover, EB flattening provides an enhanced ability of cells to recieve nutritional support via diffusion. However, EBs have traditionally been attached to collagen or gelatin-coated 2D surfaces and under these conditions cells migrate radially away from EBs (Evans et al., 1981; Takahashi and Yamanaka, 2006). Attachment to a 2D substrate only provides nutritional support above the EB and cells that are migrating away from EBs will grow in an artificial 2D environment.

3D culturing techniques such as aggregate cultures are becoming utilised more widely due to the benefits that they provide over conventional 2D techniques (Knight and Przyborski, 2014). An alternative 3D culture strategy to aggregation is the use of 3D scaffolds.

1.5.2 Scaffold Technologies

Scaffolds have been utilised widely for 3D culturing because they provide enhanced cell attachments in a 3D microenvironment that improves cell shape and better reflects the *in vivo* situation compared to 2D substrates (Knight and Przyborski, 2014). 3D scaffolds can be made from different biological and synthetic materials using a variety of techniques which have recently been reviewed by Knight and Przyborski (2014).

Biodegradable scaffolds can be made from an array of naturally occurring materials including collagen (Baharvand et al., 2006), fibrin (Willerth et al., 2006), hyaluronic acid (Gerecht et al., 2007), silk (Mauney et al., 2007), gelatin (Awad et al., 2004), alginate (Li et al., 2010), and chitosan (Duarte et al., 2009), or synthetic materials such as poly(l-lactic acid)(PLLA) and poly(lactic-*co*-glycolic acid)(PLGA)(Levenberg et al., 2003) that may be used alone or blended. Scaffolds have been used frequently to support differentiation of ESCs in a 3D environment.

For example, PLLA/PLGA synthetic scaffolds have been used to support hESC differentiation and shown to facilitate the development of neural, cartilage, and liver tissues (Levenberg et al., 2003). One of the benefits of biobiodegradable scaffolds is that they degrade making them highly suitable for tissue engineering applications where cells can penetrate and remodel the scaffold. However, this instability may be a hindrance for routine cell culture applications where degradation may be difficult to control and have undesirable effects on cell differentiation (Knight et al., 2011).

Hydrogels have a high water content and can be formed from collagen-1, matrigel, gelatin, and hyaluronic acid and have been used to support differentiation in murine EBs (mEBs) (Kothapalli and Kamm, 2013). mEBs were embedded in hydrogels that provided a 3D structure to support their growth and maintenance facilitating differentiation to neural and glial lineages in response to ATRA and Shh (Kothapalli and Kamm, 2013). One of the limitations of the use of hydrogels is that they can impact differentiation outcomes in unpredictable ways. Collagen-1 hydrogels, for example, promoted motor neuron differentiation, while matrigel stimulated development of dopaminergic neurons (Kothapalli and Kamm, 2013). Furthermore, hydrogels may not provide sufficient transfer of nutrients to support long-term differentiation (Jongpaiboonkit et al., 2008).

For routine cell culture, chemically inert scaffolds may be preferred because they provide reproducibility that is not easy to achieve with biodegradable scaffolds or hydrogels (Bokhari et al., 2007).

1.5.3 Alvetex®polystyrene scaffolds

Alvetex®is a rigid polystyrene 3D scaffold generated by polymerisation in high internal phase emulsion (polyHIPE) that is biocompatible, non-biodegradable, and highly porous (Knight et al., 2011). Alvetex®is available in a well-insert format containing a scaffold membrane of 200 μm thick. The size of the pores and interconnects within the scaffold can be tightly regulated according to polymerisation conditions (Knight et al., 2011).

A novel approach is to combine two common 3D culture strategies and to maintain stem cell aggregates on top of 3D inert synthetic scaffolds. Alvetex®has been shown to support differentiation in 3D stem cell aggregates and supported enhanced neural differentiation in TERA2.cl.SP12 aggregates (Hayman et al., 2004). Combining 3D culture techniques in this way has been shown to result in the formation of flattened tissue-discs from spheroid stem cell aggregates that may provide a mechanism to extend the culture time of EBs *in vitro* by improving nutritional support for cells throughout the entire aggregate via diffusion (E. Knight, PhD thesis). Moreover, physical attachment is a normal process during development *in utero* and could improve the recapitulation of the latter stages of embryonic development compared to aggregate suspension cultures.

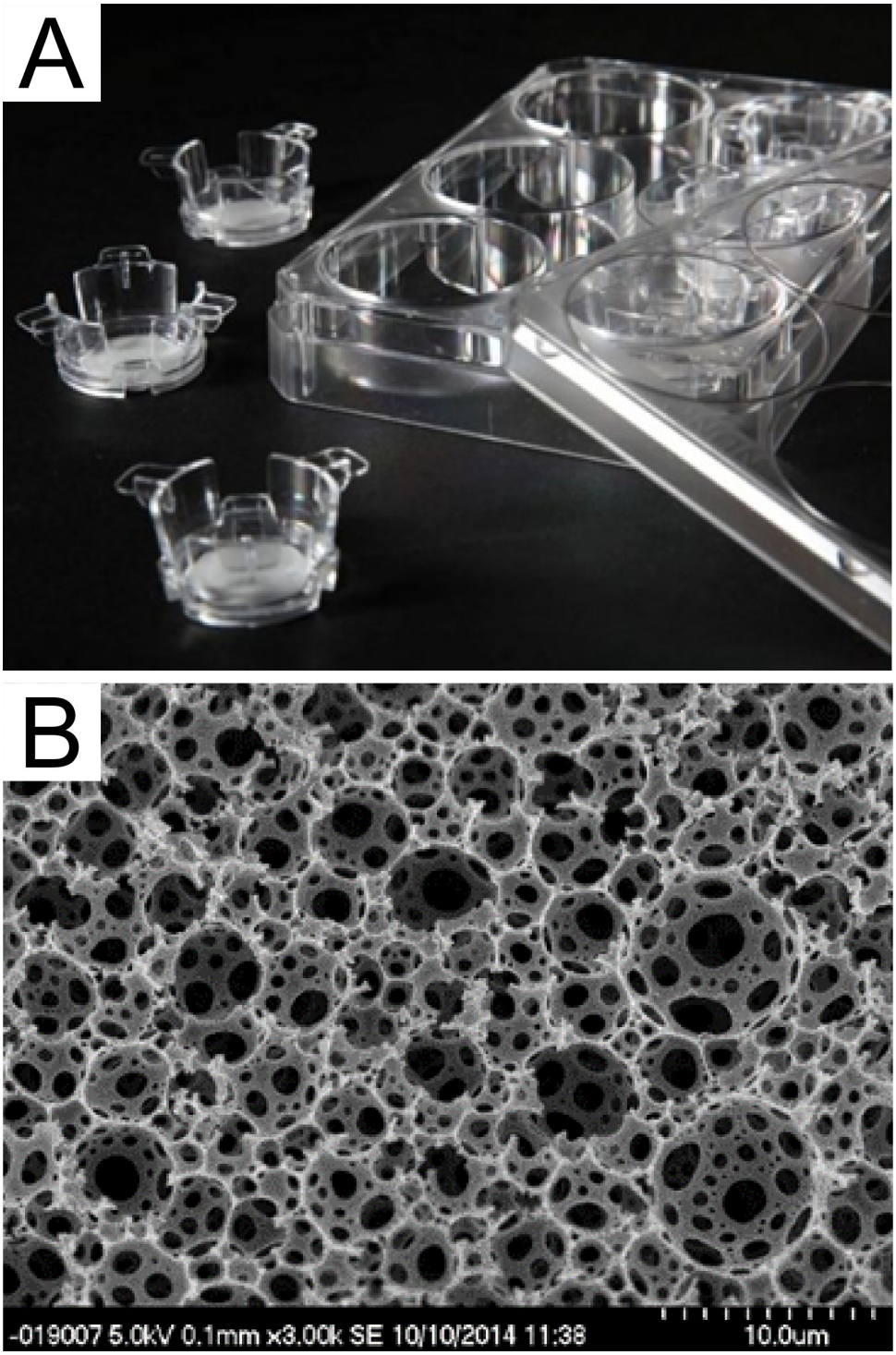

Figure 4: Images of Alvetex®porous polystyrene scaffold 6-well inserts.

Alvetex®porous polystyrene scaffolds are available as 6-well cell culture inserts (A) and consist of a porous polystyrene membrane with interconnects and voids whose size can be tightly regulated. Scanning electron micrograph (B) shows the detailed structure of Alvetex®Polaris with an average pore size of 3-4 μm. (A) was taken from www.reinnervate.com and (B) was kindly provided by R. Quelch, Durham University.

1.6 Aim and Objectives

The aim of this thesis is to investigate the maintenance of hEC aggregates and mEBs using Alvetex®3D scaffolds. Four main objectives will be explored: (1) is complex tissue development supported in tissue-discs? (2) is cell viability improved due to increased nutritional support over prolonged *in vitro* cultures? (3) can tissue-disc cultures be used to study aspects of human embryonic development? and (4) could this technique be adopted as a novel *in vitro* pluripotency assay?

2 Materials and Methods

2.1 2D Cell Culture

2.1.1 Human Embryonal Carcinoma Line TERA2.cl.SP12

The human embryonal carcinoma line TERA2.cl.SP12 was cultured according to established protocols (Przyborski, 2001). Cells were maintained using high glucose Dulbecco's Modified Eagle Medium (Lonza) supplemented with 10% heat-inactivated fetal calf serum (Gibco, Invitrogen), 2 mM L-glutamine (Lonza), and 1 ml penicillin/streptomycin (Lonza).

Frozen stocks were resuscitated by thawing cryovials as quickly as possible in a water bath at 37^{o}C and adding to 9 ml prewarmed media in a 15 ml Falcon tube (Starstedt). Cells were centrifuged at 1000 rpm for 3 minutes and supernatant removed. The cell pellet was resuspended in 10 ml prewarmed media and seeded into one T25 flask (BD Bioscience). Flasks were incubated in a humidified atmosphere with 5% CO_2 at 37^{o}C and the media was changed every 1 - 2 days. Once confluent (after about 3 days), cells were passaged by rolling sterile, acid-washed glass beads over the culture and splitting them into one fresh T75 flask, and thereafter split 1:3 into fresh T75 flasks.

In order to obtain specific cell numbers, cultures were washed in 5 ml Dulbecco's phosphate buffered saline (D-PBS, Lonza) and incubated with 3 ml trypsin/EDTA solution (Lonza) at 37^{o}C for 3 minutes to obtain a single cell suspension. Trypan blue stain (Sigma) was used to identify viable cells and a Neubauer improved haemocytometer was used to calculate cell numbers. Cells were frozen down at approximately 1x10^7 cells per ml in 90% heat-inactivated fetal calf serum and 10% DMSO (Sigma) in 1 ml cryovials (Nunc). Cells were stored at -80^oC using Nalgene's Mr Frosty for 24 hours before being transferred for long-term storage at -150^oC.

2.1.2 Mouse Embryonic Stem Cell Line CGR8

Mouse embryonic stem cell line CGR8 was obtained from Public Health England at passage 5. For routine culture, mESCs were grown using maintenance medium that consisted of Glasgow Minimum Essential Medium (GMEM, Sigma) supplemented with 10% pluripotent stem cell-qualified fetal calf serum (amsbio), 2 mM L-glutamine (Lonza), 0.05 mM 2-Mercaptoethanol (Sigma), and 1000 U/ml leukaemia inhibitory factor (LIF, amsbio).

Frozen stocks were resuscitated by thawing cryovials as quickly as possible in a water bath at 37^{o}C and adding to 5 ml prewarmed maintenance medium in a 15 ml Falcon tube. Cells were centrifuged at 1000 rpm for 3 minutes and supernatant removed. The cell pellet was resuspended in 10 ml prewarmed maintenance medium and seeded into one 0.2% gelatin coated T25 flask (Nunc). Cells were grown in 0.2% gelatin coated T25 flasks and incubated in a humidified atmosphere with 5% CO_2 at 37^{o}C. Media was changed daily and cultures were split 1:10 when they reached 70% confluency.

When splitting cells it was necessary to seed cells as a single cell suspension. Cultures were washed in D-PBS before incubating with 1 ml trypsin/EDTA solution at 37^{o}C for 3 minutes, and then pipetting up and down several times vigorously. Trypsin was

inactivated by adding 9 ml maintenance media which was then transferred to a fresh gelatin-coated T25 flask.

0.2 % gelatin solution was prepared by adding 0.2 g gelatin powder (Sigma) to 100 ml D-PBS before being autoclaved at 120^{o}C for 20 minutes in order to dissolve the gelatin. 4 ml 0.2 % gelatin solution was added to T25 flasks that were incubated for at least 4 hours at 37^{o}C before use. Flasks were stored for up to 1 week at 37^{o}C and gelatin solution was aspirated just prior to seeding the cells.

2.2 Aggregate Formation

2.2.1 TERA2.cl.SP12 Aggregates

In order to generate aggregates of TERA2.cl.SP12 human embryonal carcinoma cells, a spontaneous aggregation technique was used. 1 ml media containing 1.5x10^6 single cells in suspension were seeded into non-tissue culture treated 10 cm plates (Fisher) and topped up with media to 20 ml. Plates were incubated in a humidified atmosphere with 5% CO_2 at 37^{o}C for 24 h to allow aggregates to form before inducers were added directly to the media which was gently swirled in order to evenly distribute the inducer.

Aggregate media was changed every 3.5 days by collecting aggregates in suspension into a 50 ml Falcon tube (Starstedt) and allowing them to sediment over 2-5 minutes before aspirating spent medium and replacing with 20 ml fresh medium. Aggregates were resuspended by gently swirling the Falcon tube before pouring the suspension into a fresh 10 cm plate, adding inducers directly to the medium and gently swirling it to evenly distribute the inducers. Aggregates were maintained in suspension for up to 21 days.

2.2.2 CGR8 Murine Embryoid Bodies

AggreWell™800 plates (Stem Cell inc.) were used to obtain uniform aggregates /embryoid bodies (mEBs) of CGR8 mouse embryonic stem cells. For formation and maintenance of mEBs, mEB media was used consisting of mESC maintenance media without the addition of LIF and with the addition of either 10% or 20% heat inactivated FBS (Gibco, invitrogen).

Each well of the AggreWell™800 plate to be used for mEB formation was first rinsed with 2 ml prewarmed mEB medium that was then aspirated. 0.5 ml prewarmed mEB medium was added to the rinsed wells and the plate was centrifuged at 2000 g for 5 minutes. It was essential to balance the centrifuge correctly using another AggreWell™800 plate. An inverted phase-contrast microscope was used to check that all air bubbles inside the wells were properly displaced.

mEB formation required seeding accurate cell numbers. A single cell suspension was achieved by washing cells in D-PBS before incubating with 3 ml trypsin/EDTA solution at 37^{o}C for 3 minutes and then pipetting up and down several times vigorously. Trypsin was inactivated by adding 10 ml prewarmed mEB medium and the single cell suspension was centrifuged at 1000 rpm for 3 minutes. The cell pellet was resuspended

in 10 ml prewarmed mEB medium and trypan blue stain was used to identify viable cells and a haemocytometer was used to calculate cell numbers.

$3x10^5$ cells were added to 0.5 ml mEB medium in each well of the AggreWell™800 plate to be used and pippetted up and down several times to evenly distribute the cells. Each well containing $3x10^5$ cells generated 300 mEBs consisting of 1000 cells per mEB. Total medium in each well was adjusted to 2 ml and the plate was centrifuged at 100 g for 3 minutes.

The AggreWell™800 plate was incubated in a humidified atmosphere with 5% CO_2 at 37^oC for 72 hours with careful 1 ml media changes every 24 hours in order not to disturb the mEBs. mEBs were harvested after 72 hours by pipetting up and down with moderate force 2-3 times to ensure that all mEBs had left their microwells. mEBs in suspension were strained through a 37 µm cell strainer (VWR). Each well was washed with 2 ml mEB medium and strained again. The well was visualised using an inverted phase-contrast microscope to ensure all mEBs had been removed.

mEBs were washed into non-tissue culture treated 10 cm plates at 300 mEBs per plate with 20 ml prewarmed mEB medium. Plates were incubated in a humidified atmosphere with 5% CO_2 at 37^oC for 5 days and were physically agitated 3 times per day during the first 2 days of culture to try to prevent mEBs adhering to each other.

2.3 Small Molecules and Recombinant Proteins

Small molecules and recombinant proteins that were used as inducers of stem cell differentiation were added directly to the media of aggregates cultured in suspension. The concentrations at which inducers were used for differentiation and the suppliers from which they were acquired are shown in the table below.

Table 1: Small molecules and recombinant proteins used as inducers of stem cell differentiation.

Inducer	Concentration	Supplier
ec23	0.01 µM	ReproCELL Reinnervate
BMP-2	50 $ngml^{-1}$	amsbio
Noggin	100 $ngml^{-1}$	amsbio
Dorsomorphin	1 µM	Sigma
Chir99021	3 µM	Sigma

2.4 Alvetex® 3D Aggregate Cultures

Alvetex®3D polystyrene scaffold membranes (ReproCell Reinnervate) were prepared using an EMITECH K1050X plasma treater set to 40 W power and 5 minutes ashing time in order to render the polystyrene surfaces hydrophylic. Alvetex® 3D polystyrene scaffolds may also be prepared by dipping the membrane in 70 % ethanol followed by two washes in sterile PBS. Alvetex® 6-well inserts were placed into a 6-well culture plate (Greiner Bio-one) and hydrated by adding 8 ml of the appropriate culture media.

Aggregates in suspension were collected and passed through a 100 µm cell strainer (VWR) in order to remove any single cells before being washed back into a fresh 10 cm plate with 10 ml of prewarmed culture media. 1-2 aggregates were collected in a 1000 µl pipette tip (cut to an appropriate size for larger aggregates) and ejected on top of the Alvetex® membrane. This was repeated 2-3 times per 6-well insert in order to seed 2-6 aggregates per membrane, ensuring that aggregates were not in close proximity to each other. 3D aggregate cultures were incubated in a humidified atmosphere with 5% CO_2 at 37^{o}C for up to 32 days with 50% media changes every 3 - 4 days.

2.5 Histology

2.5.1 Paraffin Embedding of Aggregate Suspension Cultures

Aggregates in suspension were collected and passed through a 100 µm filter in order to remove any single cells before being washed back into a 15 ml falcon tube and washed three times in D-PBS, allowing aggregates to settle to the bottom of the tube between each step. Aggregates were fixed at room temperature in 4% paraformaldehyde for 30 minutes and then washed three times in D-PBS. Samples were stored in D-PBS in 15 ml Falcon tubes at 4^{o}C until ready for further processing.

D-PBS was removed and samples dehydrated at room temperature through 30% ethanol and then 50% ethanol for 10 minutes each, allowing aggregates to settle between each step. Aggregates were stained with 2 *ml* 0.05% crystal violet in 70% ethanol for 10 minutes in order to aid sectioning. Samples were then dehydrated through 80%, 90% 90% and 100% ethanol for 10 minutes each, being careful to ensure aggregates remained at the bottom of the Falcon tube.

100% ethanol was removed and aggregates resuspended in 2-3 ml Histoclear for 10 minutes at room temperature. The same amount of liquid wax at 60^{o}C was added to the Falcon tubes to achieve 50:50 wax:histoclear and incubated for 30 minutes at 60^{o}C. 50:50 wax:histoclear was aspirated using a prewarmed Pasteur pippette and replaced with 2-3 ml of liquid wax at 60^{o}C and incubated for 30 minutes. Liquid wax was replaced for a second 30 minute incubation at 60^{o}C.

Samples were set into wax blocks using dispomoulds (Cell path) and allowed to set overnight before sectioning at 6 µm using a Leica RM2125RT microtome and mounted onto Superfrost microscope slides (Fisher).

2.5.2 Paraffin Embedding of Alvetex® 3D Aggregate Cultures

Alvetex® 3D polystyrene scaffold membranes were unclipped from their inserts and placed into 2-3 ml D-PBS in fresh 6-well culture plates. D-PBS was aspirated and membranes were washed again in 2-3 ml D-PBS. D-PBS was replaced with 2-3 ml 4% paraformaldehyde and samples were fixed overnight for 16 hours at 4^{o}C. Fixative was removed and replaced with 2-3 ml D-PBS and this was repeated for a total of three PBS washes. Samples were stored at 4^{o}C in D-PBS until ready for further processing.

D-PBS was removed and samples dehydrated at 4^{o}C with 2-3 ml 30% ethanol and then 50% ethanol for 30 minutes each. Aggregates were stained with 2-3 ml 0.05% crystal

violet in 70% ethanol for 10 minutes at 4^{o}C in order to aid sectioning. Samples were then dehydrated through 80%, 90%, 95% and 100% ethanol for 10 minutes each at 4^{o}C.

Alvetex® inserts were removed from 100 % ethanol, cut in half and transferred into glass vials containing 15 ml Histoclear and incubated for 15 minutes at room temperature. The same amount of liquid wax at 60^{o}C was added to the glass vials to achieve 50:50 wax:histoclear and incubated for 30 minutes at 60^{o}C. 50:50 wax:histoclear was poured away and replaced with 30 ml of liquid wax at 60^{o}C and incubated for 60 minutes.

Samples were set into wax blocks using dispomoulds and allowed to set overnight before sectioning at 8 µm using a Leica RM2125RT microtome and mounted onto Superfrost microscope slides.

2.5.3 Haematoxylin and Eosin Staining

Slides were deparaffinised in Histoclear for 5 minutes before being rehydrated in 100% ethanol for 2 minutes, 95% ethanol for 1 minute, 70% ethanol for 1 minute and deionised water for 1 minute. Slides were stained in Mayer's Haematoxylin for 5 minutes, then rinsed for 30 seconds in deionised water and nuclei were blued in alkaline ethanol for 30 seconds. Slides were dehydrated through 70% ethanol for 1 minute and then 95% ethanol for 1 minute before staining in 0.002% eosin dissolved in 95% ethanol for 1 minute. Slides were rinsed in 95% ethanol for 10 seconds, followed by another rinse in 95% ethanol for 15 seconds and then dehydrated through 100% ethanol for 15 seconds and then 100% ethanol for 30 seconds. Slides were cleared using two incubations in Histoclear for 3 minutes each. Slides were stored in Histoclear before being mounted using DPX (Fisher) and glass coverslips (Fisher). Bright-field images were taken using a Leica ICC50HD microscope.

2.5.4 Masson's Trichrome Staining

Slides were deparaffinised in Histoclear for 5 minutes before being rehydrated in 100% ethanol for 2 minutes, 95% ethanol for 1 minute, 70% ethanol for 1 minute and deionised water for 1 minute. Slides were stained in Weigert's iron Haematoxylin for 10 minutes and then rinsed under running tap water for 10 minutes before being briefly rinsed in deionised water. Slides were stained using Biebrich scarlet for 15 minutes and then rinsed in distilled water. Slides were differentiated in phosphomolybdic/phosphotungstic acid for 15 minutes and then transferred directly to aniline blue stain for 7 minutes. Slides were rinsed in distilled water and then differentiated in 1% acetic acid for 3 minutes before being rinsed in distilled water. Slides were quickly dehyrdated through 100% ethanol and 95% ethanol for 10 seconds each to avoid losing Biebrich scarlet stain. Slides were cleared using two incubations in Histoclear for 3 minutes each. Slides were stored in Histoclear before being mounted using DPX and glass coverslips. Bright-field images were taken using a Leica ICC50HD microscope.

2.5.5 Alizarin Red Staining

Alizarin Red solution was prepared by dissolving Alizarin Red S powder (Sigma) in 100 ml deionised water and adjusting the pH to 4.1 -4.3 with 10% ammonium hydroxide.

Slides were deparaffinised in Histoclear for 5 minutes before being rehydrated in 100% ethanol for 2 minutes, 95% ethanol for 1 minute, 70% ethanol for 1 minute and deionised water for 1 minute. Slides were stained in Alizarin Red solution for 2 minutes and excess dye was shaken off before blotting slides dry. Sections were dehydrated by dipping in acetone for 20 dips, followed by dipping in 50:50 acetone:Histoclear for 20 dips. Slides were cleared using two incubations in Histoclear for 3 minutes each. Slides were stored in Histoclear before being mounted using DPX and glass coverslips. Bright-field images were taken using a Leica ICC50HD microscope.

2.5.6 Immunohistochemistry

Slides were deparaffinised in Histoclear for 10 minutes before being rehydrated in 100% ethanol for 2 minutes, 95% ethanol for 1 minute, 70% ethanol for 1 minute and deionised water for 1 minute. Heat-mediated antigen retrieval was carried out on slides submerged in citrate buffer (pH 6.0) that were microwaved for 2 minutes on full power followed by 1 minute rest with the microwave door open. This step was repeated twice for a total of 3 x 2 minutes microwave heating. Slides submerged in citrate buffer were allowed to cool for 20 minutes at room temperature. Slides were incubated for 1 hour on a rocker at 50 rpm in block/permeabilisation buffer containing 0.4% triton X-100 (Fisher) and 20% normal goat serum (Sigma) in PBS. A hydrophobic pen (Liquid blocker) was used to draw around samples on slides. Samples were incubated overnight at 4^{o}C with 50-200 µl of primary antibody diluted to an appropriate concentration in block/permeabilisation buffer.

Slides were washed three times in 300 µl PBS for 10 minutes each on a rocker at 50 rpm. Appropriate fluorescently-labelled secondary antibodies were diluted 1:1000 with 1:1000 Hoechst 33342 (Molecular probes) in PBS containing 0.1% Tween-20 (Sigma) and incubation was carried out for 1 hour in the dark at room temperature. Slides were washed three times in 300 µl PBS for 10 minutes each on a rocker at 50 rpm in the dark. Slides were mounted with a small amount of VECTASHIELD®antifade mounting medium (Vector laboratories) and a glass coverslip. Coverslips were sealed with a generous amount of nail varnish and allowed to set at room temperature for 1-2 hours before storing slides in the dark at 4^{o}C. Slides were imaged within 1 week of staining using one of the following epifluorescent microscopes (Leica DMI3000B, Zeiss Axiovert 40, Zeiss Axioskop 40), or one of the following laser-scanning confocal microscopes (Zeiss 510 CLSM, Zeiss 880 CLSM, Leica SP5 CLSM).

Table 2: Primary and secondary antibodies used in immunohistochemistry.

Antibody	Code	Manufacturer	Species and Isotype	Dilution
TUJ1	PRB-435P	Covance	Rabbit polyclonal IgG	1:600
anti-E-cadherin	ab76055	Abcam	Mouse monoclonal IgG	1:250
anti-Nestin	ab22035	Abcam	Mouse monoclonal IgG	1:100
anti-CK8	ab9023	Abcam	Mouse monoclonal IgG	1:250
anti-GATA4	ab84593	Abcam	Rabbit polyclonal IgG	1:50
anti-α-SMA	ab5694	Abcam	Rabbit polyclonal IgG	1:100
anti-col-IV	ab6586	Abcam	Rabbit polyclonal IgG	1:500
anti-Rabbit IgG AlexaFluor 488	ab150077	Abcam	Goat polyclonal IgG	1:1000
anti-Mouse IgG AlexaFluor 488	ab150113	Abcam	Goat polyclonal IgG	1:1000

2.6 Flow Cytometry

TERA2.cl.SP12 cells were grown to 90% confluency in a T75 flask and a single cell suspension was generated. Cultures were washed using 5 ml D-PBS and then incubated with 3 ml trypsin/EDTA solution at 37^{o}C for 3 minutes. Trypsin was inactivated using 7 ml prewarmed culture media and cells were pipetted up and down several times before being placed into a 15 ml Falcon tube. Cells were centrifuged at 1000 rpm for 3 minutes and supernatant aspirated. The pellet was resuspended in PBS and centrifuged again at 1000 rpm for 3 minutes. The PBS wash step was repeated for a total of 2 washes. Cells were resuspended in 0.1% Bovine Serum Albumin (BSA, Sigma) in PBS and cell numbers were counted using trypan blue viablity assay and a haemocytometer.

2x10^5 cells in 0.1% BSA were added to each well to be used of a U-bottomed 96-well plate (Greiner Bio-one). Three wells were used for each primary antibody with one extra well for the isotype control antibody anti-P3X. Plates were centrifuged at 1000 rpm at 4^{o}C for 3 minutes and supernatant removed by upturning the plate in one swift motion. Pellets were resuspended using 50 µl of the appropriate primary antibody diluted in 0.1% BSA solution and incubated on ice for 60 minutes. 100 µl of 0.1% BSA solution was added to each well to remove excess unbound antibody and the plate was centrifuged at 1000 rpm at 4^{o}C for 3 minutes. Supernatant was removed pellets were resuspended in 180 µl of 0.1% BSA solution. Plates were centrifuged at 1000 rpm at 4^{o}C for 3 minutes and the wash step was repeated for a total of 2 washes.

Plates were centrifuged at 1000 rpm and 4^{o}C for 3 minutes and supernatant removed. Cell pellets were resuspended in secondary antibody diluted to the appropriate concentration in 0.1% BSA and incubated in the dark on ice for 60 minutes. 100 µl of 0.1% BSA solution was added to each well to remove excess unbound antibody and the plate was centrifuged at 1000 rpm and 4^{o}C for 3 minutes. Supernatant was removed and pellets resuspended in 180 μl 0.1% BSA solution. Plates were centrifuged at 1000 rpm and 4^{o}C for 3 minutes and the previous wash step repeated for a total of 2 washes.

Plates were centrifuged at 1000 rpm and 4^{o}C for 3 minutes and supernatant removed. Pellets were resuspended in 200 µl 0.1% BSA for performing flow cytometry. Flow cytometry was performed using Guava Technologies EasyCyte Plus flow cytometer according to the manufacturer's instructions.

Table 3: Primary and secondary antibodies used in flow cytometry.

Antibody	**Code**	**Manufacturer**	**Species and Isotype**	**Dilution**
anti-P3X	n/a	Tonge et al. (2010)	Mouse monoclonal IgM	1:10
anti-SSEA-3	MC-631	DSHB	Mouse monoclonal IgM	1:5
anti-TRA-1-60	MAB4360	Merck Millipore	Mouse monoclonal IgM	1:50
anti-A2B5	MAB1416	R&D Systems	Mouse monoclonal IgM	1:10
anti-Mouse IgM FITC	F9259	Sigma-Aldrich	Goat polyclonal IgG	1:100

2.7 Immunocytochemistry

Cells grown in 6- or 12-well tissue culture plates were washed twice in PBS and then fixed for 15 minutes at room temperature using 4% paraformaldehyde solution in PBS. All subsequent steps were performed on ice and on a rocker at 50 rpm. Cells were permeabilised for 15 minutes using 0.01% Triton X-100 in PBS and then incubated in blocking buffer for 30 minutes containing 10% normal goat serum and 0.01% Tween-20 in PBS. Primary antibodies diluted to the appropriate concentration in blocking buffer were added to wells (200 µl per 12-well or 1 ml per 6-well) and incubated for 60 minutes. Cells were washed in 1 ml blocking buffer and this wash step was repeated twice for a total of three washes. Wells were incubated with the same amount of appropriate secondary antibody diluted in blocking buffer with 1:1000 Hoechst 33342 and plates were incubated in the dark for 60 minutes. Wells were washed three times in blocking buffer and then topped up with PBS and sealed with parafilm before imaging.

Table 4: Primary and secondary antibodies used in immunocytochemistry.

Antibody	Code	Manufacturer	Species and Isotype	Dilution
TUJ1	PRB-435P	Covance	Rabbit polyclonal IgG	1:600
anti-CK8	ab9023	Abcam	Mouse monoclonal IgG	1:250
anti-SOX-2	ab97959	Abcam	Rabbit polyclonal IgG	1:1000
anti-SSEA-1	ab16285	Abcam	Mouse monoclonal IgM	1:100
anti-Oct4	ab19857	Abcam	Rabbit polyclonal IgG	1:200
anti-Nanog	ab80892	Abcam	Rabbit polyclonal IgG	1:150
anti-Rabbit IgG Alexa Fluor 488	ab150077	Abcam	Goat polyclonal IgG	1:600
anti-Mouse IgG Alexa Fluor 488	ab150113	Abcam	Goat polyclonal IgG	1:600
anti-Mouse IgM FITC	F9259	Sigma-Aldrich	Goat polyclonal IgG	1:100

2.8 Terminal deoxynucleotidyl transferase dUTP nick end labeling (TUNEL)

DeadEnd™Fluorometric TUNEL System (Promega) was used according to the manufacturer's instructions.

Samples were deparaffinised with two incubations in Histoclear for 5 minutes each and then washed in 100% ethanol for 5 minutes. Samples were rehydrated in 100%, 95%, 85%, 70%, and 50% ethanol for 3 minutes each. Samples were washed in 0.85% NaCl for 5 minutes and then washed in PBS for 5 minutes. Tissue sections were fixed in 4% paraformaldehyde in PBS for 15 minutes at room temperature, and then washed twice in PBS for 5 minutes each. Liquid was removed and the slides were placed onto a flat surface.

100 µl Proteinase K solution [20 $\mu g ml^{-1}$] was added to each slide to cover the sample and then incubated for 10 minutes at room temperature. Samples were washed in PBS for 5 minutes, then fixed in 4% paraformaldehyde solution in PBS for 5 minutes at room temperature, and then washed again in PBS for 5 minutes.

Excess liquid was removed and samples were then incubated with 100 µl equilibration buffer for 5 minutes at room temperature. Samples were incubated in a humid chamber

for 60 minutes at 37^{o}C with 50 µl rTdT incubation buffer containing 5 µl nucleotide mix and 1 µl rTdT enzyme in 45 µl equilibration buffer. Samples were prevented from drying out by placing a small piece of parafilm on top of each slide. Slides were kept in the dark after completion of this step.

Tailing reactions were terminated by immersing slides in 2X SSC buffer for 15 minutes at room temperature. Samples were washed three times in PBS for 5 minutes each. Slides were mounted onto glass coverslips using a small amount of VECTASHIELD®hardset antifade mounting medium with DAPI (Vector Laboratories).

Slides were stored in the dark at 4^{o}C and imaging of samples was performed the following day using a Zeiss 510 CLSM.

3 Results

3.1 Human Embryonal Carcinoma Cell Line TERA2.cl.SP12

2D cultures of TERA2.cl.SP12 hEC cells were maintained according to pre-established protocols (Przyborski, 2001). Flow cytometric analysis of surface antigen expression was performed in order to characterise hEC cells maintained at high confluency in 2D. Flow cytometry revealed that the glycolipid surface antigens SSEA-3 and TRA-1-60 that are associated with pluripotency in hESCs were expressed on the majority of TERA2.cl.SP12 cells (90.1% and 98.1% respectively) (**Figure 5**) (Martí et al., 2013). The early neural lineage marker A2B5 was not found to be expressed in TERA2.cl.SP12 cells and showed similar expression levels to the isotype control antibody P3x (Chua et al., 2009). Flow cytometric analysis therefore indicated that TERA2.cl.SP12 cells cultured at high confluency in 2D were maintained as undifferentiated stem cells with no evidence of spontaneous neural differentiation.

Immunocytochemistry was undertaken in order to characterise TERA2.cl.SP12 cells cultured at different cell densities in 2D. Cells were seeded at high density ($1.5x10^4$ cells per cm^2), medium density ($1.0x10^4$ cells per cm^2), or low density ($5x10^3$ cells per cm^2) and cultured for 4 days and expression of pluripotency marker Oct4 and differentiated cell markers TUJ1 and CK8 were analysed. TUJ1 antibodies react with β-III-tubulin that is predominantly expressed in mature neurons of the central nervous system but also testis and highly proliferative cancer cells (De Gendt et al., 2011; Katsetos et al., 2003; Ferrandina et al., 2006). CK8 antibodies react with cytokeratin-8 intermediate filament protein that is commonly expressed in cultured epithelial cells and all simple epithelial tissues (Magin et al., 1986).

Expression of Oct4 (**Figure 6**), TUJ1 (**Figure 7**), and CK8 (**Figure 8**) was detected in TERA2.cl.SP12 cells cultured at high, medium, and low density. Only hEC cells cultured at high and medium density exhibited characteristic pluripotent stem cell morphology, however, including small size, rounded morphology, and high nucleus:cytoplasm ratio. hEC cells cultured at low density were considerably larger and had a distinctly lower nucleus:cytoplasm ratio. Moreover, CK8 and TUJ1 staining formed filamentous structures within hEC cells cultured at low density, indicating that they had gained a more differentiated phenotype compared to cells cultured at high density where diffuse TUJ1 and CK8 staining was seen.

Taken together these data indicate that TERA2.cl.SP12 cells were maintained in an undifferentiated state when cultured at high density in 2D culture. TERA2.cl.SP12 hEC cells were therefore chosen as a useful and an inexpensive research tool for optimisation of the technique for long-term maintenance of stem cell aggregates using Alvetex® 3D scaffold membranes.

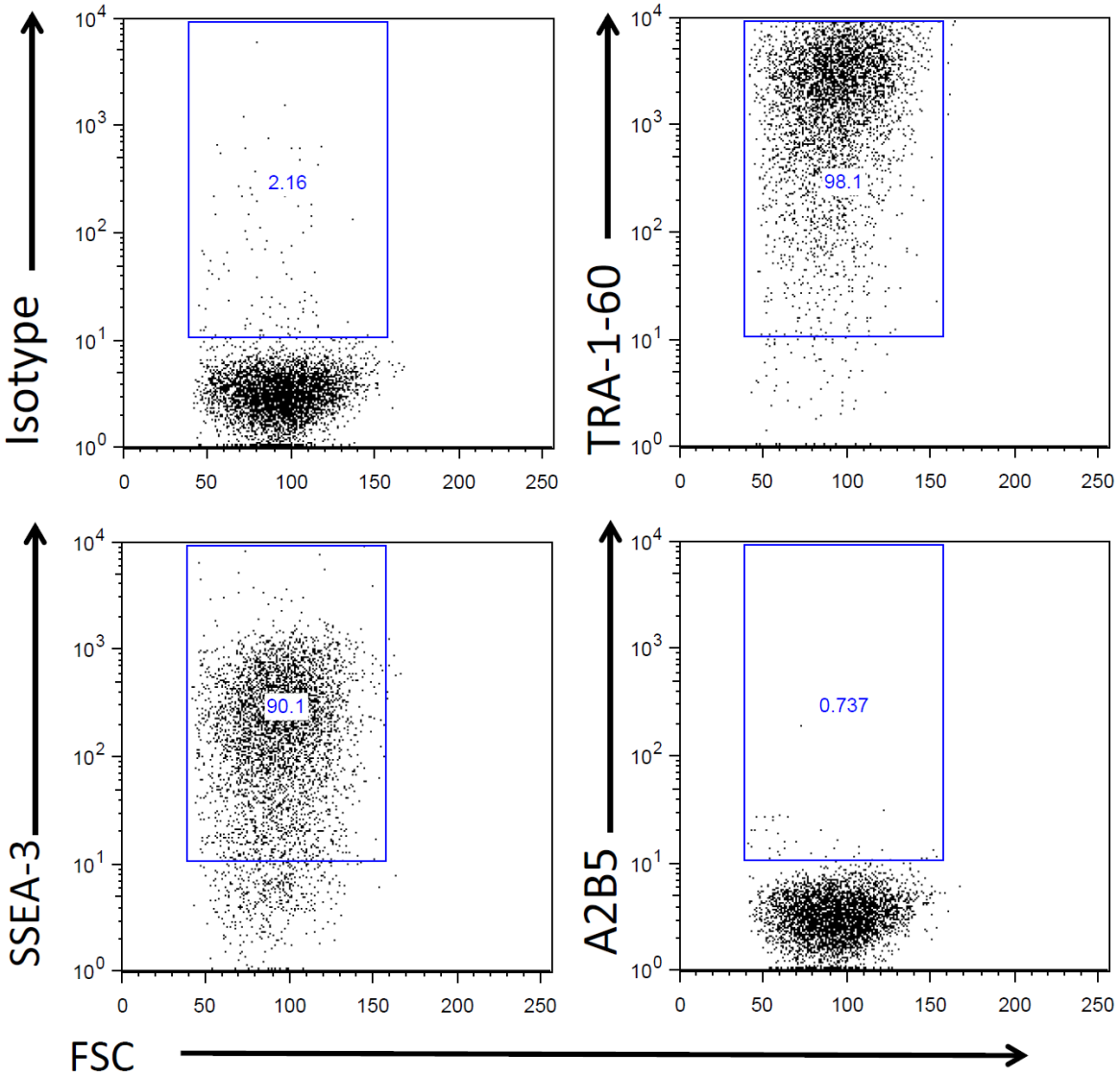

Figure 5: Flow cytometric analysis of TERA2.cl.SP12 cells cultured in 2D.

Surface antigens were detected using flow cytometry and dot plots of the data are presented with forward scatter (FSC) on the x-axis and FITC fluorescence detected for each antibody on the y-axis. Pluripotency marker TRA-1-60 expression was detected in 98.1% of cells and pluripotency marker SSEA-3 expression was detected in 90.1% of cells. A2B5 expression was not detected on TERA2.cl.SP12 cells as FITC fluorescence was at a similar level to the isotype control antibody anti-P3x.

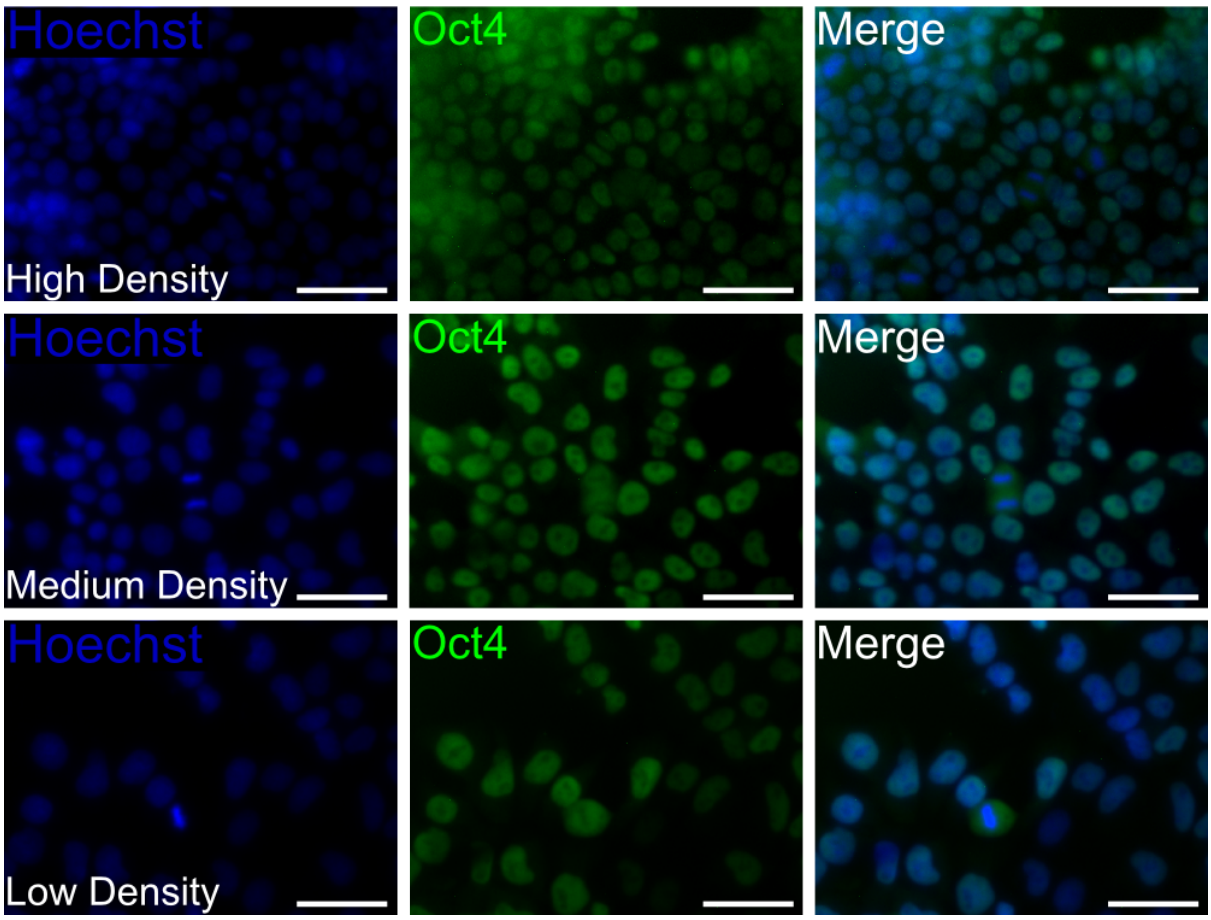

Figure 6: Oct4 expression in TERA2.cl.SP12 cells.

Immunocytochemical detection of Oct4 expression in TERA2.cl.SP12 cells seeded at high density ($1.5x10^4$ cells per cm^2), medium density ($1.0x10^4$ cells per cm^2), and low density ($5x10^3$ cells per cm^2) and cultured for 4 days in 2D. Cells cultured at all three densities showed detectable Oct4 expression. Cells cultured at high density were smaller in size than cells cultured at medium or low density. All images were taken using a Zeiss Axiovert 200 inverted epifluorescent microscope with a 63x objective. Scale bars represent 50 µm.

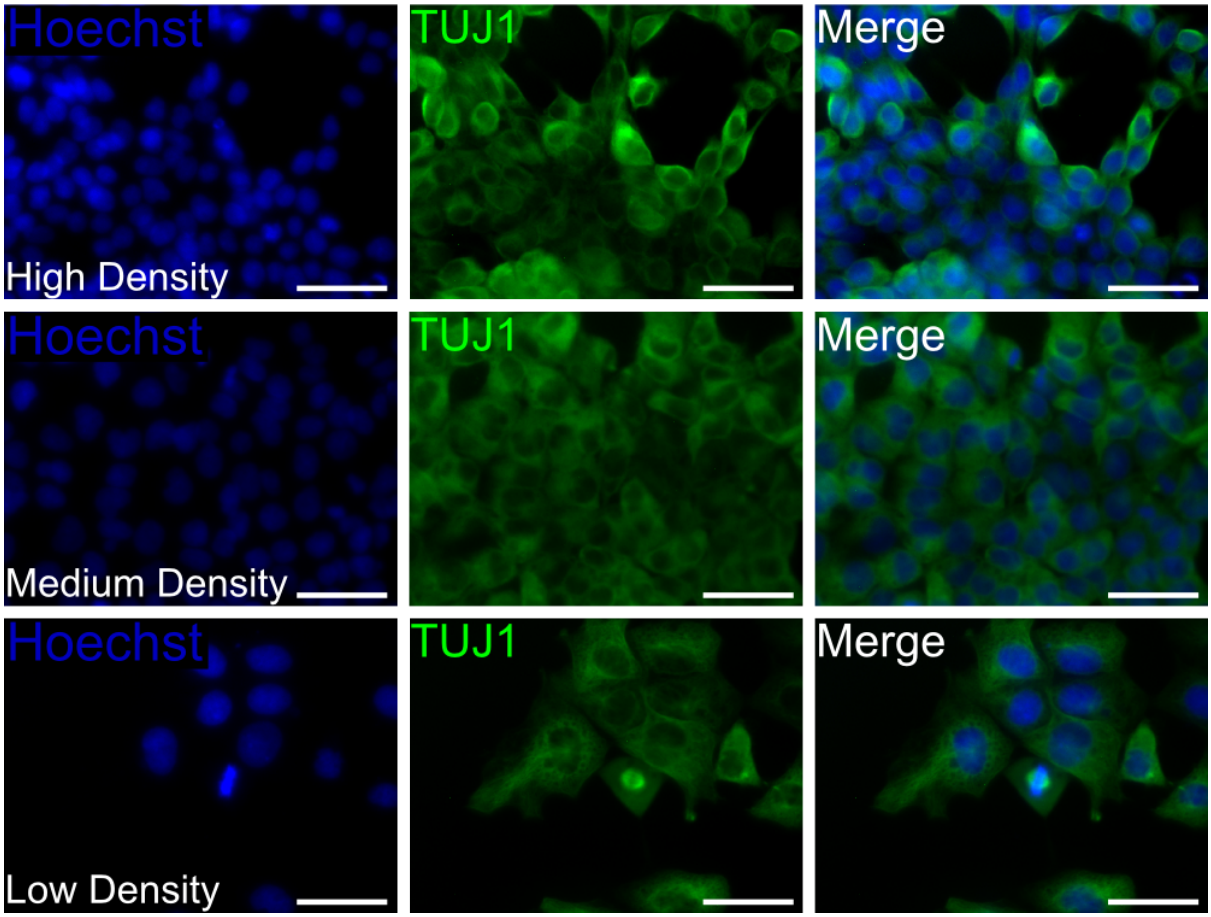

Figure 7: TUJ1 expression in TERA2.cl.SP12 cells.

Immunocytochemical detection of TUJ1 expression in TERA2.cl.SP12 cells seeded at high density ($1.5x10^4$ cells per cm^2), medium density ($1.0x10^4$ cells per cm^2), and low density ($5x10^3$ cells per cm^2) and cultured for 4 days in 2D. Cells cultured at high and medium density exhibited diffuse TUJ1 staining compared to filamentous staining seen in cells cultured at low density. All images were taken using a Zeiss Axiovert 200 inverted epifluorescent microscope with a 63x objective. Scale bars represent 50 µm.

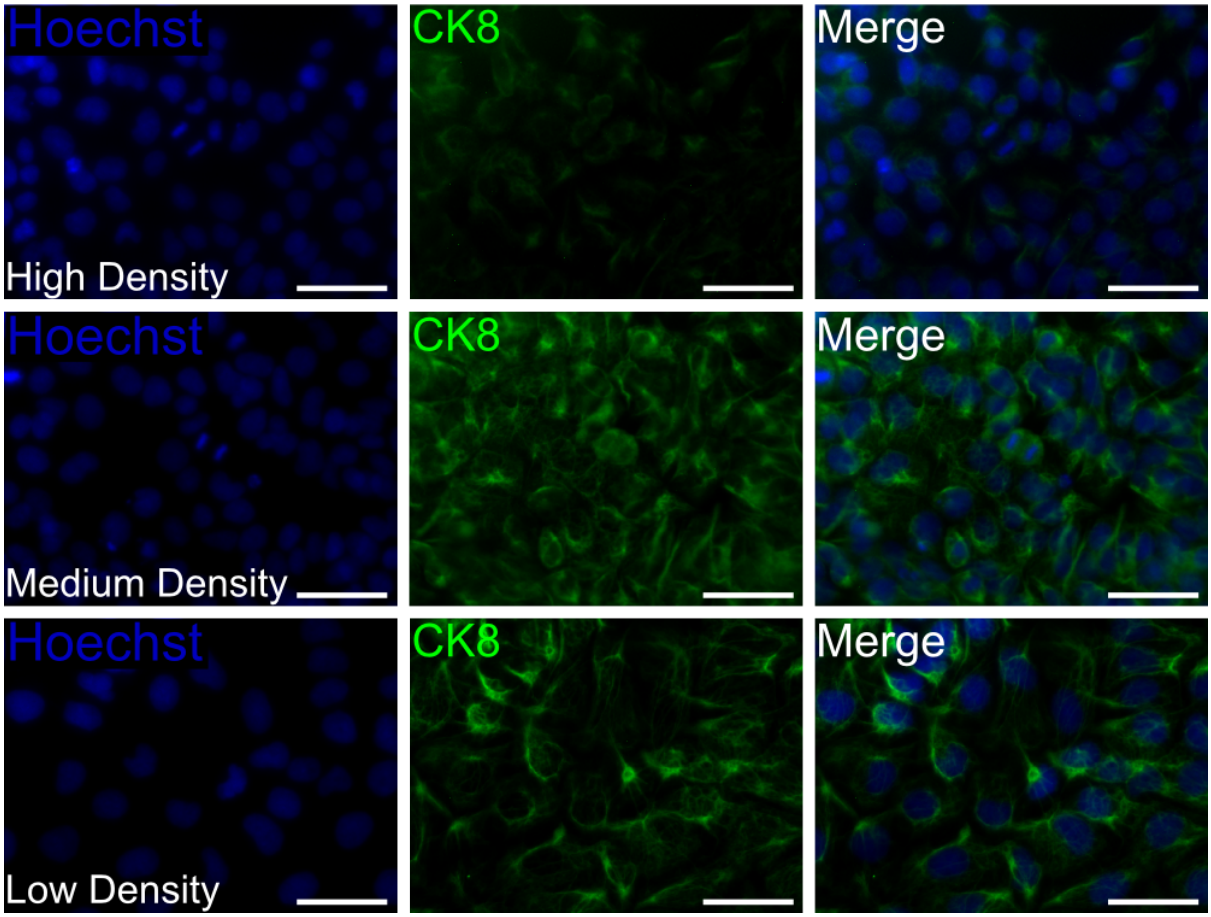

Figure 8: CK8 expression in TERA2.cl.SP12 cells.

Immunocytochemical detection of CK8 expression in TERA2.cl.SP12 cells seeded at high density ($1.5x10^4$ cells per cm^2), medium density ($1.0x10^4$ cells per cm^2), and low density ($5x10^3$ cells per cm^2) and cultured for 4 days in 2D. Cells cultured at low density exhibited filamentous CK8 staining compared to diffuse staining seen in cells cultured at high and medium density. All images were taken using a Zeiss Axiovert 200 inverted epifluorescent microscope with a 63x objective. Scale bars represent 50 µm.

3.2 TERA2.cl.SP12 Aggregates

TERA2.cl.SP12 hEC cells were cultured as a monolayer in 2D and aggregates were formed by allowing spontaneous aggregation of hEC suspension cultures to occur. Aggregates were maintained in suspension for 21 days and histological analysis was used to investigate the internal structure of hEC cell aggregates. Epithelial cavities containing polarised epithelial cells were visible in haematoxylin and eosin-stained paraffin transverse sections (arrows, **Figure 9**). Epithelial structures resembled neural rosettes that are typical of neuroepithelial development, suggesting that 3D culturing of TERA2.cl.SP12 cells as aggregates had induced spontaneous neural differentiation (Gotz and Huttner, 2005). Histological analysis also indicated that significant necrosis had occurred in TERA2.cl.SP12 aggregates after 21 days in suspension—evident as a central region of debris that contained small dark cell nuclei that were indicative of cell death (asterisks, **Figure 9**).

3.2.1 Maintenance of TERA2.cl.SP12 Aggregates using 3D Scaffolds

At the same time as maintaining TERA2.cl.SP12 cells for 21 days in suspension, after 14 days in suspension some aggregates were cultured for 7 days using Alvetex® 3D porous polystyrene scaffold membranes of three different pore sizes. TERA2.cl.SP12 aggregates cultured for 7 days using Alvetex® Scaffold (that has an average pore size of 40 µm) largely disintegrated and cells penetrated the full depth of the scaffold, approximately 200 µm (**Figure 10C**). Aggregates were also cultured using Alvetex® Strata (that has an average pore size of 20 µm) and, similarly, significant numbers of cells left the aggregate and migrated into the scaffold membrane below (**Figure 10B**). Alvetex® Polaris has the smallest average pore size of 3-4 µm, and when aggregates were cultured for 7 days on these membranes they were maintained intact with no penetration of cells into the membrane (**Figure 10A**).

Over 7 days culture, aggregates formed flattened tissue-discs and neuroepithelial differentiation took place in all tissue-discs examined (arrows, **Figure 10**). Unlike aggregates cultured in suspension, a necrotic core was not visible at the centre of any tissue-discs examined cultured using Alvetex®. For all further experiments Alvetex® Polaris was chosen due to being able to support differentiation within hEC aggregates while minimising cell loss.

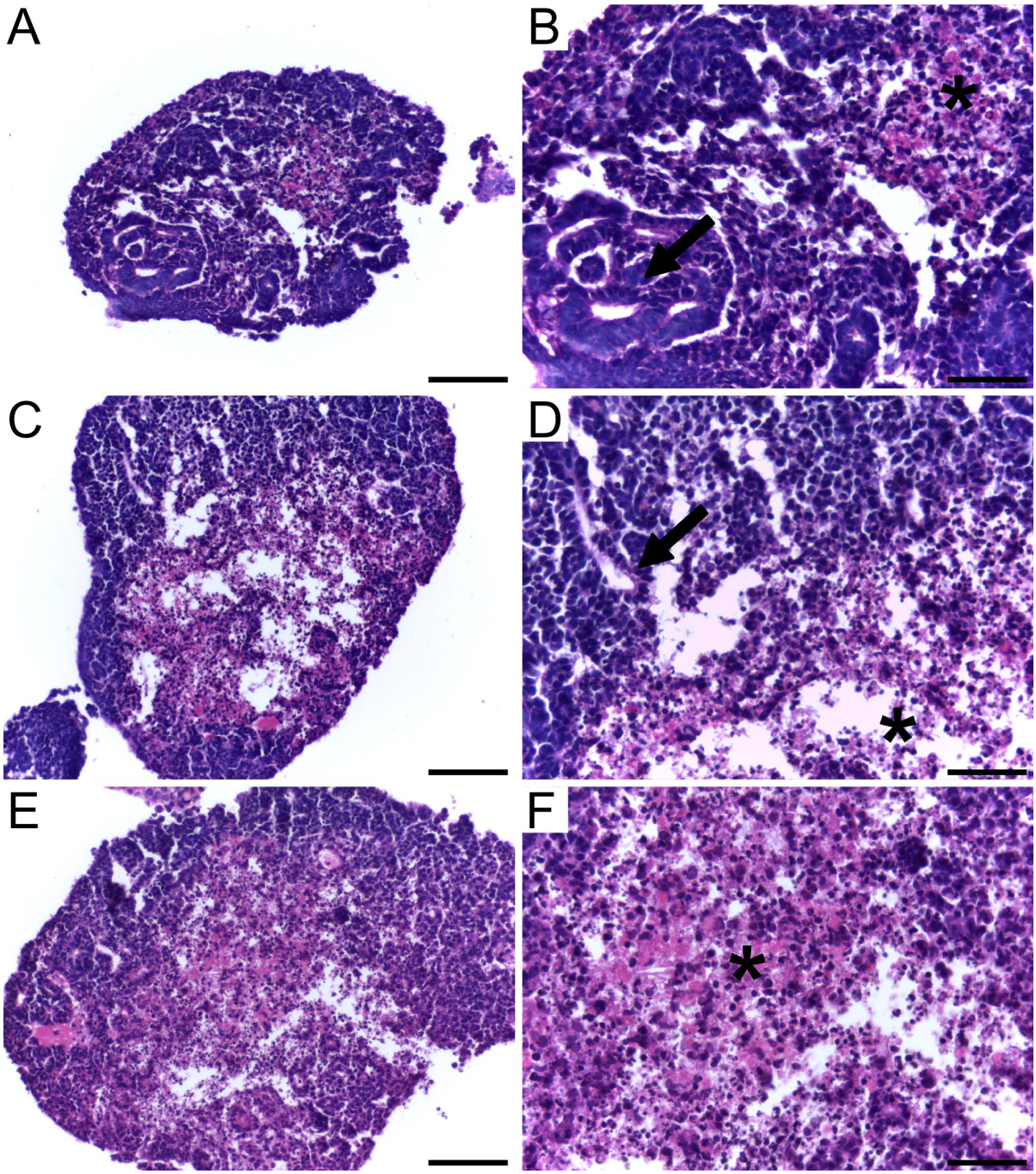

Figure 9: Histological analysis of TERA2.cl.SP12 aggregates cultured in suspension.

TERA2.cl.SP12 aggregates were maintained in suspension for 21 days and 5 µm paraffin transverse sections were generated and stained using haematoxylin and eosin to reveal internal structures. Small epithelial cavities that resembled neural rosettes were visible in many aggregates (arrows) as well as areas of apparent necrosis (asterisks) with small black cell nuclei visible. Scale bars represent 100 µm (A, C, and E) and 50 µm (B, D, and F). Bright-field images were taken using a Leica ICC50HD microscope and a 20x (A, C, and E) or 40x objective (B, D, and F).

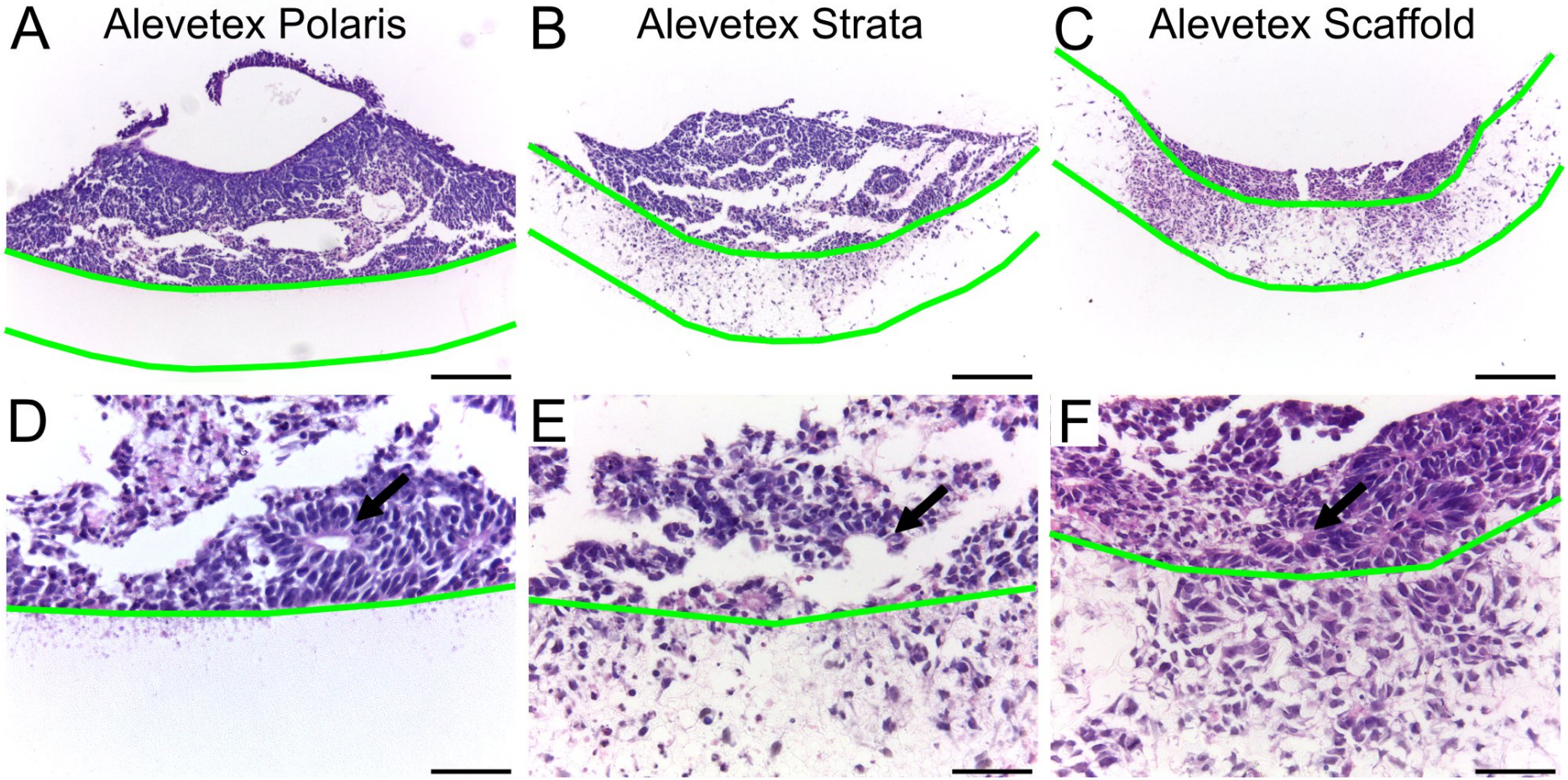

Figure 10: Histological analysis of TERA2.cl.SP12 aggregates cultured using Alvetex®3D scaffold membranes.

TERA2.cl.SP12 aggregates were maintained in suspension for 14 days followed by 7 days growth using Alvetex®3D scaffold membranes with three different pore sizes, and 8 µm paraffin transverse sections of aggregates grown in 3D were stained using haematoxylin and eosin. Aggregates maintained using Alvetex®Strata and Scaffold membranes with an average pore size of 20 µm and 40 µm, respectively, exhibited cell loss from aggregates as cells migrated through the membrane (B, and C). Aggregates cultured using Alvetex®Polaris, with a pore size of 4 µm, however, were intact after 7 days culture. Similar to aggregates cultured in suspension, neural rosette-like structures were visible in many aggregates (black arrows) but unlike aggregates cultured in suspension for 21 days, large areas of necrosis at the centre of aggregates were not seen. Green lines have been drawn to visualise the approximate boundary of the Alvetex®membrane. Scale bars represent 200 µm (A-C) and 50 µm (D-F). Bright-field images were taken using a Leica ICC50HD microscope and a 10x (A-C) or 40x objective (D-F).

3.2.2 Analysis of Apoptosis

The terminal deoxynucleotidyl transferase dUTP nick end labeling (TUNEL) assay was performed in order to identify apoptotic cells in TERA2.cl.SP12 aggregates. Aggregates cultured in suspension for 21 days exhibited large numbers of apoptotic cells at their centre (**Figure 11**, A-C). Aggregates cultured using Alvetex®Polaris on the other hand, contained fewer apoptotic cells that were sparsely distributed throughout the aggregate (**Figure 11**, D-F).

ImageJ was used to quantify the fluorescence intensity of three aggregates maintained in suspension for 21 days and of one aggregate maintained using Alvetex®Polaris (examined in two separate locations). Each aggregate was traced around and raw fluorescence intensity (integrated density) of the green channel was divided by the area of each aggregate to generate corrected fluorescence values for each aggregate. Mean fluorescence intensity of aggregates maintained in suspension was 7.9 (arbitrary units) and the mean fluorescence intensity of one aggregate maintained using Alvetex®Polaris was 2.2 (arbitrary units) (**Figure 12**). The difference in mean fluorescence between aggregates cultured in suspension and using Alvetex®Polaris was found to be not statistically significant (unpaired t-test; $P = 0.1354$). However, the robustness of this statistical test is limited due to the very small number of aggregates that could be examined. Increasing the number of aggregates examined will be necessary in order to be more confident in determining the differences between aggregate suspension cultures and 3D tissue-disc cultures in terms of cell viability.

Nonetheless, histological evidence also indicated that some aggregates cultured in suspension developed an hypoxic core (**Figure 10**). Moreover, TUNEL staining reveals that the hypoxic core that developed within some aggregates contained large numbers of apoptotic cells (**Figure 11**). Possibly due to the limited number of aggregates examined, the effect of 3D culturing aggregates as tissue-discs using Alvetex®Polaris on the number of apoptotic cells was found to be not statistically significant.

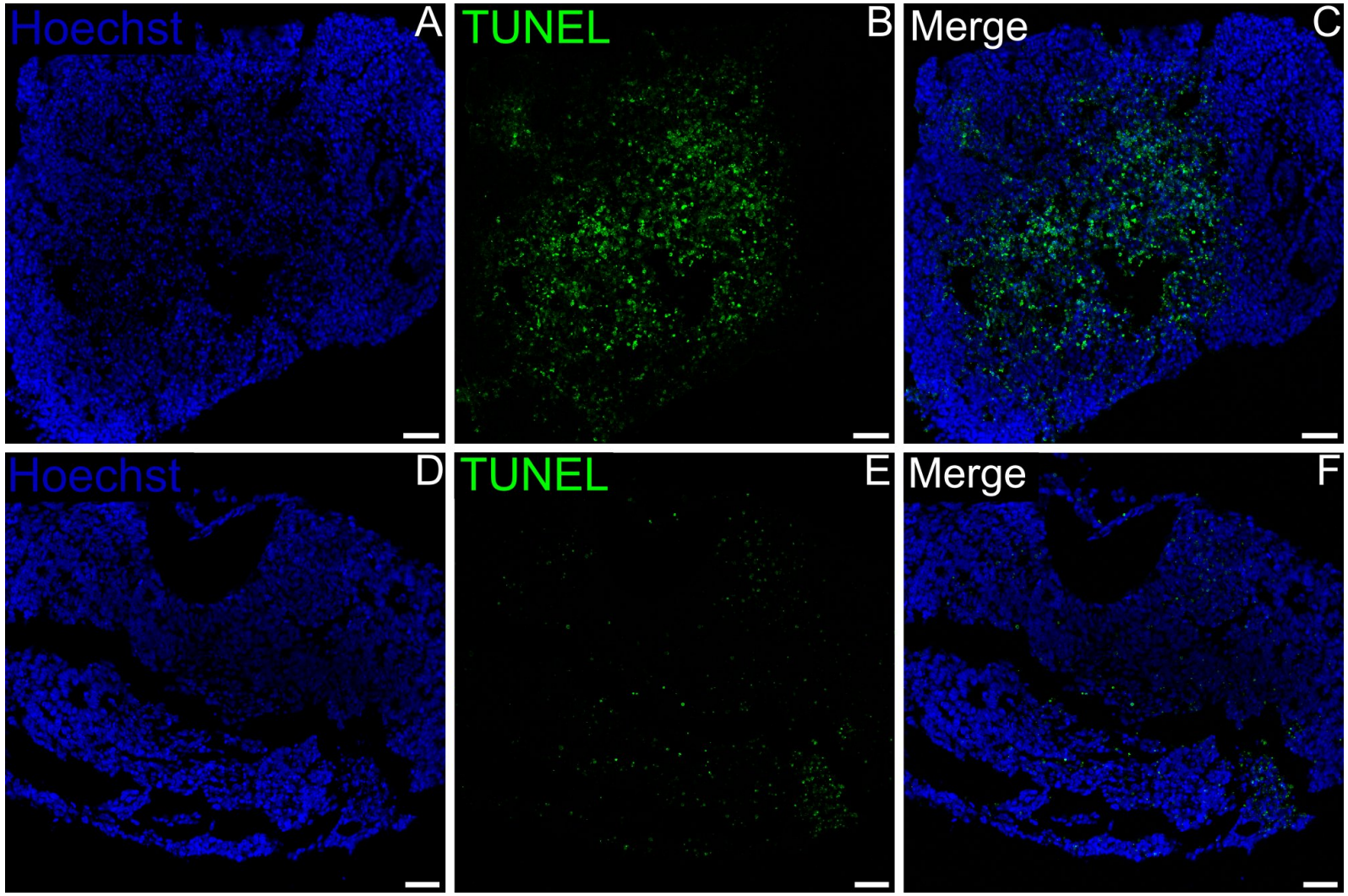

Figure 11: TUNEL stain comparing apoptosis in TERA2.cl.SP12 aggregates maintained in suspension and using Alvetex®

Fluorescence TUNEL staining of paraffin sections of TERA2.cl.SP12 aggregates maintained in suspension for 21 days (A-C) or in suspension for 14 days followed by 7 days growth using Alvetex®Polaris (D-F). A central core containing many apoptotic cells was seen in some aggregates maintained in suspension but was not present in the aggregate maintained in 3D using Alvetex®. Confocal images were taken using Zeiss 510 CLSM using a 20x objective. Scale bars represent 50 µm.

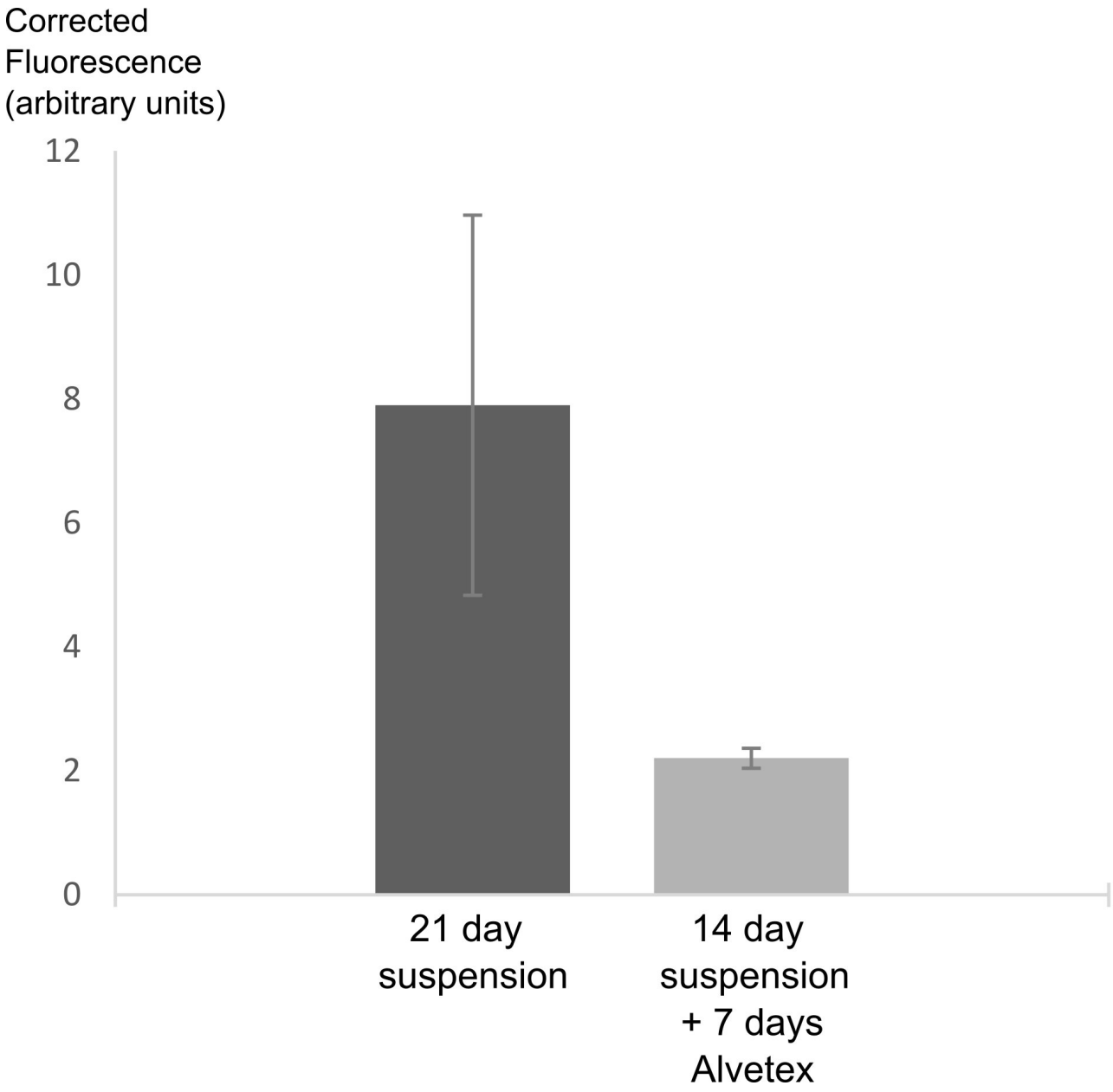

Figure 12: Quantification of fluorescent intensity of TUNEL staining in TERA2.cl.SP12 aggregates maintained in suspension and using Alvetex®

Confocal images of fluorescent TUNEL staining of paraffin sections of TERA2.cl.SP12 aggregates were taken using a Zeiss 510 CLSM. Images were loaded into ImageJ and each aggregate was traced around. The raw fluorescent intensity (integrated density) of the green channel was divided by the area of each aggregate to generate corrected fluorescence values for each aggregate. Three different 21 day suspension aggregates were analysed and one aggregate cultured for 14 days in suspension + 7 day Alvetex®Polaris was analysed in two separate locations. The mean values for suspension and 3D cultured aggregates were plotted with error bars for one standard deviation.

3.3 Manipulating Developmental Pathways to Study Aspects of Human Embryonic Development

Studying the role that developmental pathways play in human embryonic development is challenging due to the limited accessibility of human embryogenesis *in utero*. *In vitro* differentiation of hESC, hiPSC, and hEC lines allows aspects of human embryonic development to be studied. To this end, several morphogens including small molecules and recombinant proteins were used to manipulate developmental pathways in hEC aggregates in order to attempt to gain insight into the roles of developmental pathways in human embryonic development using 3D tissue-disc cultured aggregates.

3.3.1 Retinoid Pathway

TERA2.cl.SP12 cultures produce a mixture of terminally differentiated neurons and non-neural epithelial-like cells when exposed to ATRA in 2D cultures, and the purity of neural induction is increased in aggregate suspension cultures (Horrocks et al., 2003). In order to confirm the ability of aggregates cultured using Alvetex®Polaris to respond appropriately to developmental stimuli, the retinoid pathway was chosen due to its reproducible induction of neural differentiation in TERA2.cl.SP12 aggregates (Horrocks et al., 2003; Christie et al., 2008). TERA2.cl.SP12 cells were seeded into suspension and allowed to form aggregates over 24 hours before being treated with the synthetic retinoid and ATRA analogue, ec23 [0.01 µM] or DMSO (vehicle control) for 21 days in suspension. Aggregates cultured in suspension for 21 days were then cultured using Alvetex®Polaris membranes for a further 7 days. Histological analysis revealed that DMSO treated aggregates developed small neural rosette structures, while ec23 treated aggregates appeared more densely packed and neuroepithelial structures were not seen (**Figure 13**).

Immunostaining revealed high levels of TUJ1 expression within ec23-treated aggregates and extensive outgrowth of $TUJ1^+$ neurites into the Polaris membrane (arrows, **Figure 14**). In DMSO control samples, TUJ1 expression was detected although no neurites were found to have penetrated the Polaris membrane (data not shown). This indicates that hEC aggregates responded to retinoid stimulation by ec23 and agreed with previous findings that ec23 increases neurite outgrowth from TERA2.cl.SP12 aggregates cultured in 3D *in vitro* (Clarke et al., 2014).

These data demonstrate that stem cell aggregates cultured as tissue-discs for prolonged periods can be used to study the role of developmental pathways such as the retinoid pathway in human embryonic development *in vitro*.

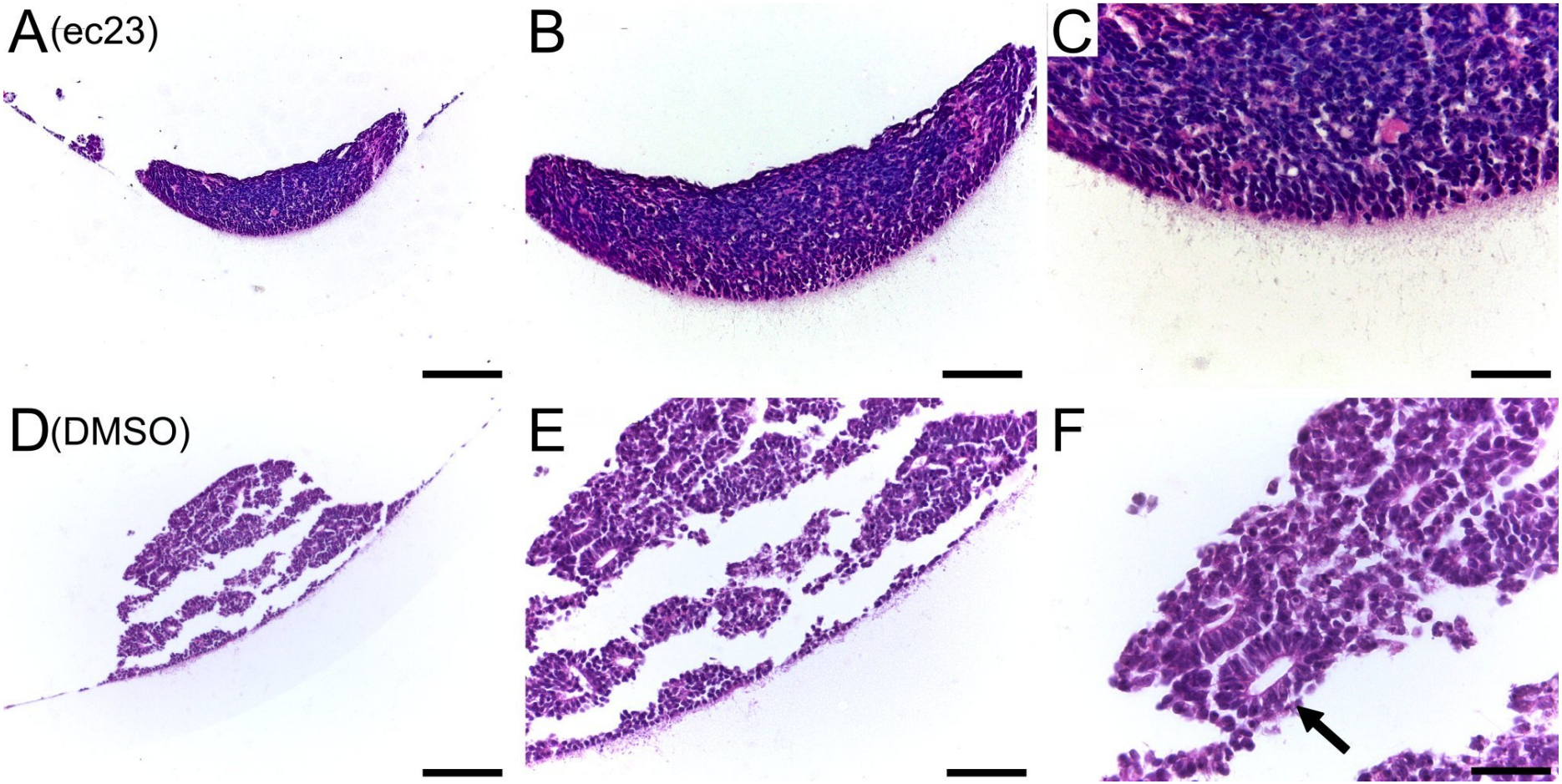

Figure 13: Histological analysis of ec23-treated TERA2.cl.SP12 aggregates.

TERA2.cl.SP12 aggregates were maintained in suspension for 21 days in the presence of ec23 [0.01 µM] or DMSO as a vehicle control followed by 7 days growth using Alvetex®Polaris. Haematoxylin and eosin staining of paraffin sections suggested that ec23 treatment induced densely packed aggregates and no neuroepithelial neural rosette structures were seen. DMSO control aggregates were shown to develop a more loosely packed internal structure with several neural rosettes visible (arrow in F). Scale bars represent 200 µm (A, and D), 100 µm (B, and E), and 50 µm (C, and F). Bright-field images were taken using a Leica ICC50HD microscope and a 10x (A, and D) or 20x (B, and E) or 40x objective (C, and F).

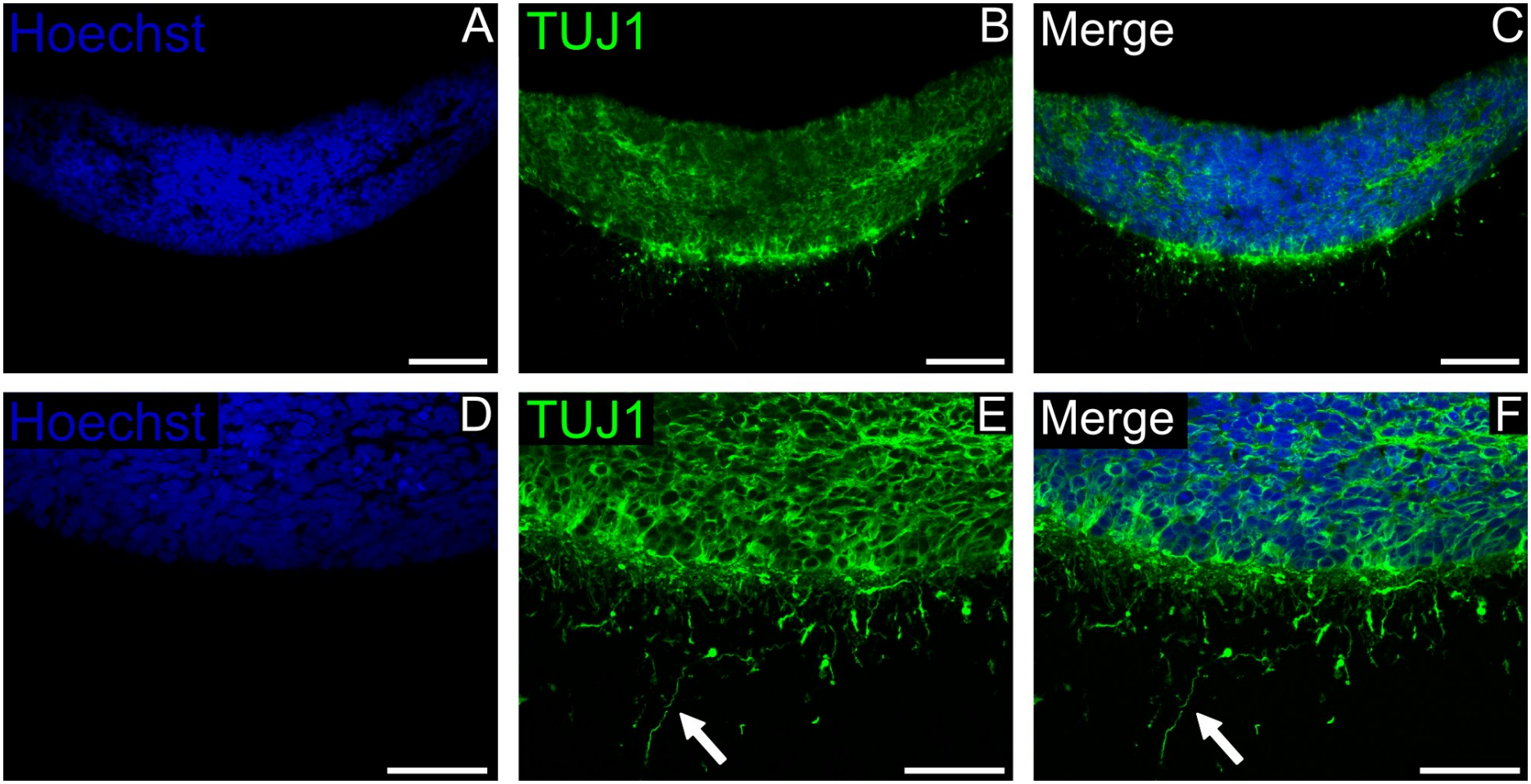

Figure 14: Immunohistochemical analysis of ec23-treated TERA2.cl.SP12 aggregates.

TERA2.cl.SP12 aggregates were maintained in suspension for 21 days in the presence of ec23 [0.01 µM] followed by 7 days growth using Alvetex®Polaris. TUJ1 was found to be highly expressed in ec23 aggregates and in neurites that could be seen penetrating the scaffold membrane (arrows). Scale bars represent 100 µm (A-C) and 50 µm (D-F). Images were taken using a Leica DMI3000B (A-C) and a 20x objective or using Leica SP5 CLSM (D-F).

3.3.2 Bone Morphogenetic Protein activation

Neural differentiation in hEC line TERA2.cl.SP12 in response to retinoid stimulation is relatively well-studied and highly reproducible in 2D, in aggregate suspension cultures, and in aggregates cultured as tissue-discs (Horrocks et al., 2003; Christie et al., 2008). It was also of interest to investigate non-neural differentiation in TERA2.cl.SP12 cells. The bone morphogenetic protein (BMP) pathway was chosen to be manipulated due to its ability to inhibit neural differentiation and promote epidermis formation during vertebrate embryonic ectoderm development (Wilson and Hemmati-Brivanlou, 1995). BMP2 was chosen as an inducer of hEC aggregates because previous work showed that it downregulated neural markers and upregulated epithelial markers in TERA2.cl.SP12 cells cultured as aggregates in suspension (Przyborski et al., 2004).

TERA2.cl.SP12 aggregates cultured for 7 days in suspension with BMP2 [50 ngml^{-1}] followed by 7 days culture using Alvetex®Strata or Polaris membranes responded to BMP2 stimulation and exhibited distinct morphological features compared to vehicle (acetic acid) control aggregates (**Figure 15**). Interestingly, histological analysis revealed heterogeneity in BMP2 treated aggregates, with distinct mesenchymal regions that contained fewer cells (asterisks, **Figure 15**), as well as more cell dense regions with an appearance more similar to vehicle control aggregates (arrows, **Figure 15**).

CK8 and TUJ1 immunostaining of aggregates treated with BMP2 for 7 days in suspension followed by growth using Alvetex®Polaris for 7 days revealed mutually exclusive expression of pan-epithelial marker CK8 in mesenchymal regions (asterisks, **Figure 16**), and TUJ1 expression in cell dense regions (arrows, **Figure 16**). CK8^{+};TUJ1^{-} mesenchymal regions were thought to represent non-neural cell types that were induced by BMP2 treatment because control aggregates never developed these CK8^{+} mesenchymal regions. TUJ1^{+};CK8^{-} cells that were visible after 7 days exposure to BMP2 may have represented groups of cells that had not yet responded to BMP2 treatment due to insufficient time for non-neural differentiation to have occurred. To examine this, hEC aggregates were maintained in suspension in the presence of BMP2 [50 ngml^{-1}] for 21 days.

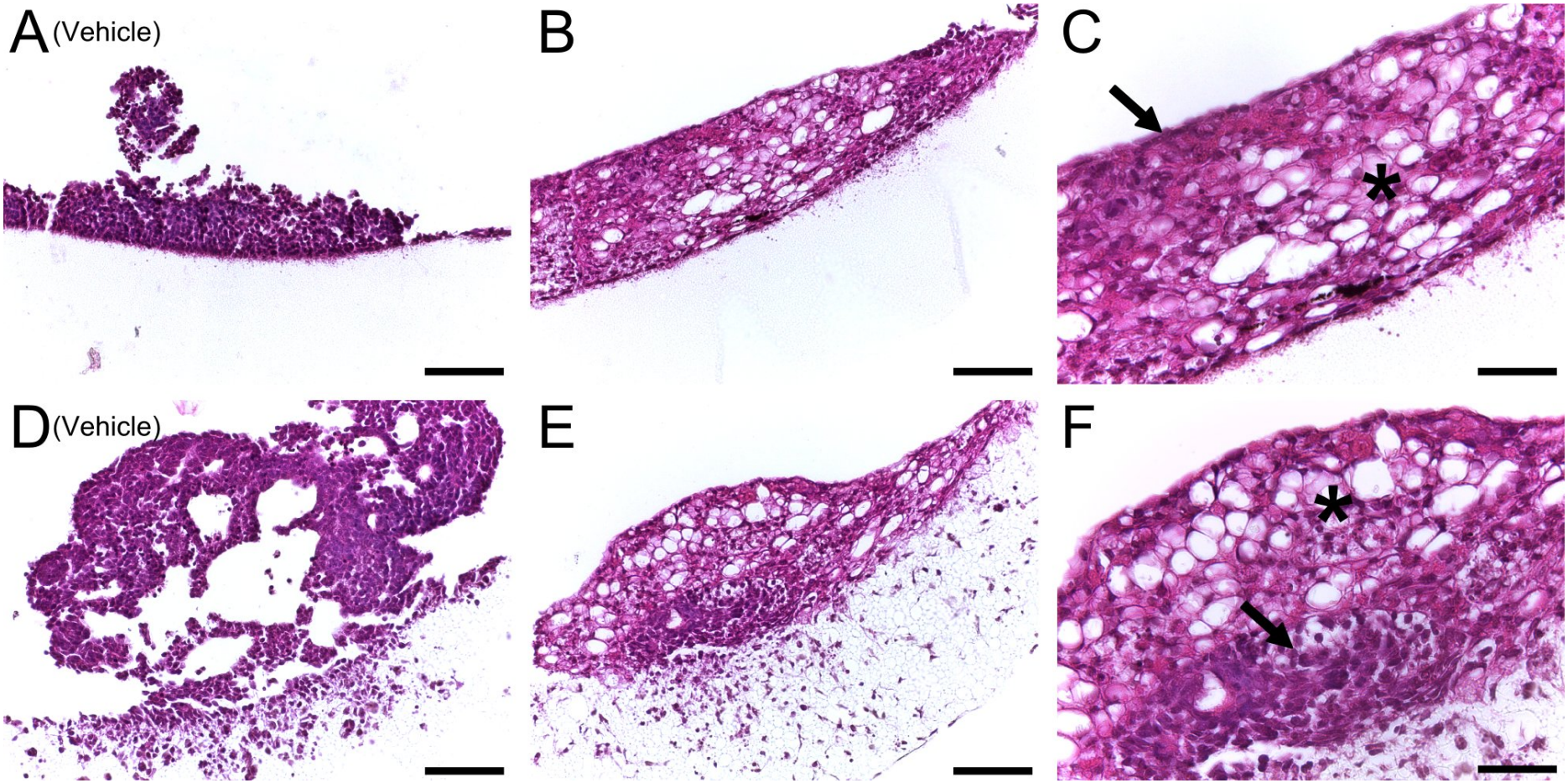

Figure 15: Histological analysis of TERA2.cl.SP12 aggregates treated with BMP2.

Haematoxylin and eosin staining of 8 µm paraffin transverse sections of hEC aggregates treated with BMP2 [50 ngml^{-}1] for 7 days revealed the induction of mesenchymal regions with few cells present (asterisks, C and E) that were not visible in control samples (A and D). BMP-2 aggregates were heterogeneous and also contained more cell dense regions that were similar to vehicle controls. Scale bars represent 100 µm (A, B, D, and E) and 50 µm (C, and F). Bright-field images were taken using a Leica ICC50HD microscope and a 20x (A, B, D, and E) or 40x objective (C, and F).

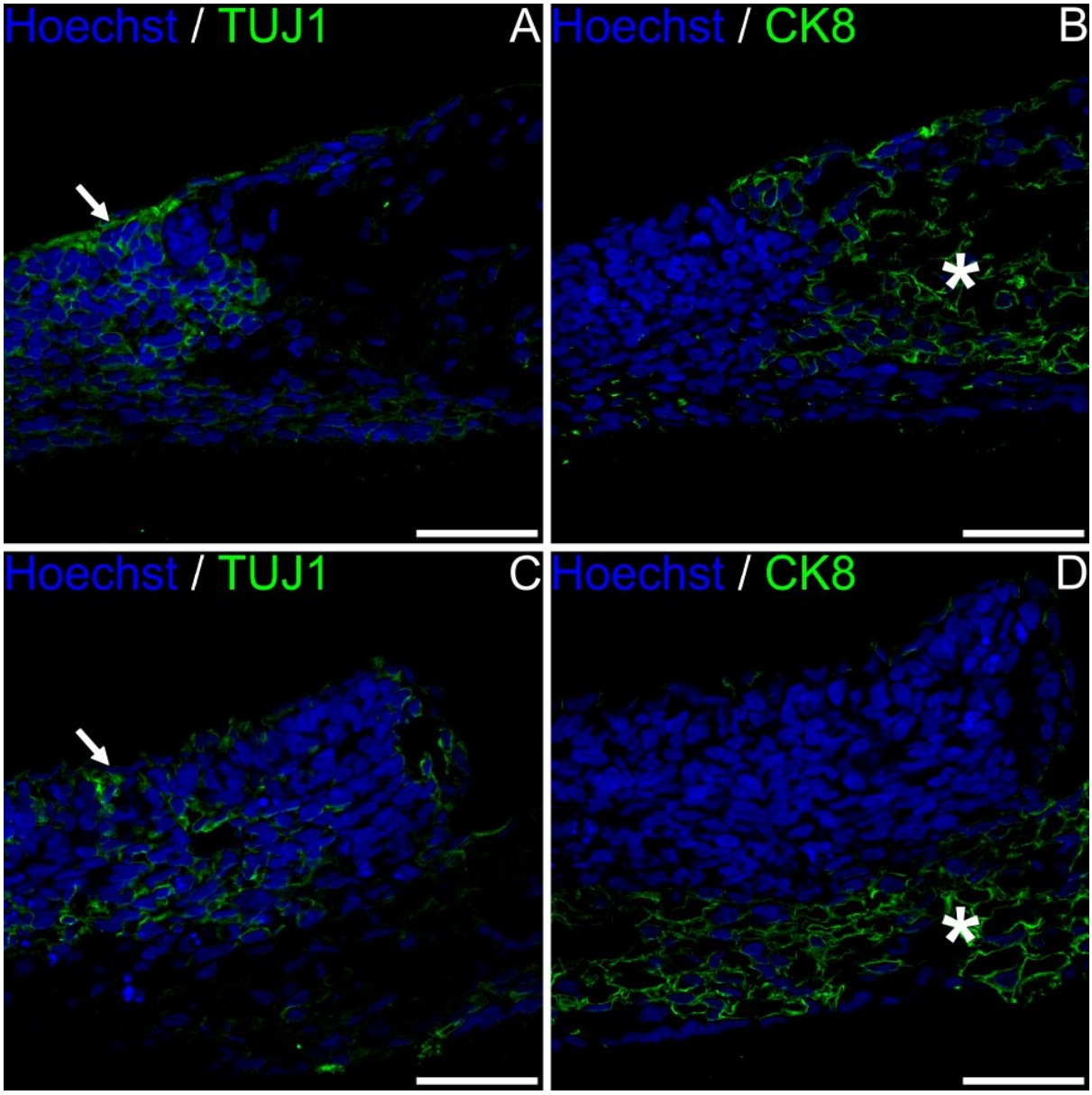

Figure 16: Immunohistochemical analysis of TERA2.cl.SP12 aggregates treated with BMP2.

Immunoflourescent staining of sequential 8 µm paraffin transverse sections of hEC aggregates treated with BMP-2 [50 ngml^{-}1] for 7 days revealed CK8 expression, but not TUJ1 expression, in mesenchymal regions with few cells present (asterisks, B and D). TUJ1 was found to be expressed in more cell dense regions that expressed minimal levels of CK8 (arrows, A and C). Scale bars represent 50 µm. Confocal images were taken using a Zeiss 510 CLSM and a 40x objective.

TERA2.cl.SP12 aggregates treated with BMP2 for 21 days followed by 7 days growth using Alvetex®Polaris generated large amounts of non-neural, $CK8^+$ mesenchymal tissue (**Figure 17E**). Notably, however, a region of highly organised neuroepithelial tissue developed at the centre of one large aggregate (**Figure 17F**). Within the neuroepithelium, mitotically active cells close to the basement membrane expressed the neural stem cell marker nestin, and mature neural marker TUJ1 expression was increased in postmitotic cells that lay outside the neuroepithelium (arrows, **Figure 18**). This staining pattern agreed with what is known about neurogenesis *in vivo* (Gotz and Huttner, 2005)—indicating the highly developed and *in vivo*-like nature of the tissue, but seemingly contradicting the hypothesis that BMP treatment for 21 days would inhibit neural development.

It was puzzling that such an *in vivo*-like neuroepithelium developed despite most of the hEC cells being directed towards non-neural lineages. One explanation considered was that due to the neural region being enveloped in mesenchymal tissue—and not in contact with the BMP2-containing media—the default neural pathway for these cells was instead being followed. However, the fact that neural regions were observed on the outside of the aggregate (top arrow, **Figure 17C**), and that the neuroepithelial tissue in the central region was far more developed than previously seen in TERA2.cl.SP12 aggregates, suggested that a neural inductive effect could also have played a role.

Developmental pathways such as the BMP pathway are tightly regulated. Antagonists are a common feature of signalling networks such as the BMP pathway, preventing excessive signal accumulation and maintaining signalling fecundity. Another possibility was that BMP2 treatment of TERA2.cl.SP12 aggregates induced the production of BMP inhibitors. Noggin has been shown to be induced in human mesenchymal stem cells in response to BMP2 (Chen et al., 2012), and is a known neural inducer that acts by antagonising the neural inhibition of BMPs (Lamb et al., 1993). BMP inhibition could have been responsible, therefore, for the development of the highly developed neuroepithelium observed in hEC aggregates treated with BMP2 for 21 days.

Together these data suggest that BMP2 induces differentiation to non-neural cell types in TERA2.cl.SP12 aggregates cultured as tissue-discs using Alvetex®. However, the inhibition of neural development by BMP2 is imperfect.

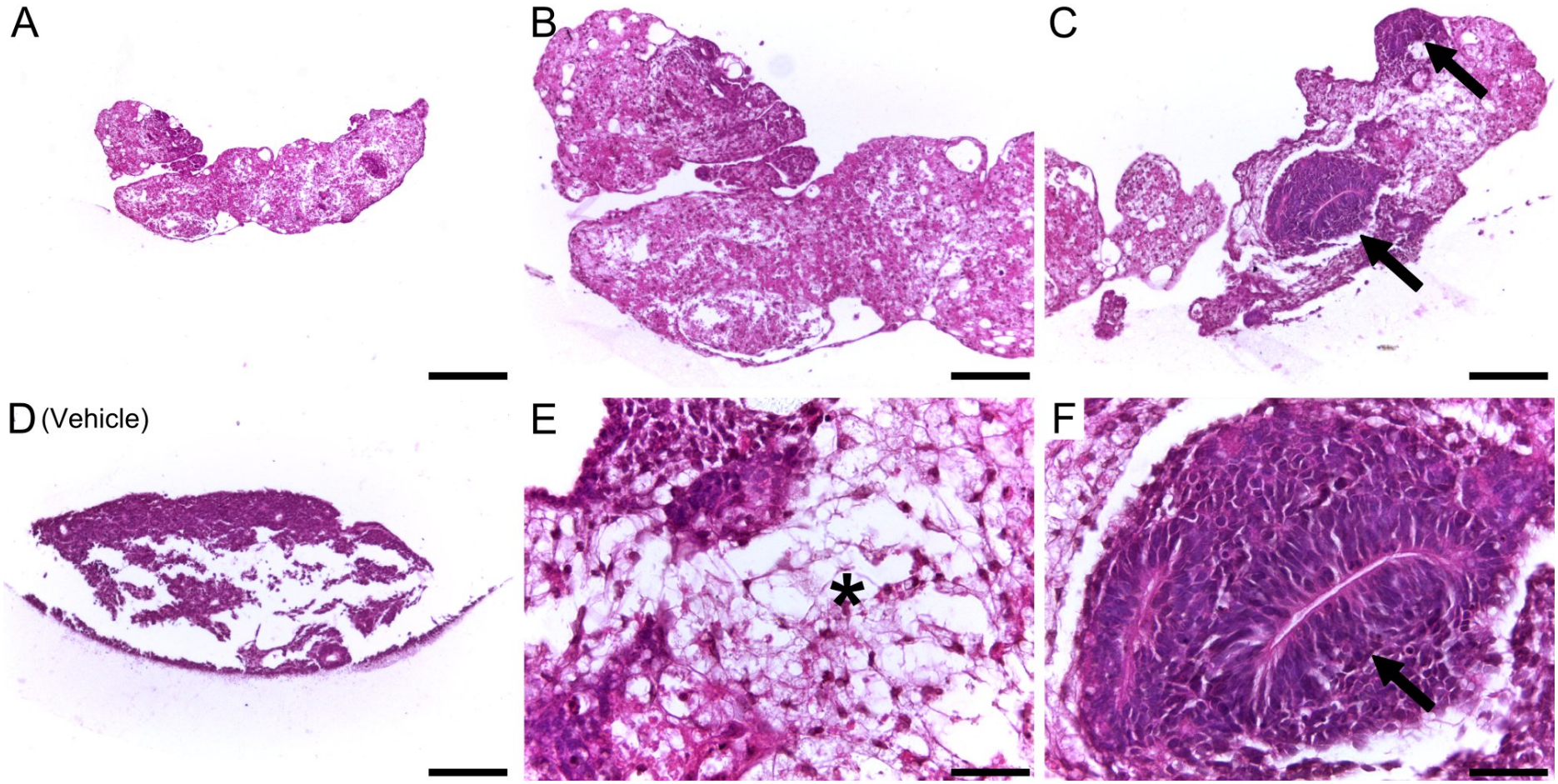

Figure 17: Histological analysis of TERA2.cl.SP12 aggregates treated with BMP2 for 21 days followed by 7 days growth using Alvetex®Polaris.

TERA2.cl.SP12 aggregates were maintained in suspension for 21 days in the presence of BMP2 [50 ngml^{-}1] followed by a further 7 days 3D culturing using Alvetex®Polaris. Haematoxylin and eosin staining showed that BMP2-treated aggregates differentiated into mainly non-neural mesenchymal tissue (asterisk, E), that was not observed in vehicle control aggregates (F). Regions of neural tissue also developed in BMP2 treated aggregates (arrows, C and F). In the centre of one aggregate, a highly developed neuroepithelium was evident (arrow, F). Scale bars represent 500 µm (A), 200 µm (B, C, and F), and 50 µm (G, and H). Bright-field images were taken using a Leica ICC50HD microscope and a 4x (A), or 10x (B, C, and F), or 40x (G, and H) objective.

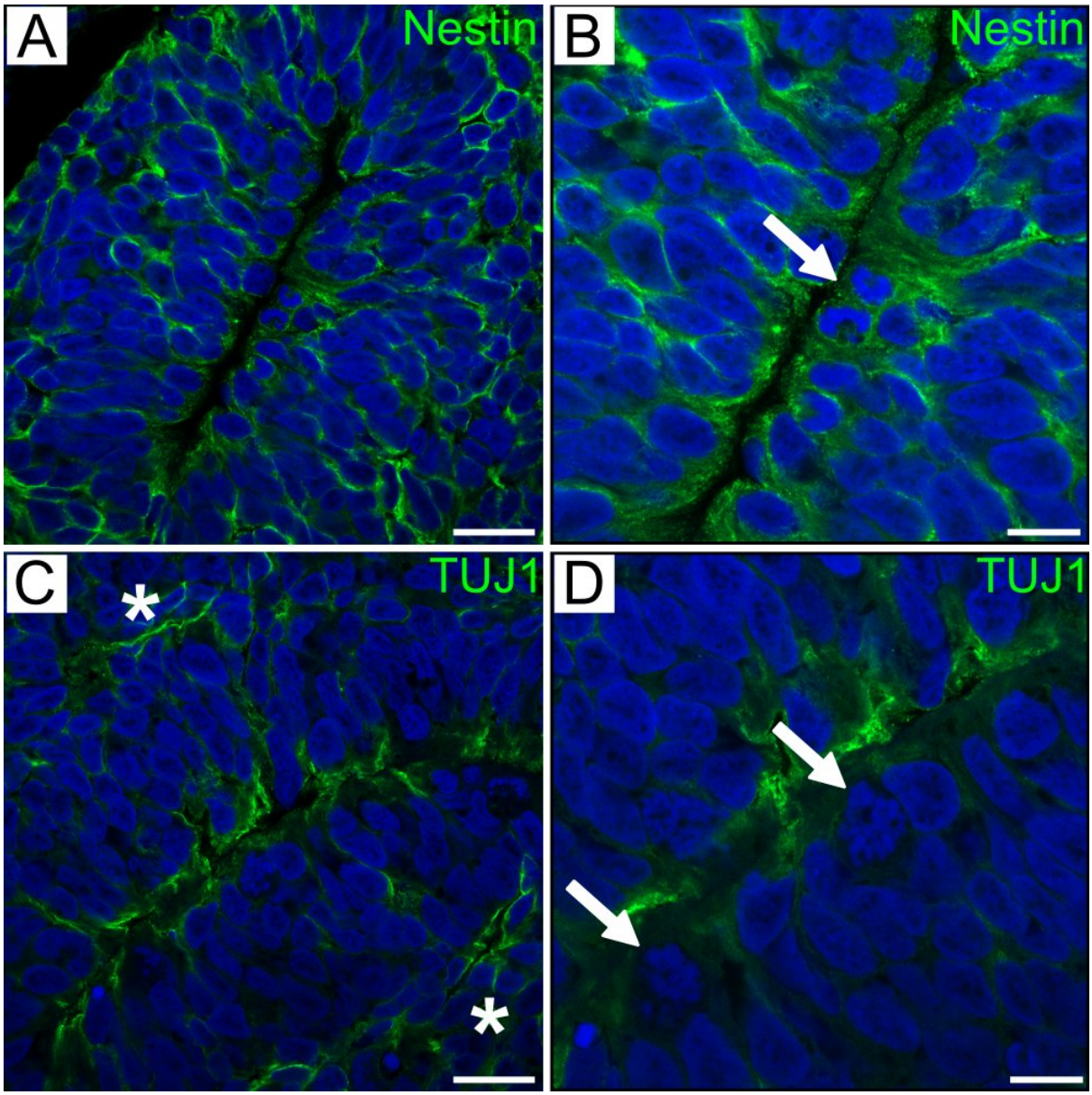

Figure 18: Immunoistochemical analysis of TERA2.cl.SP12 aggregates treated with BMP2 for 21 days followed by 7 days growth using Alvetex®Polaris.

TERA2.cl.SP12 aggregates were maintained in suspension for 21 days in the presence of BMP2 [50 ngml^{-}1] followed by a further 7 days 3D culturing using Alvetex®Polaris. Nestin expression was detected in all cells in the neural region (A), including in TUJ1^{-} neural progenitor cells that resided close to the basement membrane, some of which were actively dividing (arrows, B and D). TUJ1 expression was increased in post-mitotic neurons that lay outside of the neuroepithelium (asterisks, C). Scale bars represent 20 µm (A, and C), and 10 µm (D, and E). Confocal images were taken using a Zeiss 880 CLSM and a 63x objective.

3.3.3 Bone Morphogenetic Protein inhibition

To test the hypothesis that BMP inhibition promoted neuroepithelial differentiation in TERA2.cl.SP12 aggregates, noggin and dorsomorphin were chosen as developmental stimuli. Noggin is a cysteine knot protein that acts to inhibit BMP signalling through ligand sequestration, binding preferentially to BMP4 and BMP7 (Groppe et al., 2002). Dorsomorphin is a small molecule that was shown to dorsalise zebrafish embryos in an *in vivo* screen and antagonises BMP signalling through selective inhibition of BMP type I receptors ALK2, ALK3, and ALK6 (Yu et al., 2008).

TERA2.cl.SP12 aggregates were treated with BMP inhibitors, dorsomorphin [1 µM] or noggin [100 $ngml^{-1}$] (or their respective vehicle controls) for 21 days. Some aggregates were fixed after 21 days in suspension for further analysis while others were maintained as tissue-discs using Alvetex®Polaris for a further 7 days. Aggregates treated with BMP inhibitor dorsomorphin (**Figure 19**) or noggin (**Figure 20**) were heterogenous in structure after 21 days in suspension. Aggregates had developed large epithelial cavities as well as smaller neural rosettes. Close examination of haematoxylin and eosin stained sections revealed at least two distinct cell morphologies that formed different epithelial structures. Cells with a more narrow and long nucleus appeared to form neuroepithelial rosettes (arrows, **Figure 19D**), while larger, more cuiboidal cells formed distinct epithelial cavities (arrow, **Figure 19C**). No easily discernible differences were obvious between aggregates treated with dorsomorphin or noggin, or their respective controls, suggesting that BMP inhibition did not significantly increase neuroepithelial differentiation in hEC aggregates.

Similar results were seen in aggregates after a further 7 days 3D growth using Alvetex™ Polaris. Aggregates formed tissue-discs that contained neuroepithelial tissue (arrow, **Figure 21B**) as well as distinct epithelial structures made up of cuiboidal cells (arrow, **Figure 21C**). Only results from noggin and vehicle control (BSA) treated aggregates are shown in the interest of saving space, but dorsomorphin and DMSO-treated aggregates showed similar features.

Immunohistochemistry was undertaken to try to characterise cell types in TERA2.cl.SP12 aggregates and elucidate if any effects on protein expression patterns could be detected in response to BMP inhibition. Neuroepithelial regions containing neural rosettes were found to express the neural markers nestin and TUJ1, while they expressed lower levels of CK8 (**Figure 22**). Larger epithelial structures expressed lower levels of neural markers and expressed higher levels of pan-epithelial marker CK8 (**Figure 22**). Sequential sections taken from one aggregate treated with dorsomorphin [1 µM] for 21 days in suspension are shown in **Figure 22** because they clearly demonstrate the switching between neural and non-neural epithelial cell types but all aggregates examined showed similar results.

The development of both neural and non-neural epithelial tissues within hEC aggregates treated with BMP inhibitors dorsomorphin and noggin indicate that BMP inhibition does not have a strong neural inductive effect in TERA2.cl.SP12 hEC cells.

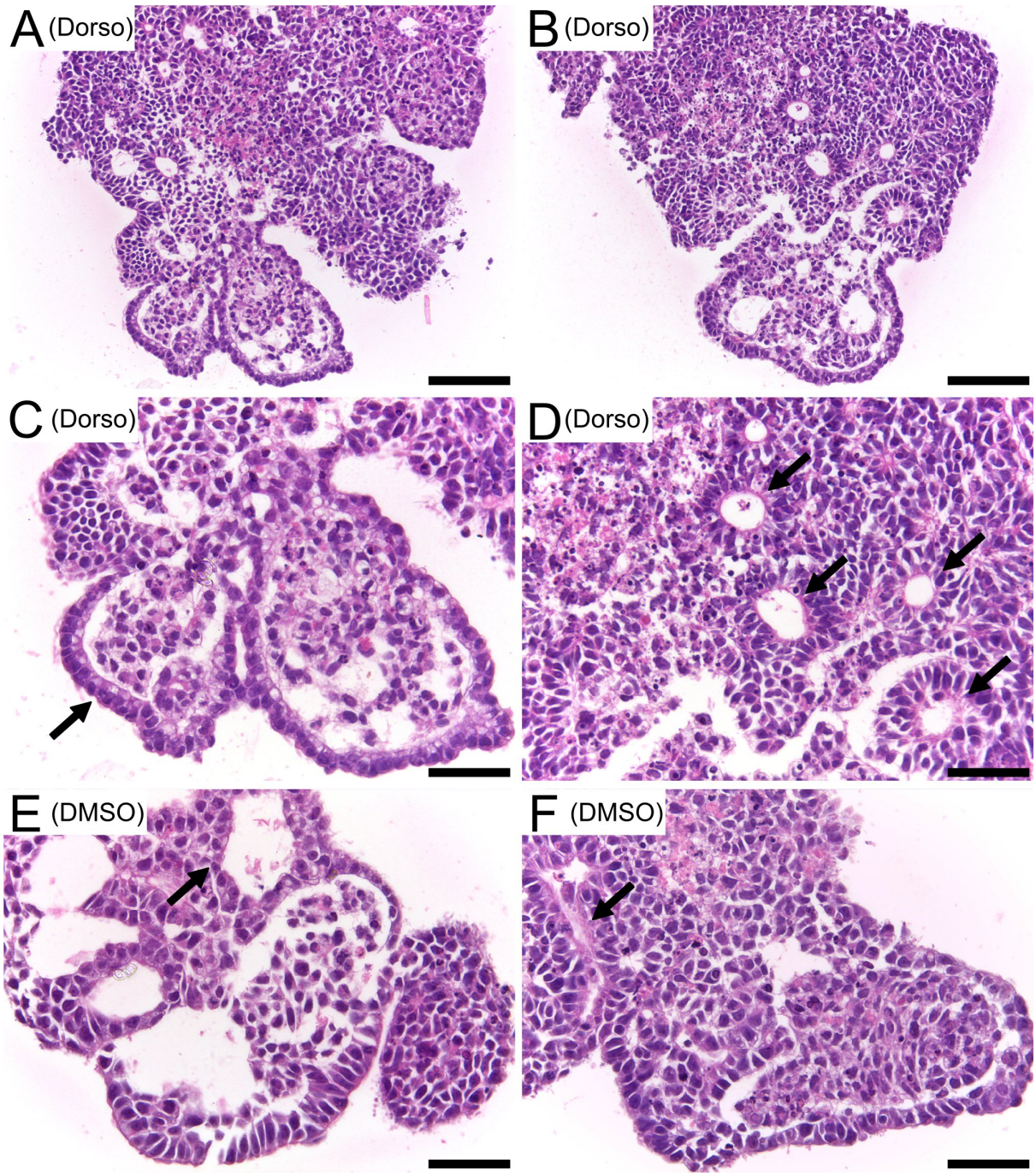

Figure 19: Histological analysis of TERA2.cl.SP12 aggregates cultured in suspension for 21 days in the presence of dorsomorphin

TERA2.cl.SP12 aggregates were cultured in the presence of the BMP inhibitor dorsomorphin (Dorso) [1 µM] or DMSO (vehicle control) and maintained in suspension for 21 days. Haematoxylin and eosin staining of 6 µm paraffin transverse sections revealed that DMSO-treated vehicle control aggregates exhibited similar mixed differentiation to aggregates treated with dorsomorphin. At least two distinct cell types that formed different epithelial structures were visible within aggregates. Narrow cells produced neural rosette-like structures (arrows, D, and F) while more cubiodal cells produced larger epithelial cavities (arrows, C and E). Scale bars represent 100 µm (A, and B), and 50 µm (C-F). Bright-field images were taken using a Leica ICC50HD microscope and a 20x (A, and B) or 40x objective (C-F).

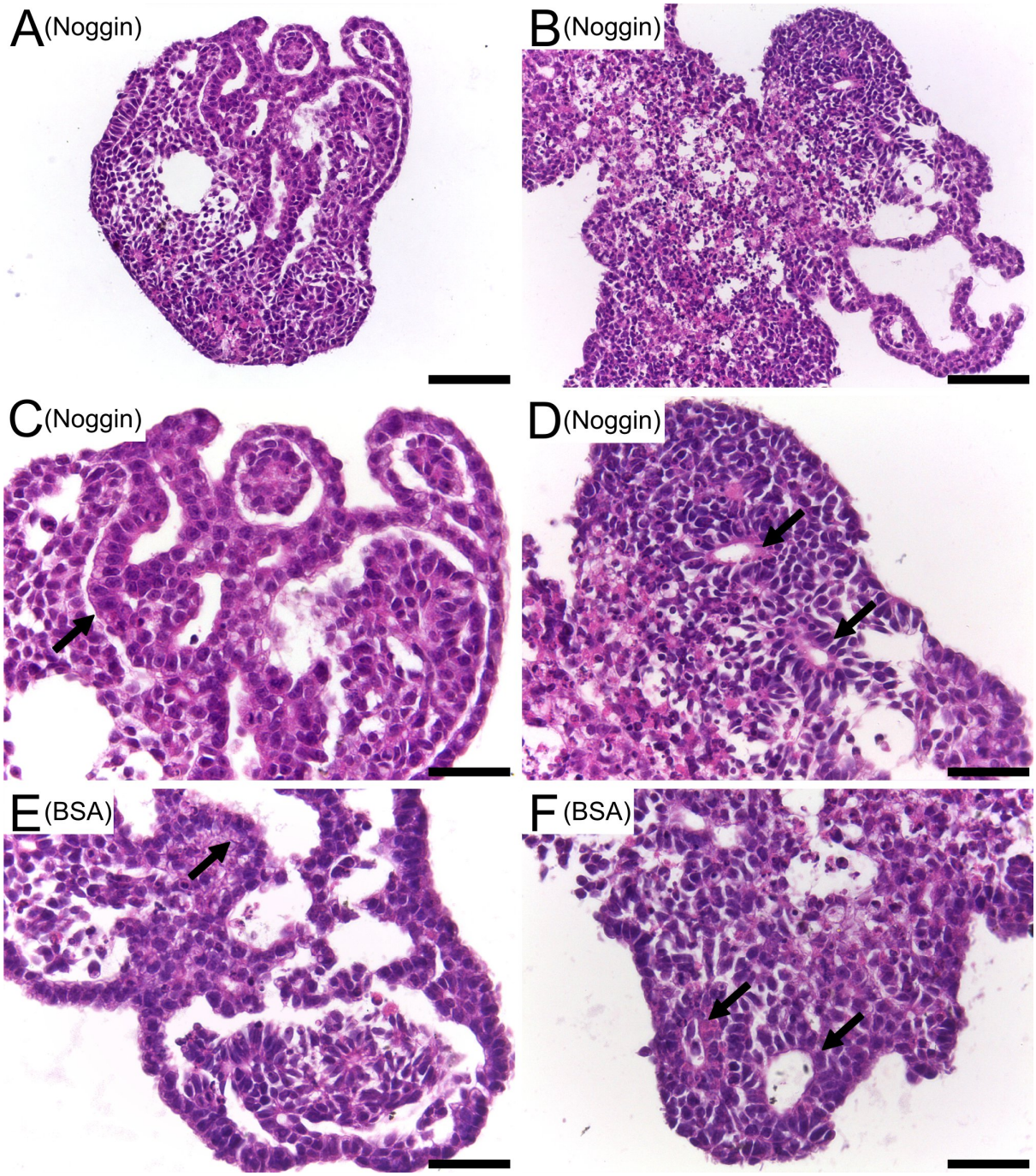

Figure 20: Histological analysis of TERA2.cl.SP12 aggregates cultured in suspension for 21 days in the presence of noggin

TERA2.cl.SP12 aggregates were cultured in the presence of the BMP inhibitor noggin [100 ngml^{-}1] or bovine serum albumin [0.1%] (vehicle control) and maintained in suspension for 21 days. Haematoxylin and eosin staining of 6 µm paraffin transverse sections revealed that BSA-treated vehicle control aggregates exhibited similar mixed differentiation to aggregates treated with noggin. At least two distinct cell types that formed different epithelial structures were visible within aggregates. Narrow cells produced neural rosette-like structures (arrows, D and F) while more cuboidal cells produced larger epithelial cavities (arrow, C and E). Scale bars represent 100 µm (A and B), and 50 µm (C-F). Bright-field images were taken using a Leica ICC50HD microscope and a 20x (A, and B) or 40x objective (C-F).

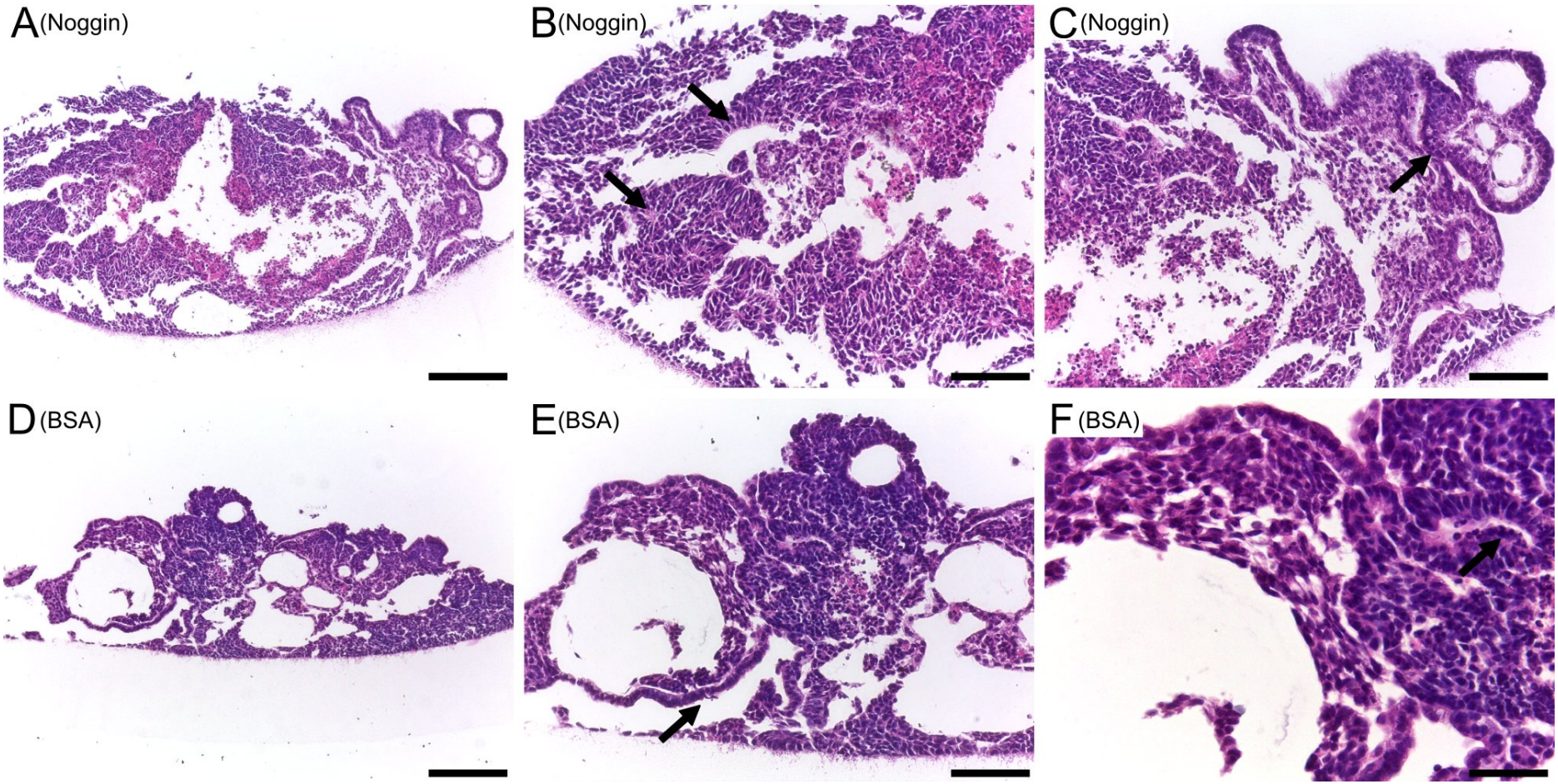

Figure 21: Histological analysis of aggregates cultured in suspension for 21 days in the presence of noggin followed by 7 days growth using Alvetex®Polaris

TERA2.cl.SP12 aggregates were cultured in the presence of the BMP inhibitor noggin [100 ngml^{-}1] or bovine serum albumin (BSA) [0.1%] and maintained in suspension for 21 days, followed by maintenance in 3D using Alvetex®Polaris. Both noggin (A-C) and vehicle control (D-F) aggregates exhibited mixed differentiation. Aggregates developed neuroepithelial regions containing longer, narrow cells (arrows, B, and E) as well as regions of non-neural epithelial tissue consisting of larger, cuiboidal cells (arrows, C, and F). Scale bars represent 200 µm (A, and D), 100 µm (B, C, and E) 50 µm (F). Bright-field images were taken using a Leica ICC50HD microscope and a 10x (A, and D), 20x (B, C, and E), or 40x objective (F).

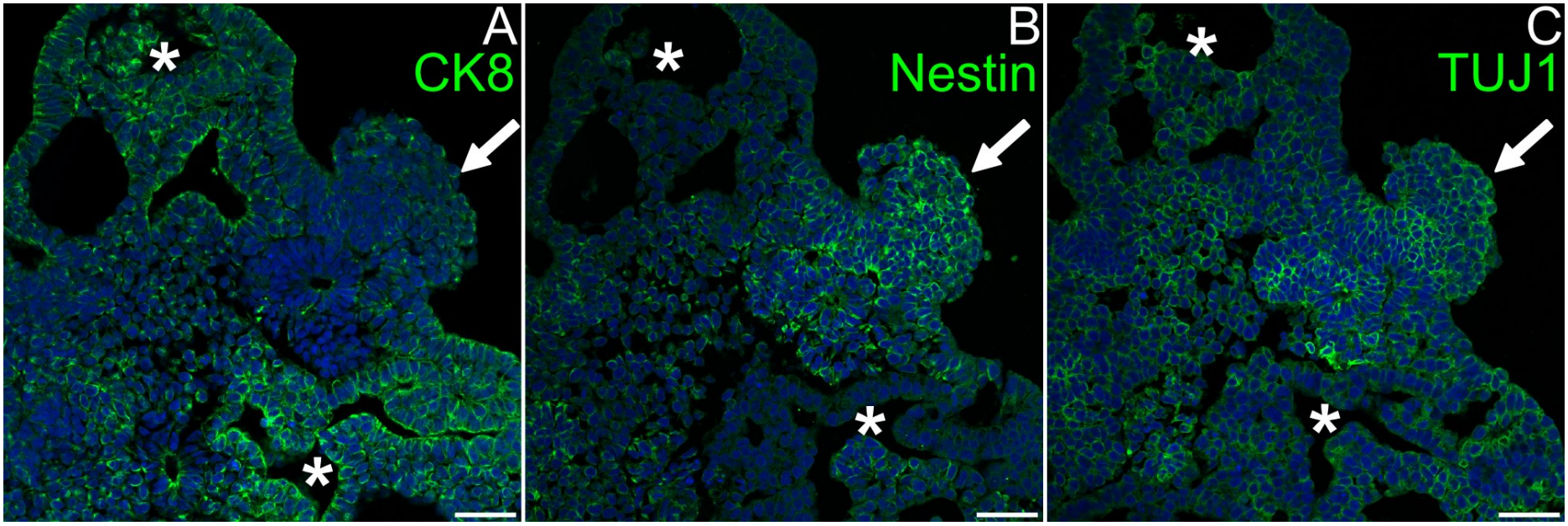

Figure 22: Immunohistochemical analysis of aggregates cultured in suspension for 21 days in the presence of dorsomorphin

TERA2.cl.SP12 aggregates were cultured in the presence of the BMP inhibitor dorsomorphin [1 µM] and immunostained against pan-epithelial marker cytokeratin-8 (CK8) (A), early neural marker nestin (B), and mature neural marker TUJ1 (C). Serial sections of one aggregate showed that the expression of neural markers was highest in regions of neuroepithelium (arrows), with highest CK8 expression seen in the regions of non-neural epithelial tissue (asterisks). Scale bars represent 50 µm. Confocal images were taken using a Zeiss 880 CLSM and a 20x objective.

3.3.4 Wnt/β-catenin Pathway

Next, Chiron99021 (Chi) was used to study the role of the canonical Wnt/β-catenin pathway in TERA2.cl.SP12 differentiation (Przyborski et al., 2004). The small molecule glycogen synthase kinase 3β (GSK3β) inhibitor, Chi, acts to agonise the canonical Wnt/β-catenin pathway by blocking the proteolysis of β-catenin and allowing its nuclear translocation (Wray et al., 2011). In the nucleus, β-catenin mediates gene-regulatory effects through interactions with TCF/LEF factors that activate transcription of target genes when bound to β-catenin (Behrens et al., 1996).

Histological analysis revealed a striking lack of epithelial structures in TERA2.cl.SP12 aggregates treated with Chi [3 µM] for 7 days when compared to vehicle control (DMSO) treated aggregates (**Figure 23**). Control aggregates had developed large numbers of epithelial cavities after 7 days in suspension (mean = 9 cavities per aggregate, n = 4) while the majority of Chi-treated aggregates completely lacked epithelial structures after 7 days (mean = 0.2 cavities per aggregate, n = 5). This suggested that epithelial morphogenesis was strongly inhibited in TERA2.cl.SP12 aggregates by exposure to Chi [3 µM] for 7 days in suspension and this difference was extremely statistically significant (unpaired *t*-test; $P = 0.0008$).

Aggregates treated with Chi for 21 days in suspension similarly exhibited a lack of epithelial structures compared to DMSO controls (**Figure 24**) (Chi-treated mean = 1.2 cavities per aggregate, n = 7; control mean = 8.5 per aggregate, n = 4; unpaired *t*-test; $P = 0.0012$). Interestingly, Chi-treated aggregates were also substantially larger than control aggregates (Chi mean diameter = 801 µm, n = 3; control mean diameter = 349 µm, n = 4; unpaired *t*-test; $P = 0.0064$). A large central cavity that was devoid of cells was seen in some aggregates (asterisk, **Figure 24B**). These cavities may have represented a necrotic core of cells that developed due to the increased size of the aggregates, or an artefact of the process of aggregates adhering together that has previously been shown to produce such hole defects (Beachley et al., 2014). It was interesting to note whorls of cells that formed a circular cluster in some Chi-treated aggregates maintained in suspension for 21 days (arrows, **Figure 24B&D**). These circular clusters of cells were thought to have developed as a consequence of blocking epithelial morphogenesis in TERA2.cl.SP12 cells.

Aggregates treated with Chi for 21 days in suspension and maintained on Alvetex®Polaris for a further 7 days also showed highly reduced epithelial tissue development. A typical example is shown where only one cavity could be seen in a Chi-treated aggregate and 9 in a control aggregate (**Figure 25**). The development of highly reduced numbers of epithelial structures in Chi-treated aggregates maintained in suspension and using Alvetex®further supported that epithelial differentiation is reduced in response to Chi.

These data suggest that the canonical Wnt/β-catenin pathway plays a role in epithelial morphogenesis in TERA2.cl.SP12 aggregates. It was not immediately obvious whether Chi-treatment led to other changes in differentiation, however, and so immunohistochemistry was used to characterise protein expression in Chi-treated aggregates.

Only aggregates after 21 days in suspension were chosen for immunohistochemical analysis to allow for a greater number of aggregates to be examined per slide. Expression of the neural markers nestin and TUJ1 was seen in aggregates treated with Chi for 21

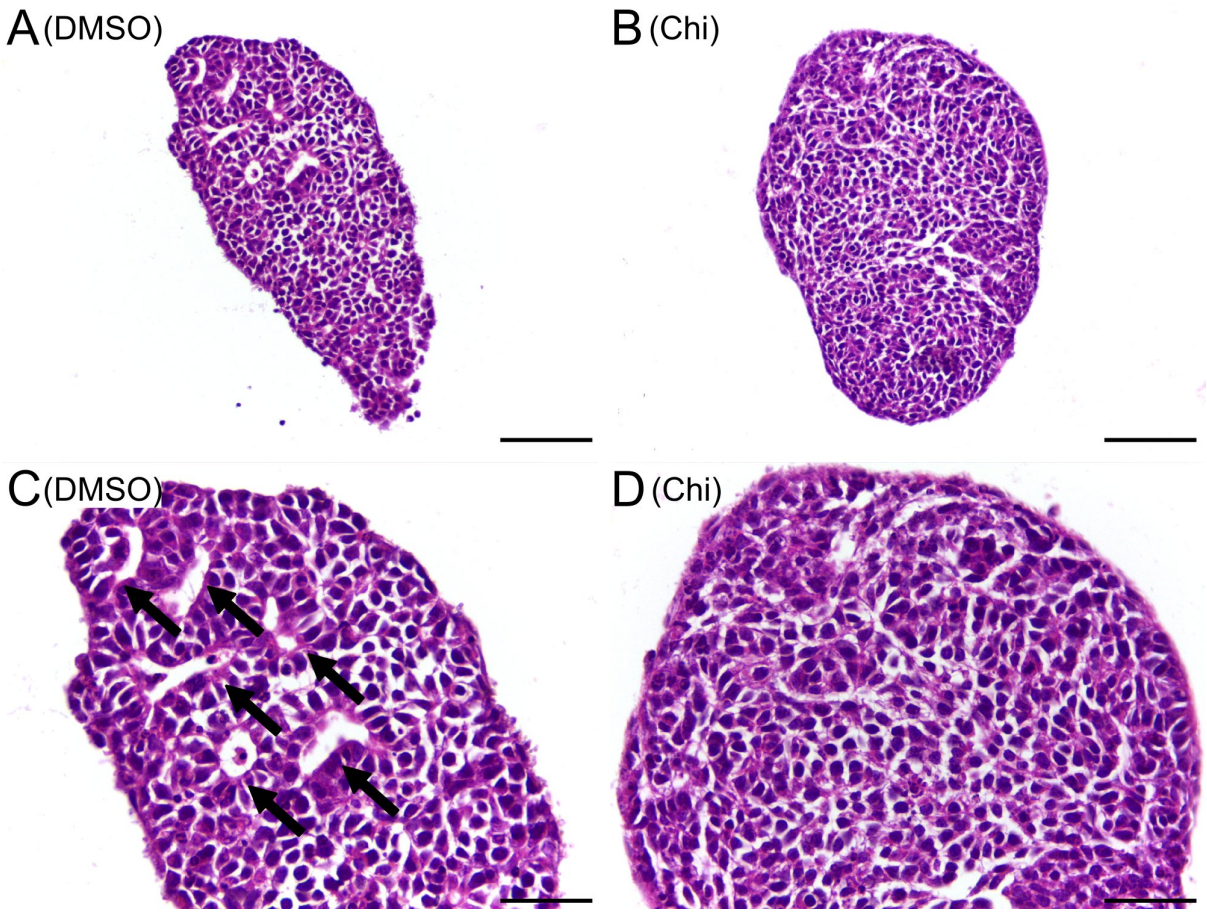

Figure 23: Histological analysis of TERA2.cl.SP12 aggregates treated with Chiron99021 for 7 days in suspension

TERA2.cl.SP12 aggregates were maintained in suspension in the presence of Chiron99021 (Chi) [3 µM] for 7 days and histological analysis carried out. Haematoxylin and eosin staining revealed that small neural rosette-like structures that developed in control aggregates (A, and arrows in C) were absent in Chi-treated aggregates (B, and D). Scale bars represent 100 µm (A, and B), and 50 µm (C, and D). Bright-field images were taken using a Leica ICC50HD microscope and 20x (A, and B), or 40x objective (C, and D).

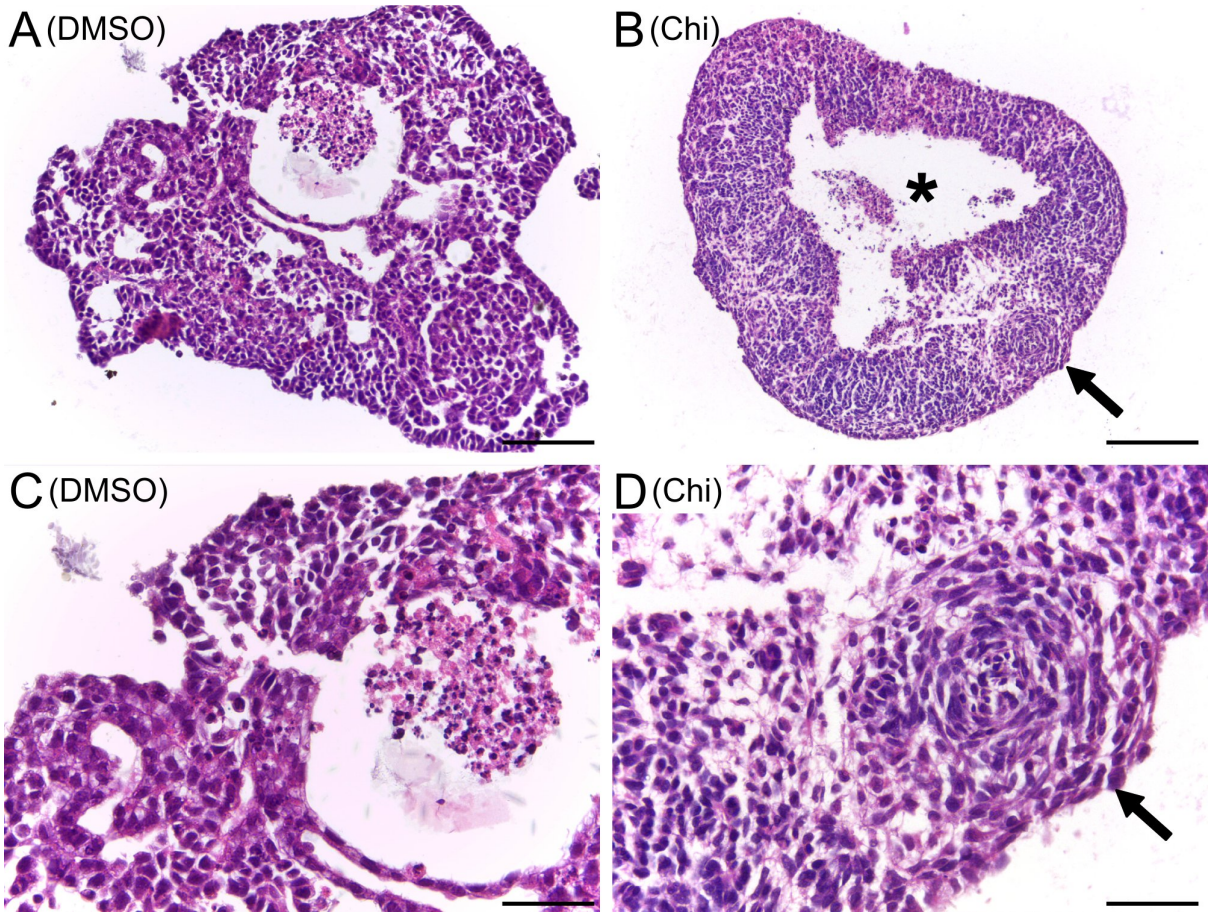

Figure 24: Histological analysis of TERA2.cl.SP12 aggregates treated with Chiron99021 for 21 days in suspension

TERA2.cl.SP12 aggregates were maintained in suspension in the presence of Chiron99021 (Chi) [3 µM] for 21 days and histological analysis performed. Haematoxylin and eosin stained paraffin transverse sections revealed that large epithelial structures that developed in control aggregates (A, and C) were absent in Chi treated aggregates and epithelial structures were rarely seen (B, and D). A large central cavity was evident in some Chi-treated aggregates (asterisk, B) that was thought to represent a necrotic core or hole defects due to the process of smaller aggregates adhering together. A circular whorl of cells was sometimes visible in Chi-treated aggregates (arrows, B and D) that was thought to be induced by Chi treatment blocking epithelial morphogenesis. Scale bars represent 200 µm (B), 100 µm (A), and 50 µm (C, and D). Bright-field images were taken using a Leica ICC50HD microscope and a 10x (B), 20x (A), or 40x objective (C, and D).

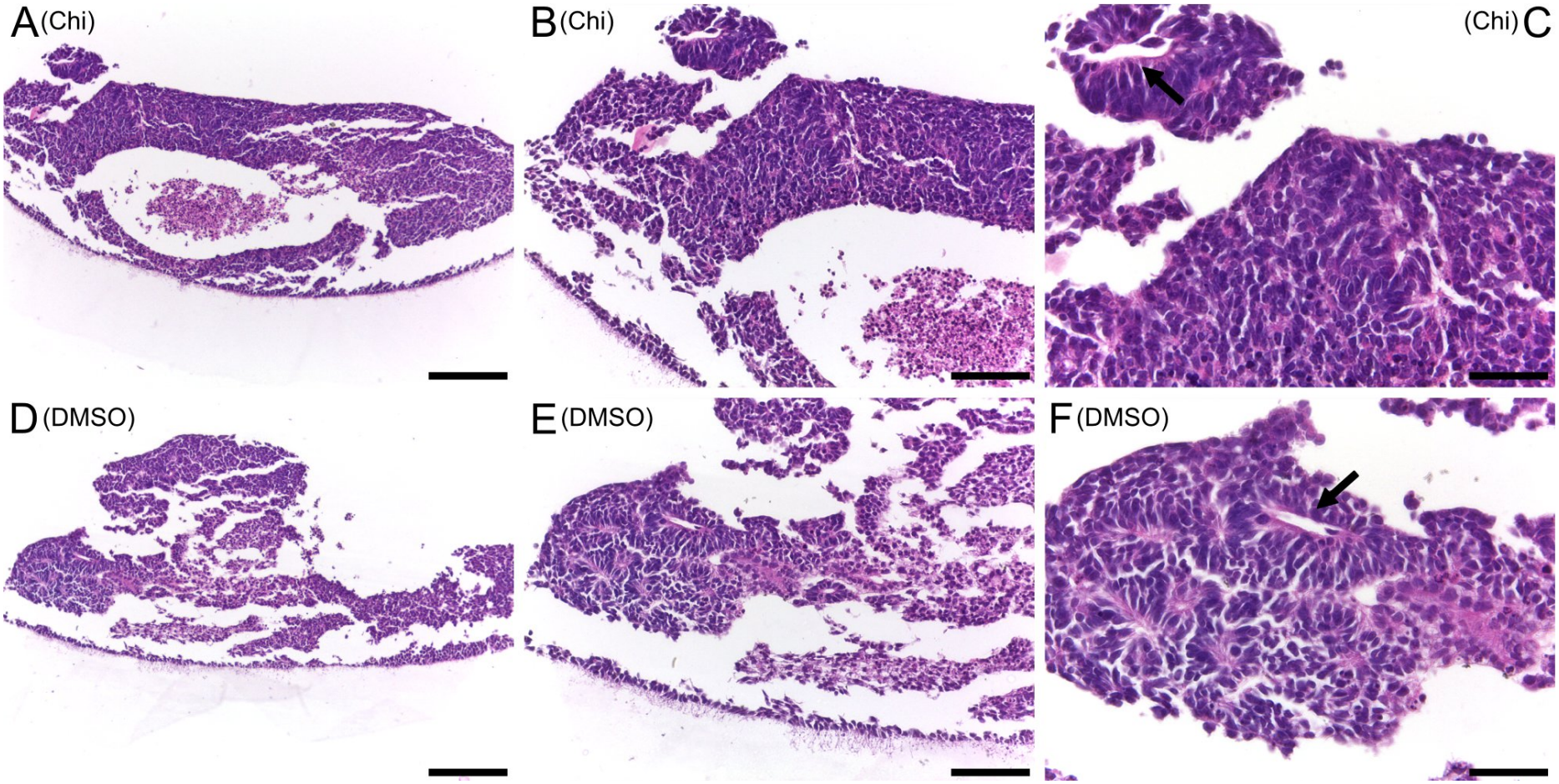

Figure 25: Histological analysis of TERA2.cl.SP12 aggregates treated with Chiron99021 for 21 days in suspension followed by 7 days growth using Alvetex®Polaris

TERA2.cl.SP12 aggregates were maintained in suspension in the presence of Chiron99021 (Chi) [3 µM] for 21 days followed by 7 days growth using Alvetex®Polaris and histological analysis performed. Haematoxylin and eosin stained paraffin transverse sections revealed that neuroepithelial structures (arrow, A and F) that developed in control aggregates were numerous (D-F) but were very rarely seen in Chi-treated aggregates (A-C). Scale bars represent 200 µm (A, and D), 100 µm (B, and E), and 50 µm (C, and F). Bright-field images were taken using a Leica ICC50HD microscope and a 10x (A, and D), 20x (B, and E), or 40x objective (C, and F).

days in suspension (**Figure 26**). CK8 expression, however, was absent from all aggregates examined (**Figure 26A**). As was previously noted, a proportion of aggregates were found to contain small epithelial structures and these were found to be CK8$^-$ but expressed nestin. The staining pattern observed is therefore indicative of the development of neuroepithelial tissue in Chi-treated TERA2.cl.SP12 aggregates.

Together these data reveal that Chi has a strong inhibitory effect on epithelial tissue formation in TERA2.cl.SP12 aggregates. However, Wnt/β-catenin activation does not completely block neuroepithelial development.

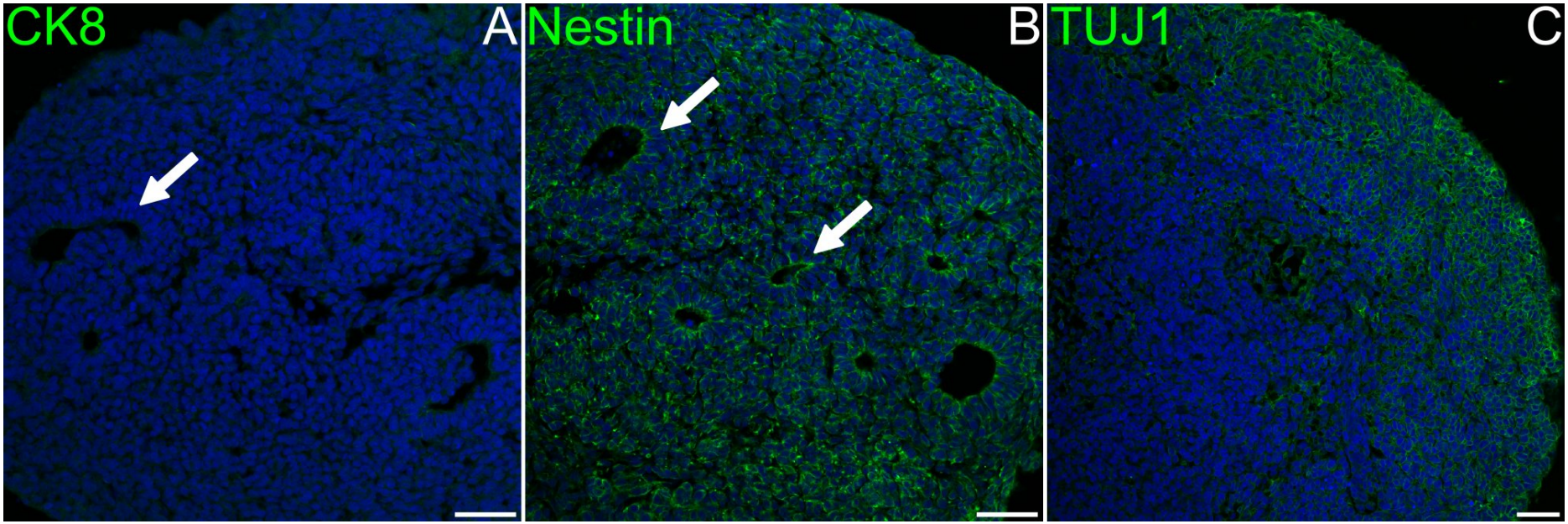

Figure 26: Immunohistochemical analysis of TERA2.cl.SP12 aggregates treated with Chiron99021 for 21 days in suspension

TERA2.cl.SP12 aggregates were maintained in suspension in the presence of Chiron99021 [3 µM] for 21 days and immunostaining against CK8 (A), nestin (B), and TUJ1 (C) performed. Aggregates were not found to express the pan-epithelial marker, CK8 (A) but expression of neural markers nestin and TUJ1 was seen (B and C). Neuroepithelial structures developed that were $CK8^{-}$ and expressed nestin (arrows, A and B). Scale bars represent 50 µm. Confocal images were taken using a Zeiss 880 CLSM and a 20x objective.

3.4 TERA2.cl.SP12 Teratoma formation

In order to compare the tissues produced *in vitro* to tissues produced *in vivo*, teratoma formation from TERA2.cl.SP12 cells was examined. Teratoma samples were derived from an animal study that was previously performed with permission of the institution at Durham University, UK, School of Biological and Biomedical Sciences, in accordance with UK Home Office guidelines. $0.5x10^6$ undifferentiated TERA2.cl.SP12 cells were implanted subcutaneously into the flank of adult male nude (nu/nu) mice and formed teratomas over 6-8 weeks.

Histological analysis of teratomas revealed multiple distinct differentiated cell types and formed complex epithelial tissues including neuroepithelium (arrows, **Figure 27B&C**), and larger non-neural epithelial structures that have previously been shown to express CK8 (asterisks, **Figure 27D-F**)(Cooke et al., 2006). Epithelial tissues seen in hEC teratomas were well developed but overall tissue organisation was haphazard (**Figure 27A**).

Comparatively speaking, epithelial tissue structures were generally larger and more developed than those seen in aggregates cultured *in vitro*, possibly due to interactions with host vasculature or the larger size and greater cell number in teratomas. However, neuroepithelium that developed in one BMP2-treated aggregate cultured as a tissue-disc (**17**) was at least as highly developed as those seen in teratomas, suggesting that under certain conditions *in vitro* culturing of hEC aggregates as tissue-discs for extended periods provides a suitable microenvironment to allow differentiation to occur in a manner comparable to *in vivo*.

It has been shown that TERA2.cl.SP12 cells could be maintained in an undifferentiated state in culture and that their spontaneous differentiation was induced by aggregation. The culturing of hEC aggregates as 3D tissue-discs using Alvetex®Polaris facilitated the formation of a flattened tissue-disc that reduced the formation of a necrotic core over prolonged culture. Tissues produced in hEC tissue-discs included neuroepithelial tissue and other non-neural epithelial tissues that were similar to tissues produced in teratomas *in vivo*. Culturing human stem cell aggregates for extended periods *in vitro* as tissue-discs using Alvetex®Polaris may, therefore, offer a novel alternative to the teratoma assay for pluripotency testing.

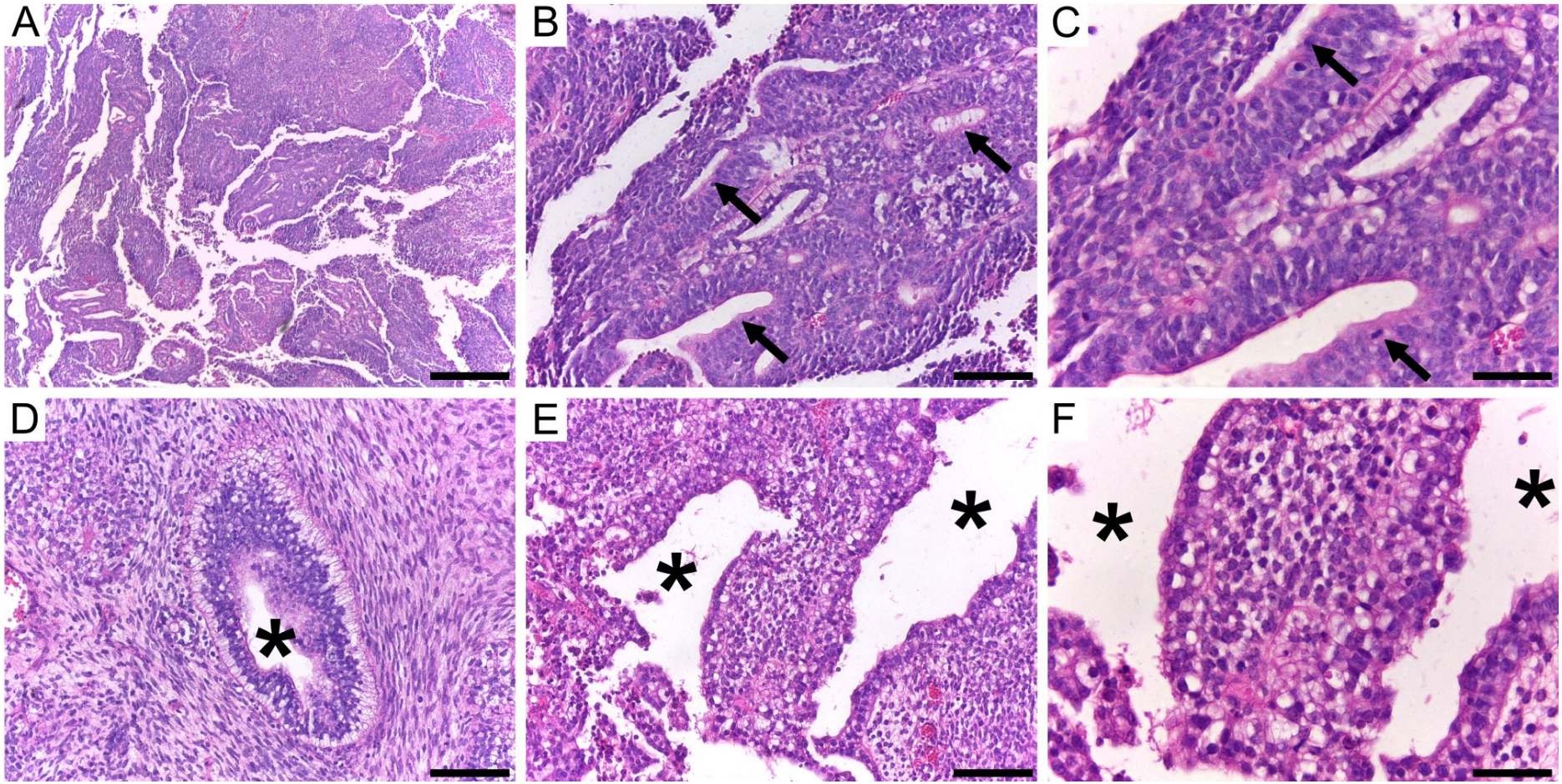

Figure 27: Histological analysis of teratomas derived from TERA2.cl.SP12 cells.

$0.5x10^6$ undifferentiated TERA2.cl.SP12 cells were injected into the flank of male nude (nu/nu) and teratoma formation occurred over 6-8 weeks. Paraffin transverse sections were generated and stained using haematoxylin and eosin to reveal internal structure. The overall tissue architecture of teratomas was haphazard (A). Teratomas contained multiple differentiated cell types and complex epithelial tissues. Distinct, large epithelial structures consisting of cuiboidal cells were visible (D-F) as well as neuroepithelial tissues (B, and C). Scale bars represent 500 µm (A), 100 µm (B, D, and E), and 50 µm (C, and F). Bright-field images were taken using a Leica ICC50HD microscope and a 4x (A), 20x (B, D and E), or 40x objective (C, and F).

3.5 Mouse Embryonic Stem Cell Line CGR8

CGR8 mESCs were chosen for validation of the method of using stem cell aggregates cultured as tissue-discs using Alvetex® 3D scaffold membranes as a novel *in vitro* pluripotency assay. CGR8 cells were maintained feeder-free in 2D culture with the addition of LIF to the media to prevent spontaneous differentiation (Williams et al., 1988). Immunocytochemistry revealed that markers typically associated with pluripotency in mESCs including SSEA-1 (Solter and Knowles, 1978), Nanog (Chambers et al., 2003), Oct4 (Scholer et al., 1989), and SOX2 (Yuan et al., 1995) were expressed in colonies of CGR8 mESCs grown in 2D culture (**Figure 28**). CGR8 cells also exhibited morphological features typical of mESCs including small size, rounded morphology, high nuclear:cytoplasm ratio, and prominent nucleoli. As an initial *in vitro* characterisation, these findings were indicative of the pluripotency of CGR8 mESCs maintained in 2D culture.

3.6 Murine Embryoid Bodies

CGR8 mESCs were formed into aggregates or embryoid bodies (mEBs) using AggreWell™ plate technology. The benefits of using such a method to aggregate cells over spontaneous aggregation is that the size of EBs and number of cells per EB can be regulated more precisely. mEBs containing 1000 cells were cultured in suspension in the presence of 10% fetal bovine serum (FBS) and underwent cavitation after 5 days. Cavities were visible in most aggregates in suspension under phase-contrast microscopy as lighter coloured areas, and as cavities in haematoxylin and eosin stained sections (asterisk, **Figure 29D&E**). Several differentiated cell types were visible within mEBs after 5 days suspension culture (arrow, **Figure 29F**) and appeared to form an extrusion of cells on the surface of many mEBs (arrow, **Figure 29C**).

These initial mEB experiments were conducted using relatively late passage number stocks of the CGR8 mESC cell line (passage number 26, p26). In order to maintain the greatest level of developmental potency cells of as early passage number as possible should be used. Passage number 9 stocks (p9) of the CGR8 cell line were also used to generate mEBs that were subsequently cultured in suspension with 20% FBS to try to maximise spontaneous differentiation.

Histology was performed on p9 mEBs cultured in 20% FBS after 5 days suspension culture and images of haematoxylin and eosin stained 6 µm paraffin transverse sections are shown in (**Figure 30**). Similar to p26 mEBs, large cystic cavities were seen in the majority of mEBs examined (**Figure 30A**). Differentiated cell types were also visible and had formed an extrusion of cells on the surface of many aggregates (**Figure 30B**). Unlike mEBs cultured in 10% FBS, however, large areas of mesenchymal tissue were seen that resembled embryonic mesenchyme (**Figure 30C**)—a mesoderm-derived transitional tissue formed during mouse embryonic development that contains stellate-shaped cells and facilitates nutrient transfer (Greep and Weiss, 1977). p9 mEBs cultured with 20% FBS were larger than p26 mEBs cultured with 10% FBS, possibly due to reduced cell density within aggregates (mean diameter p9 mEBs = 679 µm, n = 7; mean diameter p26 mEBs = 383 µm, n = 11; unpaired t-test; $P = 0.0013$).

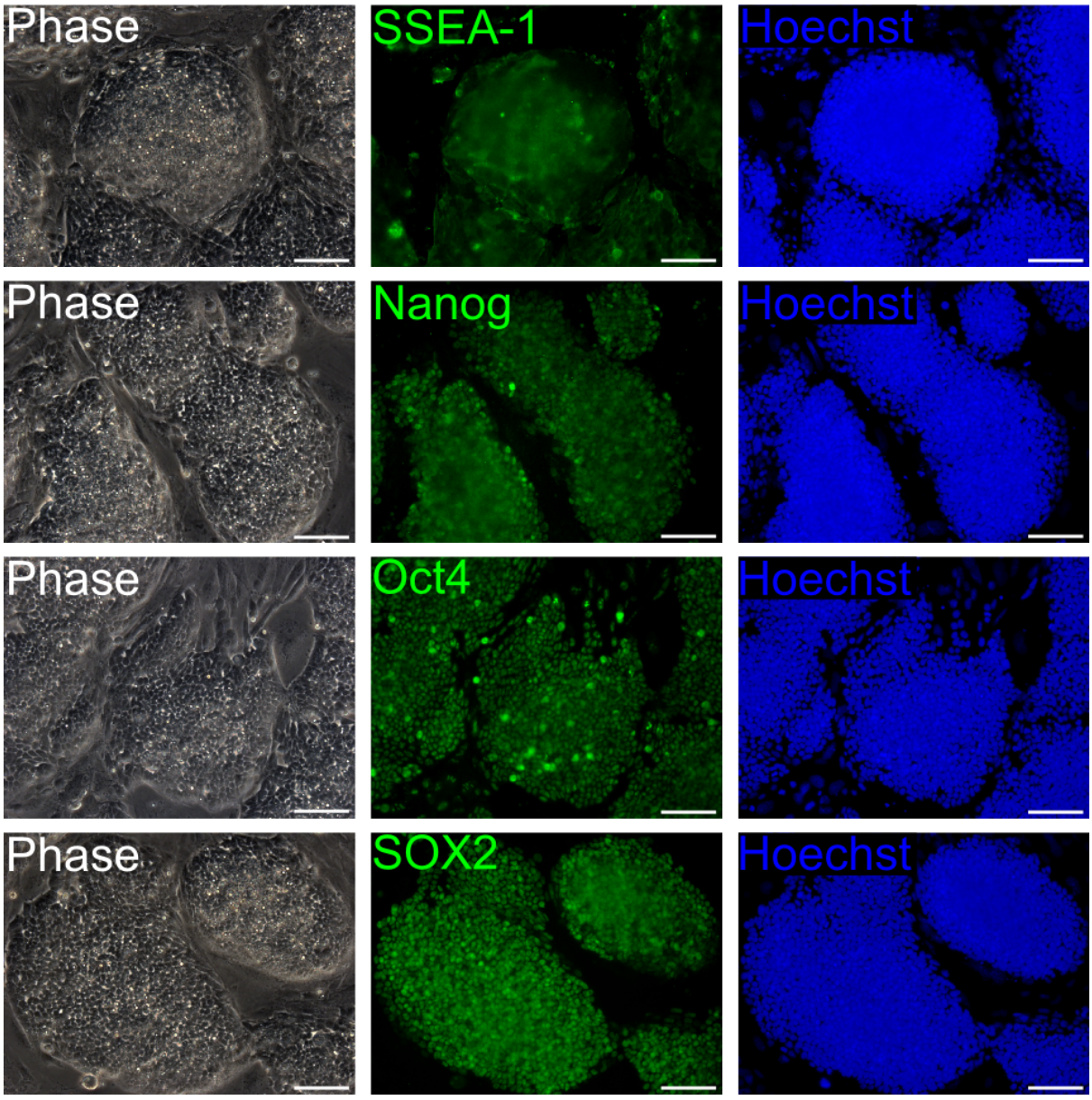

Figure 28: Pluripotency marker expression in CGR8 mESCs cultured in 2D.

Immunocytochemistry revealed expression of the pluripotency markers SSEA-1, Nanog, Oct4, and SOX2 in CGR8 mESCs cultured in 2D in the presence of LIF. Phase-contrast images revealed typical mESC morphology including small size, rounded morphology, high nuclear:cytoplasm ratio, and prominent nucleoli. Scale bars represent 100 µm. Phase-contrast and flourescent images were taken using a Leica DMI3000B inverted epifluorescent microscope and a 20x objective.

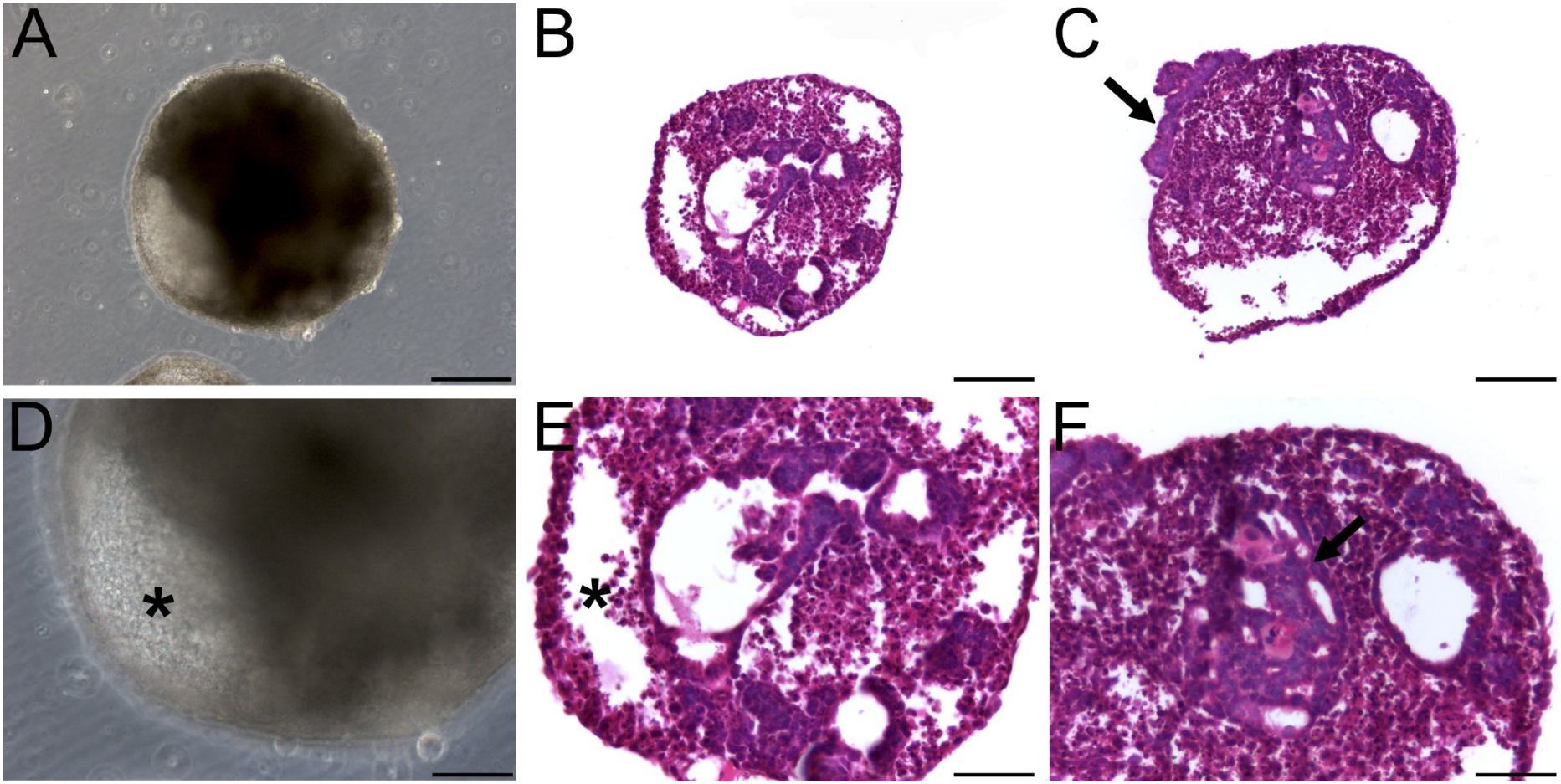

Figure 29: Murine Embryoid Bodies after 5 days suspension culture with 10% FBS.

Haematoxylin and eosin stained 6 µm paraffin sections and phase-contrast images of p26 mEBs after 5 days in suspension culture. Cavities were visible in many mEBs after 5 days (arrows) indicating that cavitation had taken place. Distinct differentiated cell types were visible indicating that spontaneous differentiation was occurring. Scale bars represent 100 µm (A, B, and C) and 50 µm (D, E, and F). Bright-field images were taken using a Leica ICC50HD microscope and a 20x (A, B, and C), or 40x objective (D, E, and F).

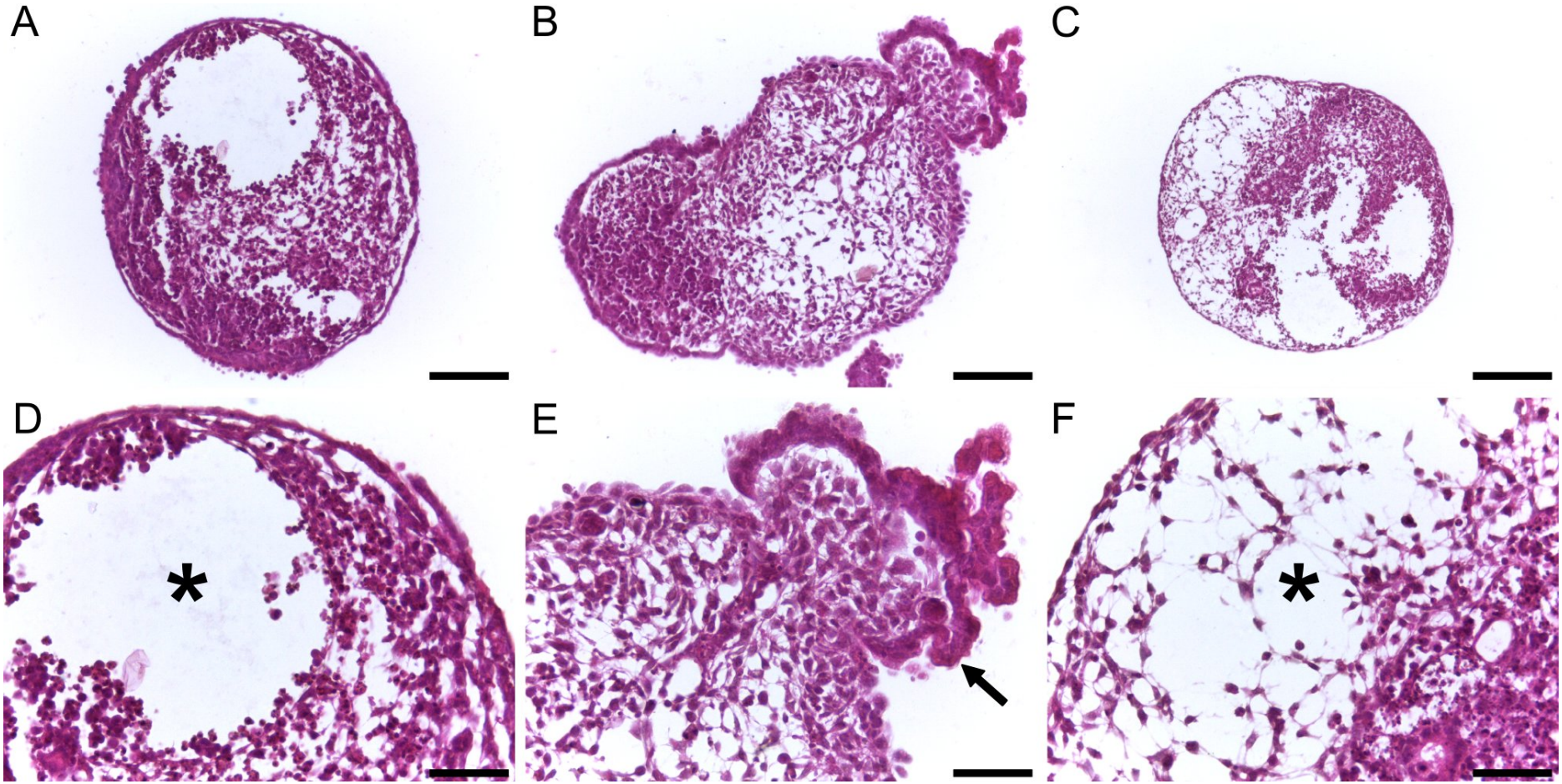

Figure 30: Murine Embryoid Bodies after 5 days suspension culture with 20% FBS.

Haematoxylin and eosin stained 6 µm paraffin sections of p9 mEBs cultured for 5 days in suspension. Cavities were visible in many mEBs after 5 days (asterisk, D) indicating that cavitation had taken place. Differentiated cell types were visible and formed extrusions on the surface of many mEBs (arrow, E). Mesenchymal tissue was evident that may have represented mesodermal or parietal endodermal mesenchyme. Scale bars represent 200 µm (C), 100 µm (A, and B) and 50 µm (D, E, and F). Bright-field images were taken using a Leica ICC50HD microscope and a 4x (C), 20x (A, and B), or 40x objective (D, E, and F).

To identify the differentiated cell types that had formed in mEBs after 5 days in suspension, immunohistochemistry was employed. Immunostaining against E-cadherin (E-cad), GATA4, and collagen-IV (col-IV) indicated the development of endodermal lineages in p26 and p9 mEBs cultured with 10% and 20% FBS, respectively. E-cad$^+$ epithelial cells partially covered the surfaces of mEBs, frequently covering an extrusion of cells at the surface, and also formed rudimentary internal epithelial structures or small clusters of E-cad$^+$ cells (**Figure 31A&D** and **Figure 32**). Col-IV staining was frequently observed in association with E-cad$^+$ cells, suggesting that these epithelial cells produced a basement membrane (**Figure 31C&F** and **Figure 34**). GATA4 was expressed in many cells within E-cad$^+$ epithelial regions of mEBs, including internal epithelial structures and external epithelial coverings (**Figure 31B&E** and **Figure 33**). Interestingly, col-IV expression was also seen in some E-cad$^-$ regions (asterisk , **Figure 34A&C**), and one region of external epithelial tissue covering one p9 mEB had not produced a basement membrane (asterisk, **Figure 34D**).

The E-cad$^+$;GATA4$^+$;col-IV$^+$ epithelial cells identified in mEBs after 5 days suspension culture were indicative of visceral or definitive endoderm development—as both endodermal lineages share the expression of many genes inlcuding E-cad, GATA4, and col-IV (Rojas et al., 2010). Using only these markers, however, it was difficult to determine the exact identity of these endodermal tissues. It was likely that multiple lineages had developed because not all of the cell populations identified shared the same characteristics (e.g. produced a basement membrane) or showed expression of all three markers. GATA4 expression was detected in many cells of the mesenchyme that developed within p9 mEBs (arrows, **Figure 33A**), which is consistent with *in vivo* analyses where GATA4 is expressed in the embryonic mesoderm (Arceci et al., 1993; Rojas et al., 2010). Immunostaining, therefore, indicated the development of endodermal and mesodermal lineages.

Some mEBs were also maintained for longer periods in suspension. After around 9 days in suspension, spontaneous pulsatile contractions within p9 mEBs became apparent under phase-contrast microscopy. Spontaneous contraction was observed in the majority of mEBs after 9 days in suspension (71%, n = 14). Cardiomyocte differentiation and spontaneous contraction is a well-known phenomenon in mEBs and has been reported previously (Doevendans et al., 2000). Phase-contrast images of mEBs in suspension revealed that contractile activity occurred in regions of reduced cell density where aggregates appeared translucent (black asterisk, **Figure 35**). mEBs also contained more cell dense regions that appeared opaque under phase-contrast microscopy and were non-contractile (white asterisk, **Figure 35**). In one mEB, a band of contractile cells appeared to have formed a tube that contracted in unison (arrows, **Figure 35A&D**). Unfortunately, these samples were lost and further histological analysis was unable to be performed.

It was interesting that contractions originated from less cell dense regions that may have corresponded to embryonic mesenchyme identified in haematoxylin and eosin stained sections of 5 day p9 mEBs (**Figure 30**). GATA4 is expressed early in cardiomyocyte differentiation and is important for cardiac development (Arceci et al., 1993). GATA4 expression that was detected in a proportion of cells in the mesenchyme of p9 mEBs after 5 days in suspension may be indicative of early cardiomyocyte differentiation that later resulted in spontaneous contractions.

Together, these data reveal that mEB formation from CGR8 mESCs induces spontaneous differentiation towards mesodermal and endodermal lineages. In order to determine the development potential of mEBs cultured as tissue-discs for extended periods, mEBs were maintained using Alvetex®3D polystyrene scaffold membranes.

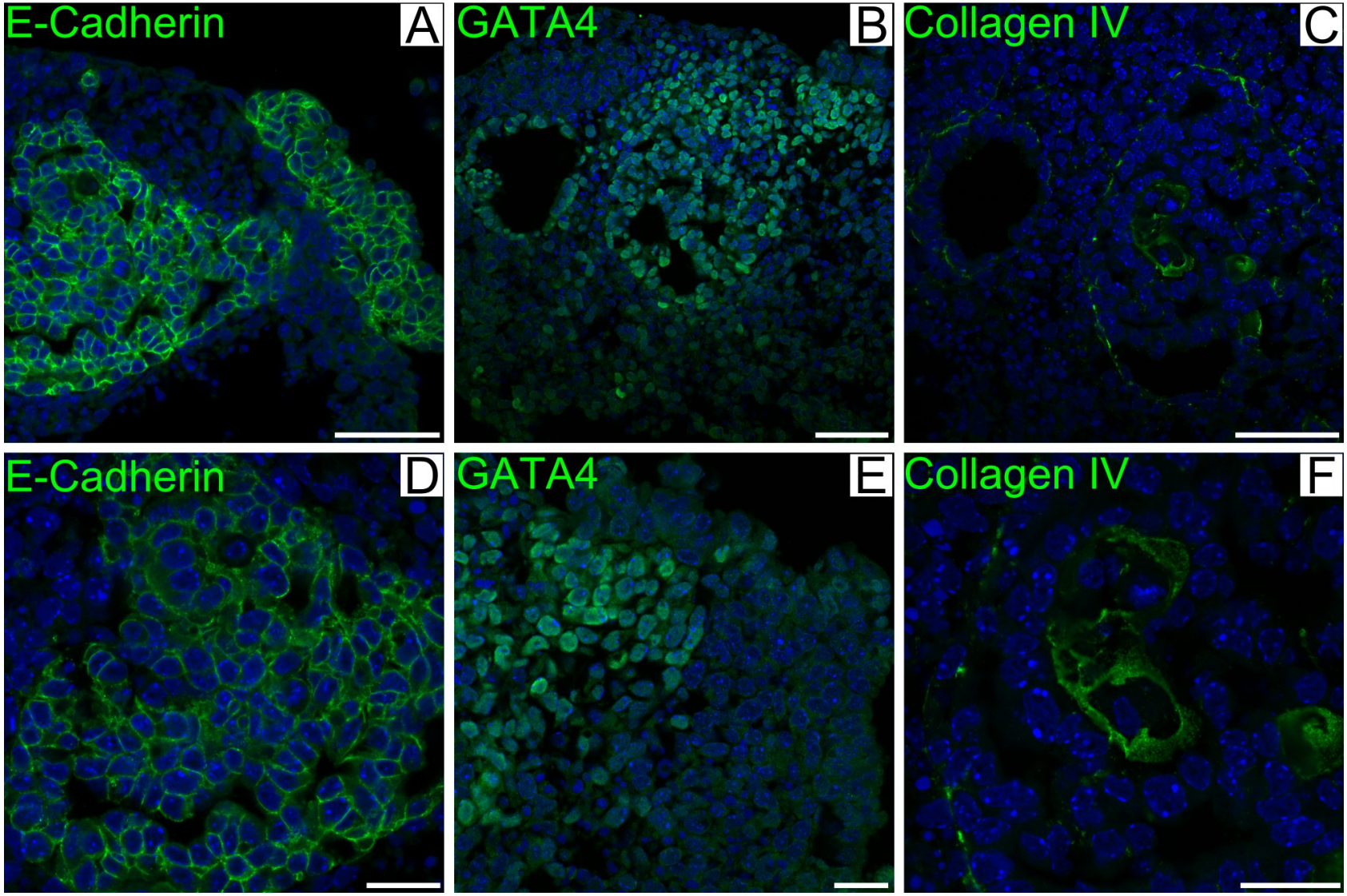

Figure 31: Immunohistochemical analysis of p26 CGR8 mEBs after 5 days suspension culture

Immunostaining against E-cadherin (E-cad), GATA4,, and collagen-IV (col-IV) was performed on 6 µm paraffin transverse sections of p26 CGR8 mEBs cultured in suspension with 10% FBS for 5 days. E-cad$^+$ cells were seen as an extrusion on the mEB surface and formed internal epithelial structures within aggregates (A, and D). Many E-cad$^+$ cells were also GATA4$^+$ (B, and E) and col-IV$^+$ (C, and F), indicative of endodermal differentiation. Scale bars represent 50 µm (A-C) and 20 µm (D-F). Images were taken using a Zeiss 880 CLSM using a 40x (A-C) and 63x objective (D-F).

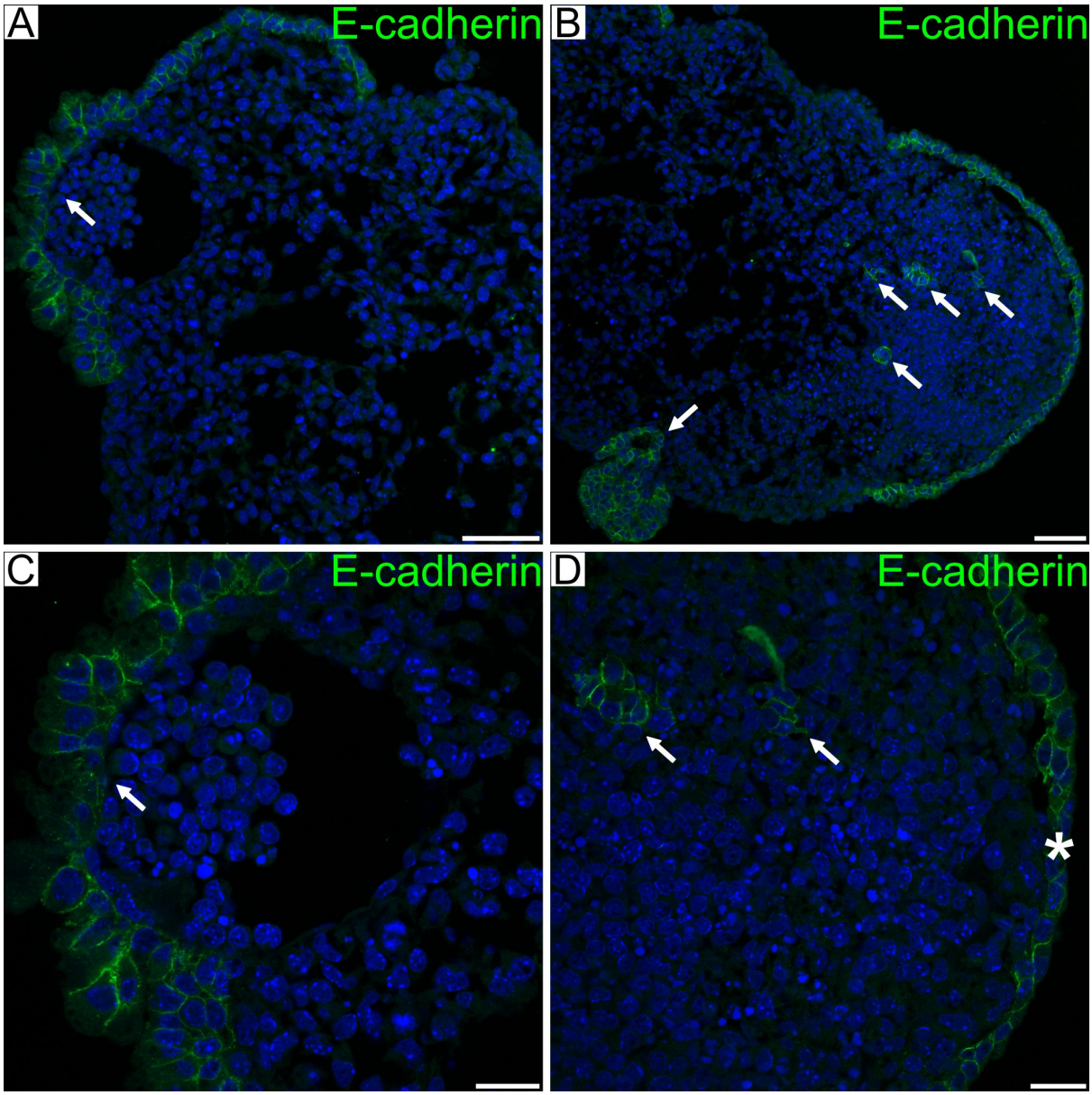

Figure 32: E-cadherin expression in p9 mEBs after 5 days suspension culture.

Immunostaining against E-cadherin (E-cad) was performed on 6 µm paraffin transverse sections of p9 CGR8 mEBs cultured in suspension with 20% FBS for 5 days. E-cad was expressed in cells that partially covered the exterior of mEBs (arrows, A, and asterisk, D) as well as in a small number of cells within cell dense regions of aggregates (arrows, B, and D). Scale bars represent 50 µm (A, and B) and 20 µm (C, and D). Images were taken using a Zeiss 880 CLSM using a 20x (A, and B) and 63x objective (C, and D).

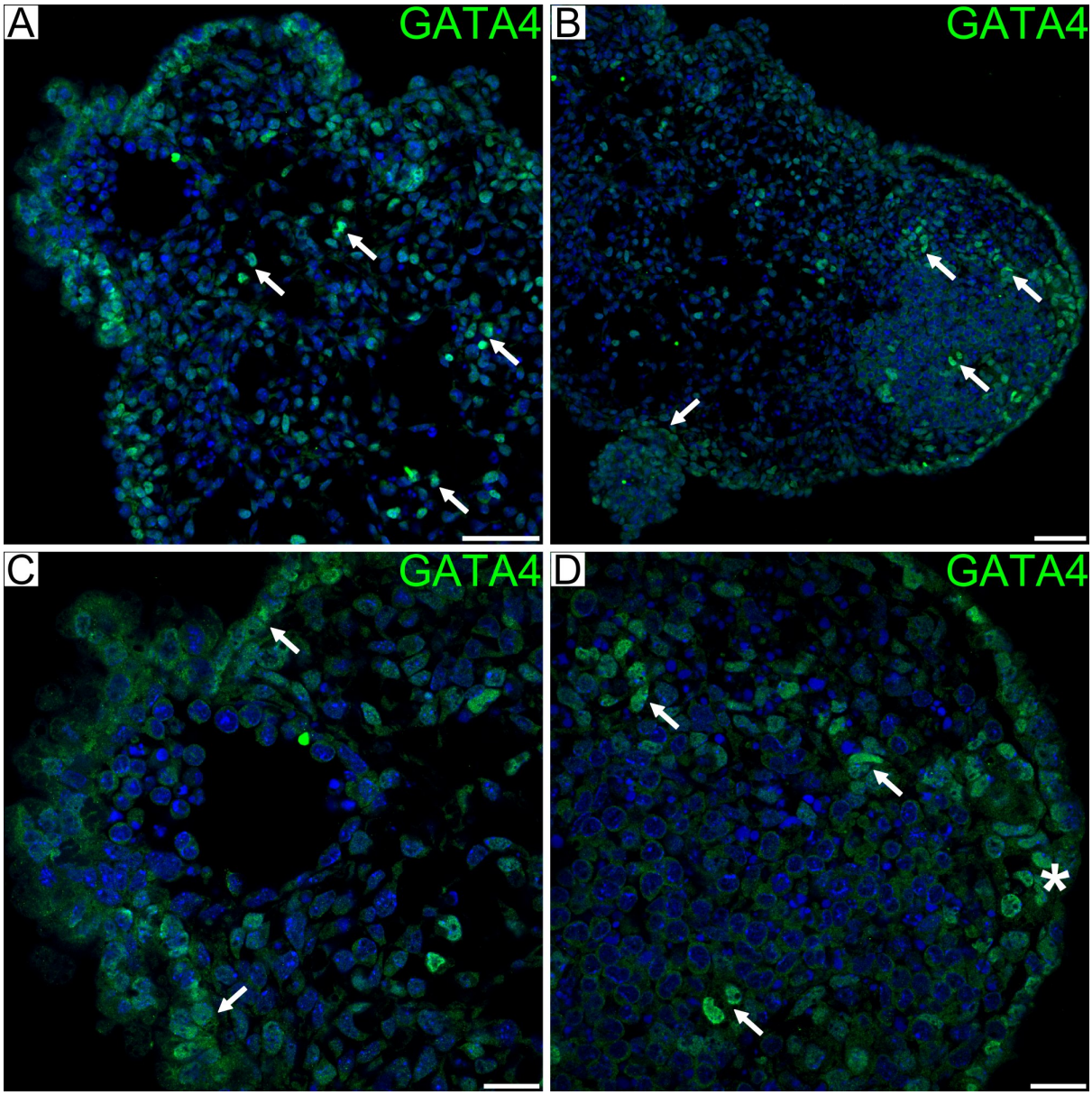

Figure 33: GATA4 expression in p9 mEBs after 5 days suspension culture.

Immunostaining against GATA4 was performed on 6 µm paraffin transverse sections of p9 CGR8 mEBs cultured in suspension with 20% FBS for 5 days. GATA4 was expressed in the majority of E-cad$^+$ epithelial cells that formed external epithelial coverings of mEBs (arrows, C, and asterisk, D) and a small number of cells in cell dense regions (arrows, C, and D) that corresponded to E-cad$^+$ cells that were observed in these regions. GATA4 expression was also detected in a proportion of cells in mesenchymal regions within mEBs (arrows, A). Scale bars represent 50 µm (A, and B) and 20 µm (C, and D). Images were taken using a Zeiss 880 CLSM using a 20x (A, and B) and 63x objective (C, and D).

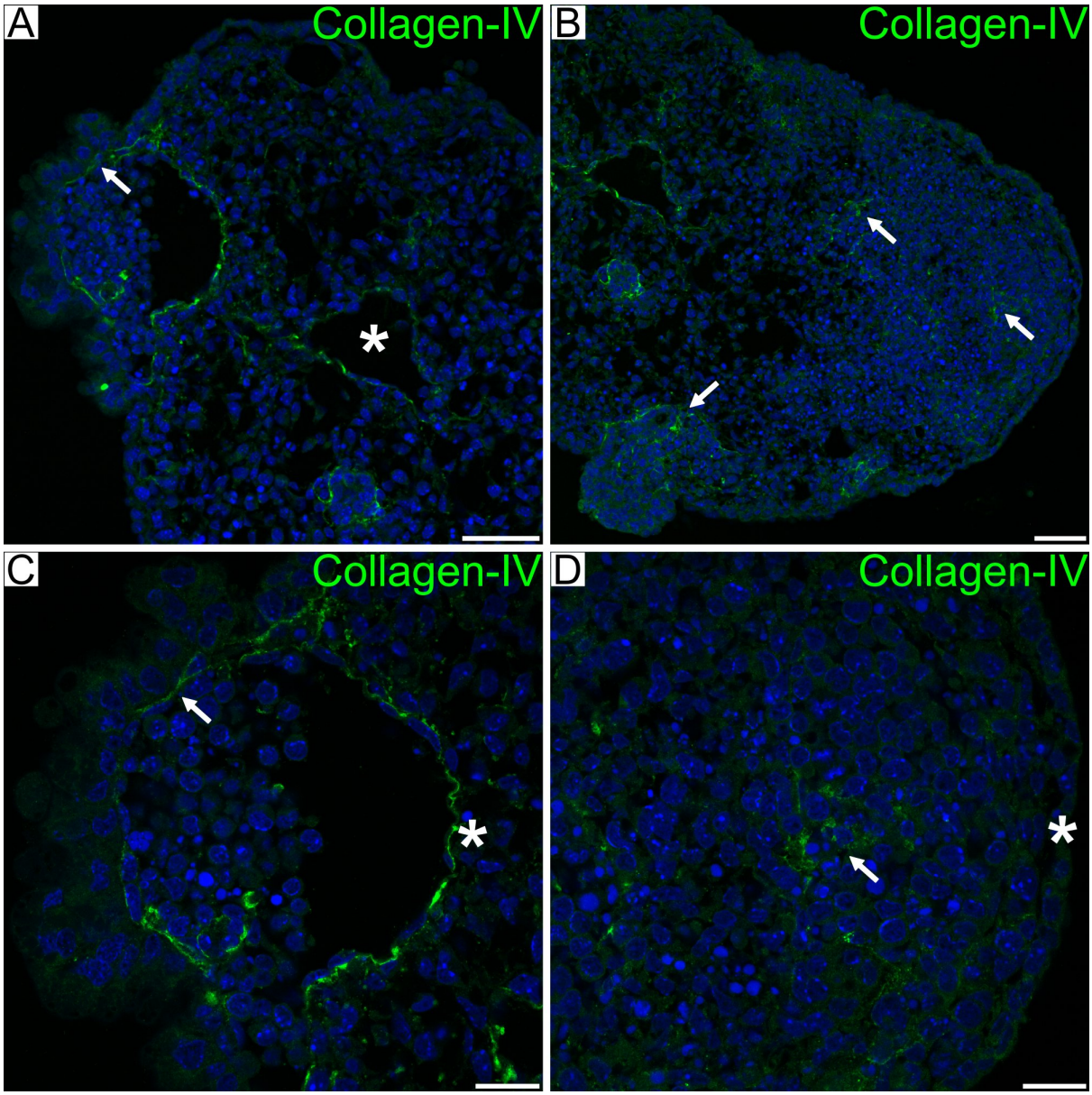

Figure 34: Collagen-IV expression in p9 mEBs after 5 days suspension culture.

Immunostaining against collagen-IV (col-IV) was performed on 6 µm paraffin transverse sections of p9 CGR8 mEBs cultured in suspension with 20% FBS for 5 days. Col-IV staining was detected in external and internal regions that were E-cad^{+};GATA4^{+} indicating that these epithelial cells had produced a basement membrane (arrows in A, B, C, and D). However, one external epithelial covering was found to not express col-IV (asterisk, D), and col-IV staining was seen in other regions that did not express E-cad (asterisk, A and C). Scale bars represent 50 µm (A, and B) and 20 µm (C, and D). Images were taken using a Zeiss 880 CLSM using a 20x (A, and B) and 63x (C, and D) objective.

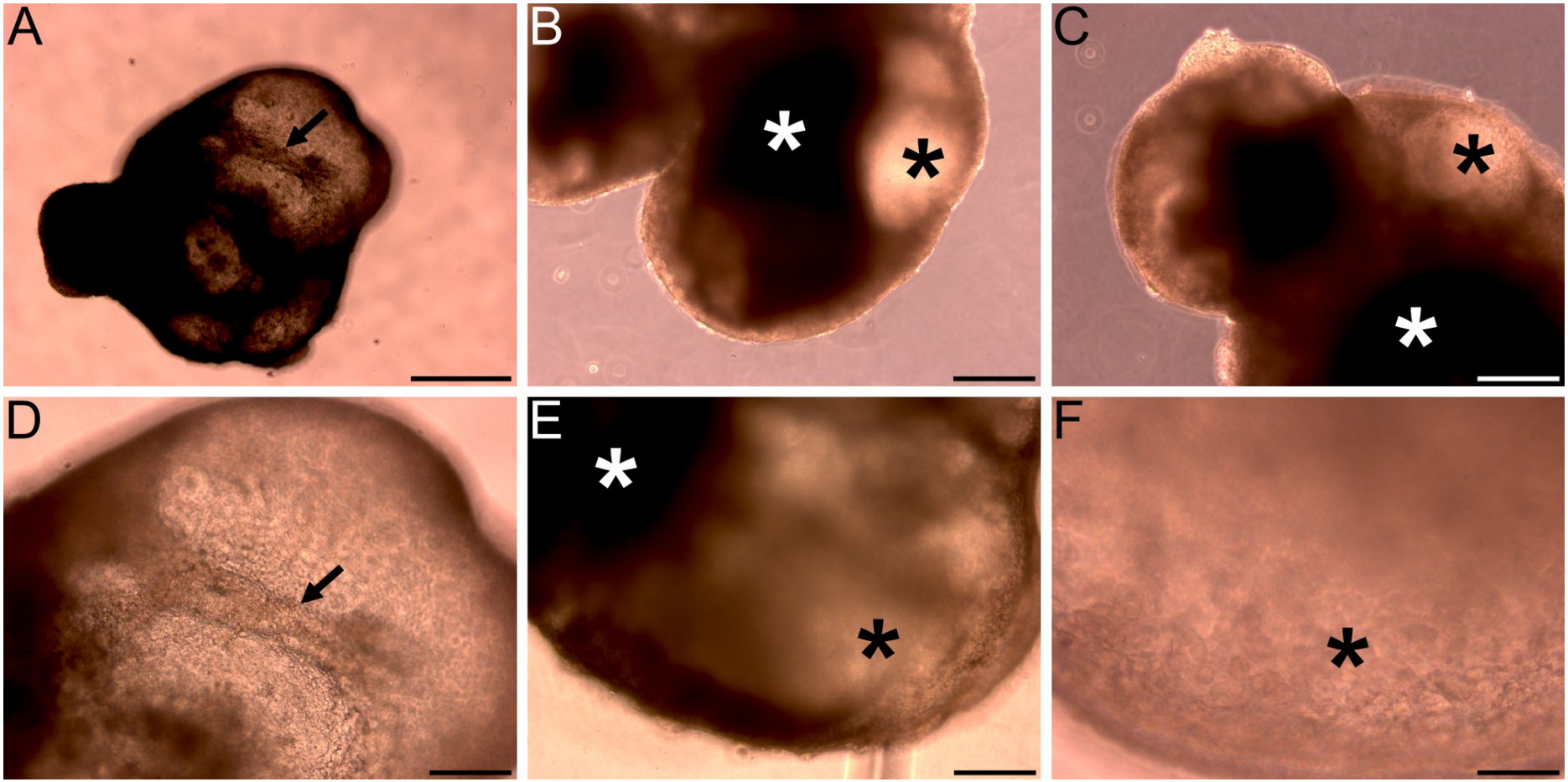

Figure 35: Phase-contrast images of p9 mEBs after 9 days suspension culture.

p9 mEBs were heterogeneous in structure and contained regions of high (white asterisks) and low cell density (black asterisks). mEBs underwent spontaneous contractions that originated in cells within translucent regions (white asterisks). In one mEB, a band of contractile cells formed a fibre that contracted in unison. Scale bars represent 500 µm (A), 200 µm (B, and C), 100 µm (D, and E), 50 µm (F). Images were taken using a Leica DMI300B inverted phase-contrast microscope using 4x (A), 10x (B, and C), 20x (D, and E), and 40x (F) objectives.

3.6.1 Murine Embryoid Bodies Cultured Using 3D scaffolds

p26 mEBs were cultured in suspension with 10% FBS for 5 days followed by a further 14 days culture using Alvetex®Scaffold (40 µm average pore size), Strata (20 µm average pore size), and Polaris (4 µm average pore size). Cells migrated long distances away from aggregates within the scaffold of mEBs cultured using Alvetex®Scaffold and Strata (**Figure 36**). It was evident from haematoxylin and eosin stained paraffin transverse sections that cells from aggregates cultured using Alvetex®Scaffold migrated significantly further (mean = 4475 mm, n = 4) than cells from aggregates cultured using Alvetex®Strata (mean = 1425 mm, n = 3) and this difference was found to be extremely statistically significant (unpaired t-test; $P < 0.0001$). Similar to hEC aggregates, mEBs developed into an intact tissue-disc when cultured using Alvetex®Polaris, with no evidence of cells penetrating the membrane below (asterisks, **Figure 37A&D**).

Organised tissue structures could be identified by routine histology and qualitative observation of p26 mEBs cultured using Alvetex®Polaris. Internal cavities lined with cuboidal epithelial cells were seen (asterisks, **Figure 37C&F**). These epithelial cavities may have represented the development of extraembryonic structures such as the yolk sac, or alternatively, embryonic structures such as the primitive gut tube (Rojas et al., 2010). Distinct epithelial cell types including columnar epithelial cells were located at the external surface of some aggregates and in one aggregate formed villi (asterisks, **Figure 37B&D**)(Bosse et al., 2006). Proteinaceous regions were associated with epithelia (arrows, **Figure 37C&F**) and were thought to represent mesodermal connective tissues that support epithelial tissues during embryonic development (Rojas et al., 2010).

Immunohistochemical analysis confirmed mesodermal differentiation through detection of α-smooth muscle actin (αSMA) expression in supportive connective tissue underlying internal epithelial cavities and in a small number of cells throughout the aggregate (**Figure 38B&D**). Ectodermal differentiation was indicated through positive staining for the neural marker TUJ1 (**Figure 38A&C**). However, the morphology of TUJ1$^+$ cells seemed inconsistent with neuroectodermal development and neuroepithelial structures were absent. It is also possible that TUJ1 expression reflected the development of the testis (as CGR8 is a male mESC line) or of highly proliferative cells, that both express β-III-tubulin (De Gendt et al., 2011; Katsetos et al., 2003; Ferrandina et al., 2006).

In further experiments mEBs were maintained using Alvetex®Polaris because it was shown to promote formation of an intact tissue-disc that supported the development of complex tissues over prolonged *in vitro* culture.

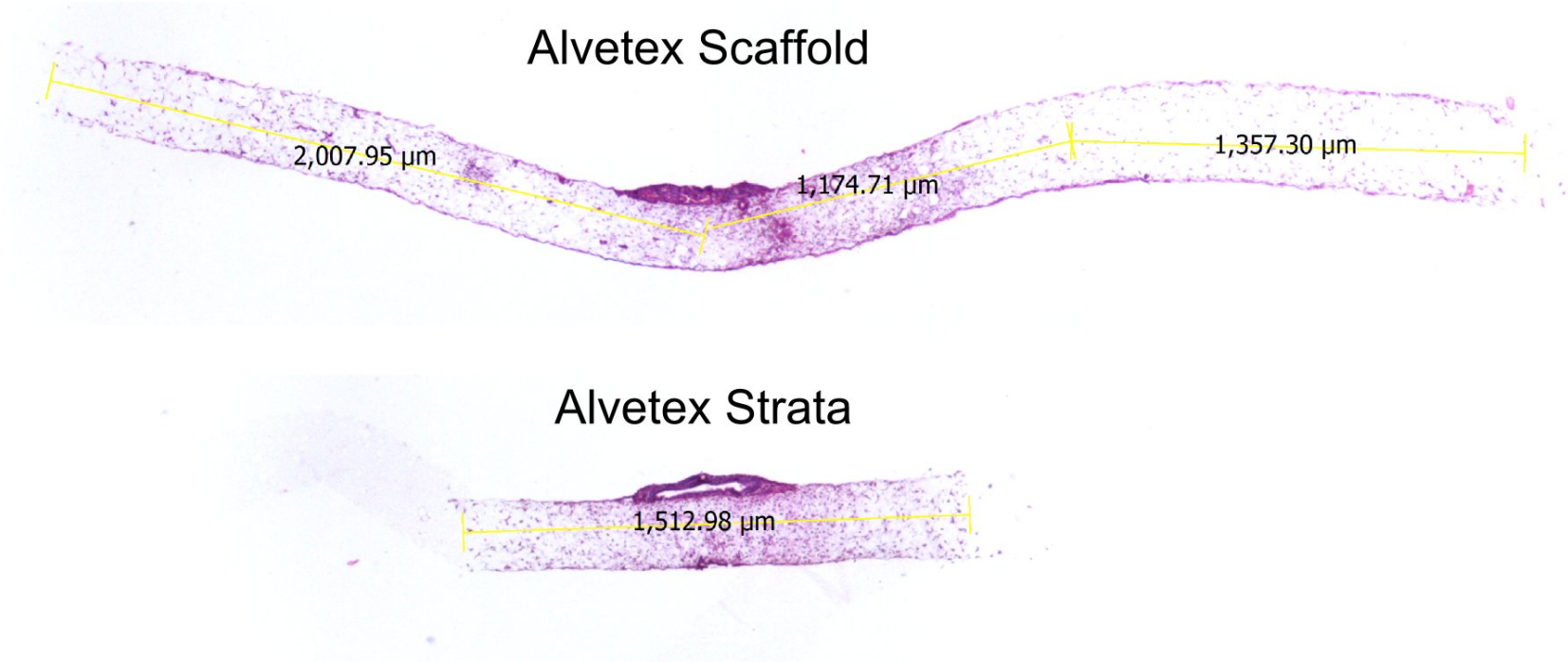

Figure 36: Histological analysis of mEBs after 5 days suspension culture followed by 14 days maintenance using Alvetex®Scaffold and Strata.

Haematoxylin and eosin stained 8 µm paraffin transverse sections of p26 mEBs cultured for 5 days in suspension with 10% FBS followed by 14 days maintenance using Alvetex®Scaffold and Strata. Cells left aggregates and migrated extensive distances within the scaffold of mEBs cultured using Alvetex®Scaffold and Strata. Alvetex®Scaffold (with a pore size of 40 µm) facilitated an average migration of 4475 µm and cells migrated an average of 1425 µm within Alvetex®Strata (unpaired t-test; $P < 0.0001$). Bright-field images were taken using a Leica ICC50HD microscope and a 4x objective.

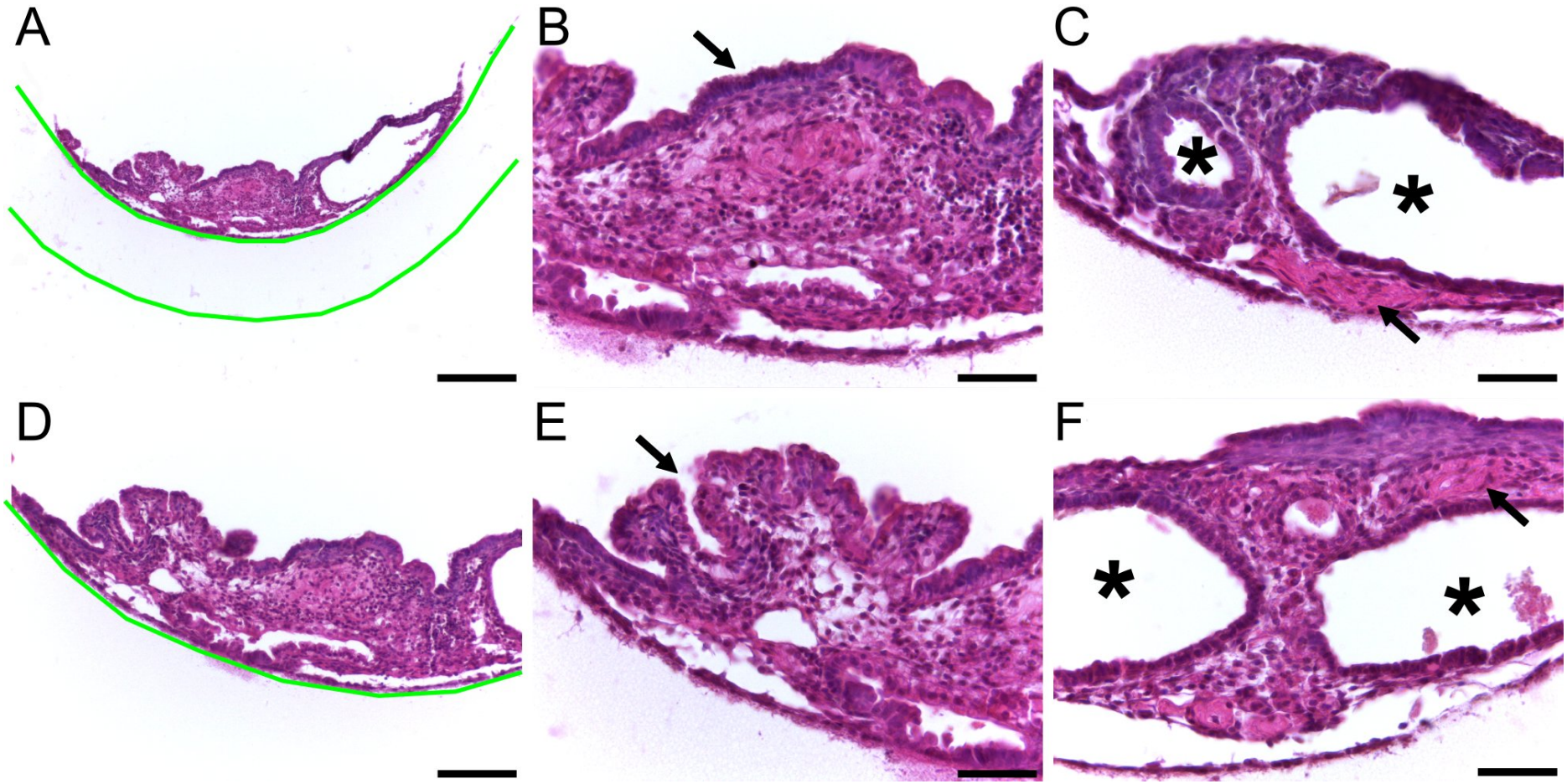

Figure 37: Histological analysis of mEBs after 5 days suspension culture followed by 14 days maintenance using Alvetex®Polaris.

Haematoxylin and eosin stained 8 µm paraffin transverse sections of p26 mEBs cultured for 5 days in suspension followed by 14 days maintenance using Alvetex®Polaris. No cells were found to have left mEBs or migrated within the Polaris membrane (A, and D). Endoderm-like internal epithelial cavities were seen that contained cuboidal epithelial cells (asterisks, C and F) and were surrounded by proteinaceous connective tissues (arrows, C and F). Columnar epithelial cells were seen on the exterior of mEBs (arrows, B and E) that appeared to have formed villi possibly representating gastrointestinal epithelium (arrows, E). Scale bars represent 200 µm (A), 100 µm (D), and 50 µm (B, C, E, and F). Bright-field images were taken using a Leica ICC50HD microscope and 10x (A), 20x (D), and 40x (B, C, E, and F) objectives.

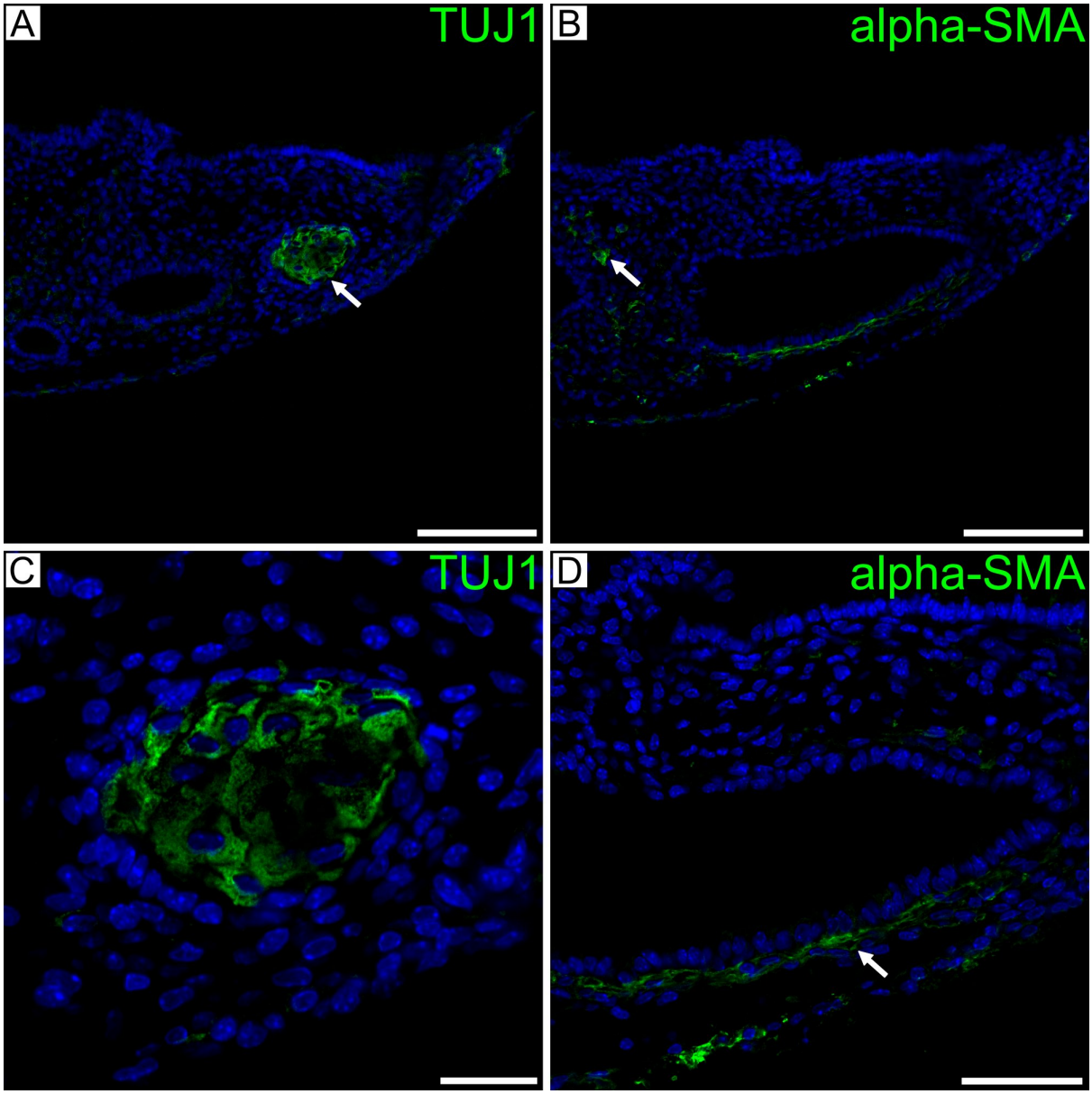

Figure 38: Immunohistochemical analysis of mEBs after 5 days suspension culture followed by 14 days growth using Alvetex®Polaris.

Immunostaining against TUJ1 and αSMA in 8 μm paraffin transverse sections of p26 mEBs cultured for 5 days in suspension followed by 14 days growth using Alvetex®Polaris indicated neurectodermal and mesodermal differentiation, respectively. TUJ1$^+$ cells were located in a small cluster (arrow, A) and were not typically neural in appearance with no evidence of neuroepithelial structures (C). αSMA staining was seen in a layer of connective tissue below an internal epithelial cavity (arrow, D) as well as in individual cells throughout the aggregate (arrow, B). Scale bars represent 100 μm (A, and B) and 50 μm (D), and 20 μm (C). Images were taken using a Zeiss 510 CLSM and a 20x (A and B) and 40x (C, and D) objective.

p9 mEBs that were maintained in suspension for 5 days with 20% FBS were grown as tissue-discs using Alvetex®Polaris. Histological analysis of one p9 mEB maintained as a tissue-disc for 16 days revealed the development of tissues representative of all three emrbyonic germ layers. Haematoxylin and eosin staining alongside Masson's trichrome staining facilitated the identification of internal endoderm-like epithelial tissue (asterisk, **Figure 39B&E**), mesodermal connective tissue (asterisk, **Figure 39C&F**), and an ectodermal keratin pearl (arrow, **Figure 39C&F**). Immunohistochemical analysis was used to examine tissue-specific marker expression in p9 mEBs cultured as tissue-discs for 16 days.

Columnar endoderm-like epithelial cells that developed in p9 mEBs after 16 days were E-cad$^+$ and supported by mesodermal connective tissue that contained α-SMA$^+$ fibroblastic cells, as is typically observed in the lamina propria underlying endodermal epithelial tissues *in vivo* (**Figure 40A&B**) (Storch et al., 2007; Young et al., 2000). The endodermal lineage that the epithelium derived from was difficult to identify histologically because there are a large number of embryonic and extraembryonic endodermal epithelial structures that exhibit similar features. E-cad staining supported histological evidence that a keratin pearl was seen (**Figure 40C**). However, staining for epidermal keratins such as keratin-14 would have been useful to investigate the developmental origins of the tissue further.

Immunohistochemical analysis suggested that complex tissues representative of all three embryonic germ layers developed in p9 mEBs cultured as tissue-discs for 16 days using Alvetex®Polaris. Next, p9 mEBs were maintained for up to 32 days using Alvetex®Polaris to determine if prolonged culture times impacted tissue development.

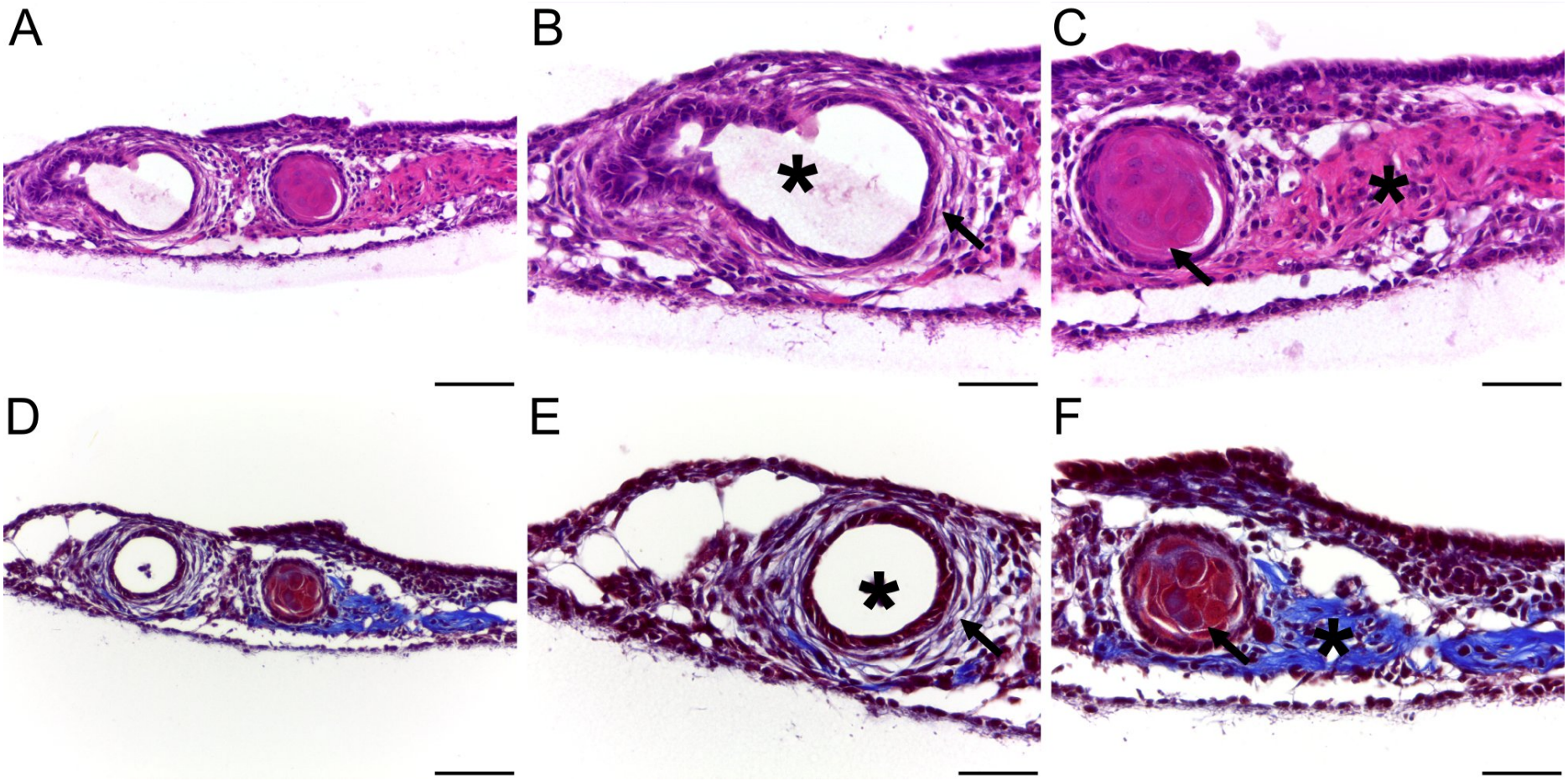

Figure 39: Histological analysis of one p9 mEB after 5 days in suspension followed by 16 days growth using Alvetex®Polaris

p9 mEBs were maintained in suspension for 5 days with 20% FBS and then cultured for a further 16 days using Alvetex®Polaris. Internal endoderm-like epithelium was evident (asterisk, B and E) and was surrounded by collagenous connective tissue that resembled the lamina propria (arrow, B and E). A large proteinaceous region of connective tissue was observed that was shown to contain collagen as it stained blue in Masson's trichrome (asterisk, C and F), indicative of mesodermal differentiation. A circular region of cells morphologically resembled a keratin pearl (arrow, C and F) and the fact that these cells were stained red in Masson's trichrome stain (indicative of keratin) supported this. Scale bars represent 100 µm (A, and D) and 50 µm (B, C, E, and F). Bright-field images were taken using a Leica ICC50HD microscope and a 20x (A, and D) or 40x (B, C, E, and F) objective.

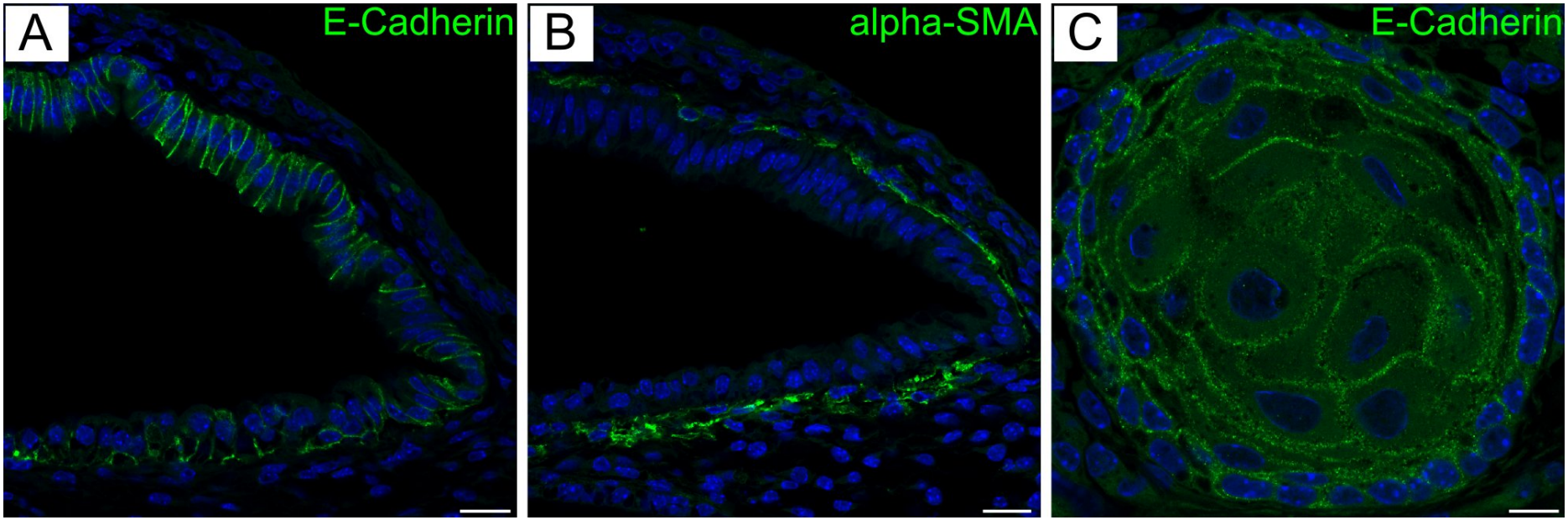

Figure 40: Immunohistochemical analysis of mEBs after 5 days in suspension followed by 16 days growth using Alvetex®Polaris

p9 mEBs were maintained in suspension for 5 days with 20% FBS and then cultured for a further 16 days using Alvetex®Polaris. Columnar endodermal cells expressed E-cadherin (A) and had a supporting layer of mesodermal connective tissue that resembled the lamina propria and contained fibroblastic cells expressing α-smooth muscle actin (B). Cells within a keratin pearl also expressed E-cadherin (C). Scale bars represent 20 µm (A, and B) and 10 µm (C). Images were taken using a Zeiss 880 CLSM and a 63x objective.

One p9 mEB that was maintained for 32 days using Alvetex®Polaris after 5 days in suspension developed to a significant size (2.3 mm in length and 946 µm in height) and contained a large cystic cavity with a diameter of 685 µm (asterisk, **Figure 41**). Histological analysis of this mEB revealed complex tissues including large amounts of collagenous fibrous connective tissue (**Figure 42A&D**), endoderm-like epithelium (**Figure 42B&E**), and neuroepithelium (**Figure 42C&F**).

Connective tissues that developed contained large amounts of collagen as indicated by blue staining in Masson's trichrome (**Figure 42A&D**). Cells were sparsely distributed through the collagenous ground substance that resembled the structure of elastic or hyaline cartilage that contains sparsely distributed chondrocytes contained within lacunae (Greep and Weiss, 1977). Alizarin Red staining was performed to investigate whether mineralisation of the connective tissue had occurred—which would have been indicative of early osteogenesis—but staining failed to identify any calcium deposition (data not shown).

Immunohistochemistry was employed to investigate the structure more closely of the endoderm-like epithelium identified in histologic sections. Immunostaining and high-resolution confocal microscopy revealed granules within cells that resembled mucin-containing granules found in goblet cells of secretory epithelia (arrows, **Figure 43B&C**) (Diaspro et al., 2006), suggesting that the epithelial tissue represented a secretory endodermal epithelium such as those lining the digestive and respiratory tracts (Greep and Weiss, 1977). Alternatively, the granules identified may also have represented vacuoles that are frequently observed in visceral endoderm (Wada et al., 2013). Analysis of tissue-specific markers such as muc2 (a marker of goblet cells) would be useful in order to identify the specific endodermal lineage that the endoderm-like epithelium derived from.

Immunohistochemistry was also used to detect neural marker TUJ1 expression in the region of tissue that resembled neuroepithelium. A neural rosette of $TUJ1^-$ neuroepithelial cells was visible (asterisks, **Figure 44B&C**) that was surrounded by $TUJ1^+$ mature neural cells (arrows, **Figure 44B&C**), demonstrating the *in vivo*-like nature of the neuroepithelium (Gotz and Huttner, 2005).

Culturing p9 mEBs for 5 days in suspension followed by 32 days using Alvetex®Polaris increased the diversity and complexity of differentiated tissues that developed in comparison to aggregates cultured for 16 days. Qualitative analysis of one 32 day mEB facilitated identification of highly complex differentiated tissues representative of all three germ layers including connective tissue, endodermal epithelium, and neural tissue. Taken together, these findings suggest that maintaining mEBs for extended periods as tissue-discs allows differentiation into complex *in vivo*-like tissues representative of all three germ layers. Maintenance of stem cell aggregates using 3D polystyrene scaffolds therefore offers a novel *in vitro* differentiation technique that may be used as an *in vitro* pluripotency assay.

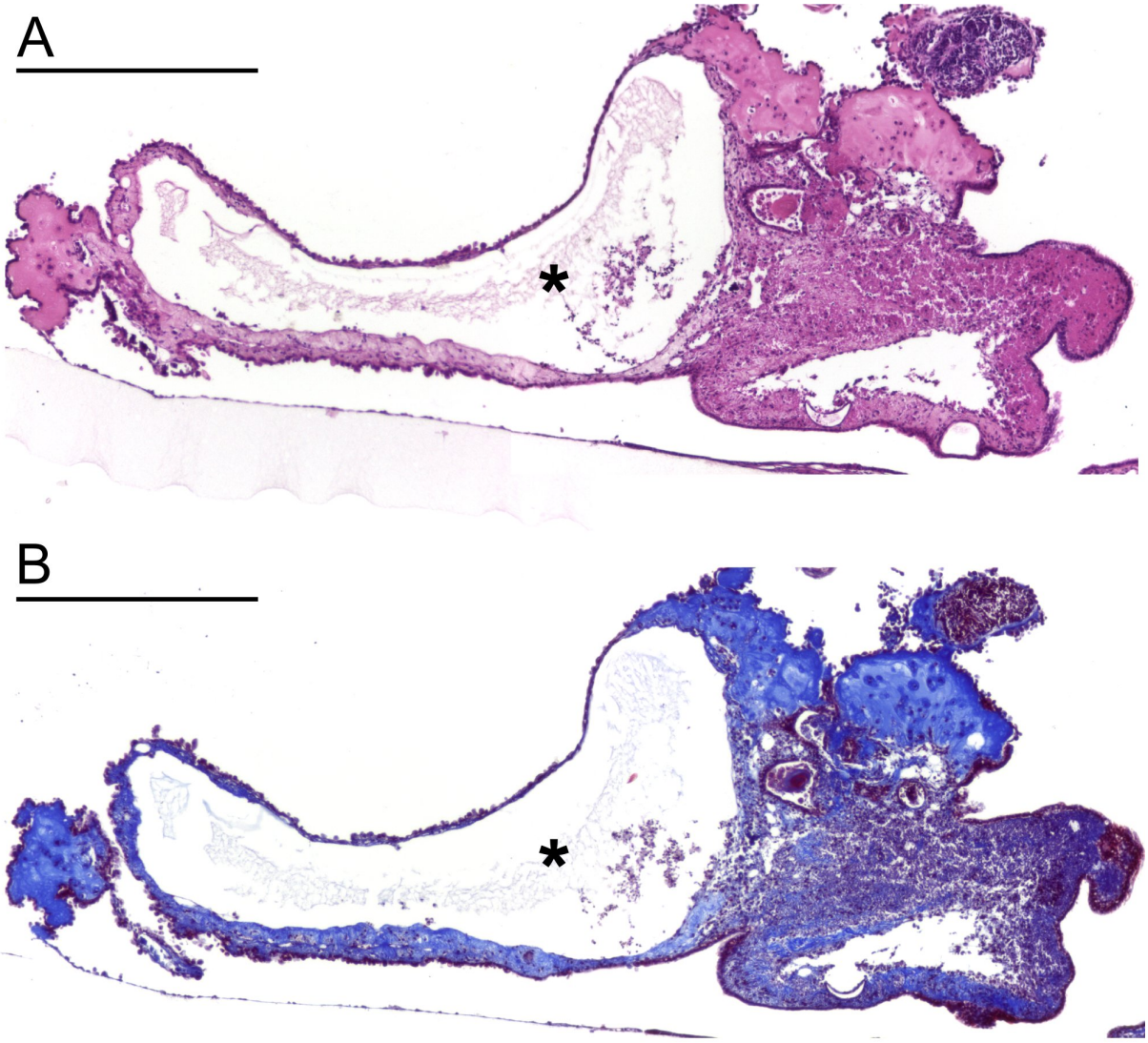

Figure 41: Gross morphology of one p9 mEB cultured for 5 days in suspension and then 32 days using Alvetex®Polaris.

Haematoxylin and eosin stain (A) and Masson's trichrome stain (B) of 8 µm paraffin transverse sections of one p9 mEB cultured for 5 days in suspension with 20% FBS followed by 32 days growth using Alvetex®Polaris. The aggregate grew to a substantial size with a length of 2.3 mm and a maximum height from the membrane of 946 µm. The aggregate contained a large epithelial cavity with a diameter of 685 µm (asterisks) and large amounts of collagenous connective tissue that appeared blue in Masson's trichrome stain (B). Scale bars represent 500 µm. Bright-field images were taken using a Leica ICC50HD microscope and a 4x objective.

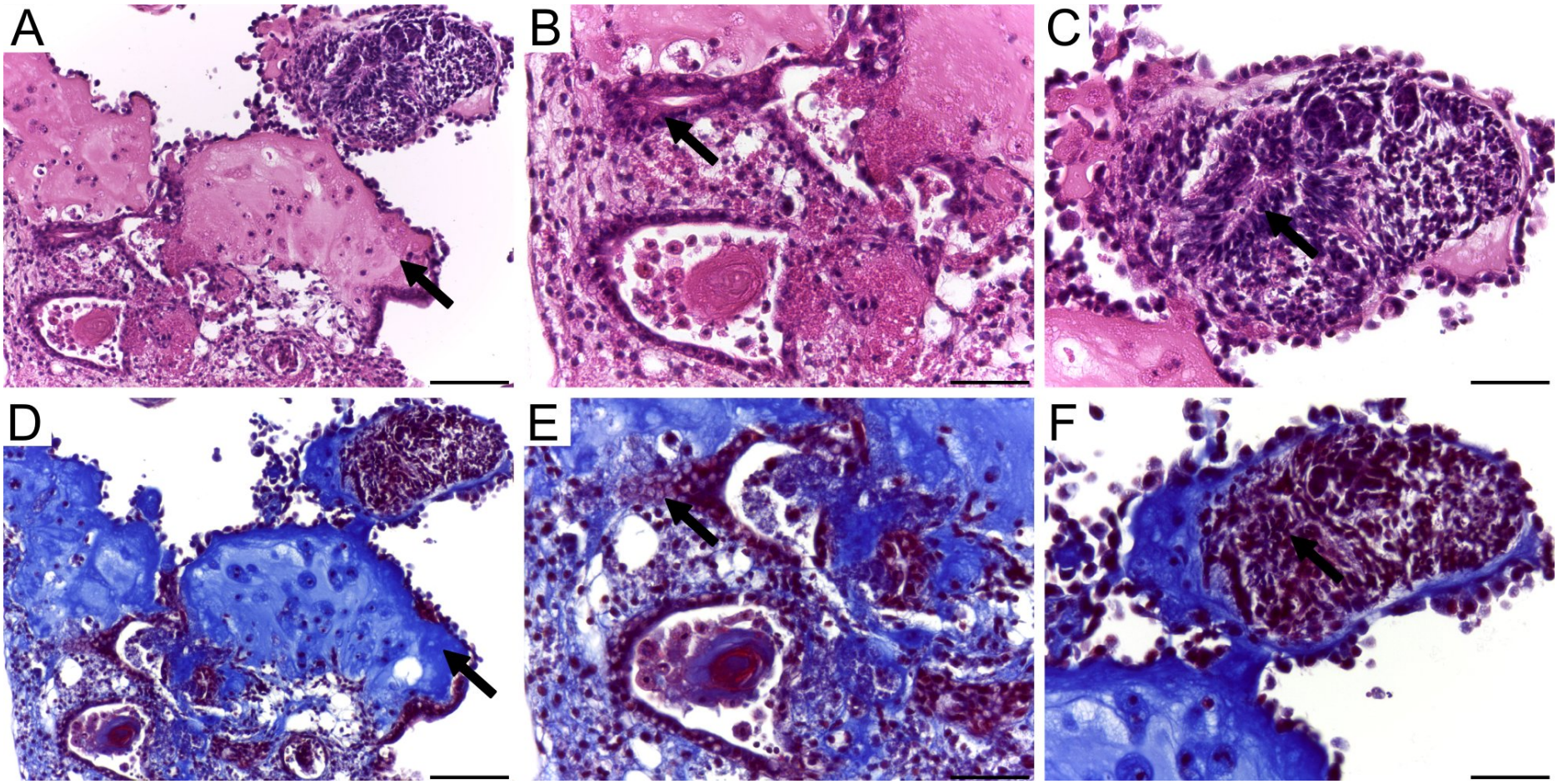

Figure 42: Histological analysis of one p9 mEB cultured in suspension for 5 days followed by 32 days maintenance using Alvetex®Polaris.

Haematoxylin and eosin staining (A-C) and Masson's trichrome staining (D-F) of 8 µm paraffin transverse sections of one p9 mEB cultured for 5 days in suspension with 20% FBS followed by 32 days growth using Alvetex®Polaris revealed the development of large and complex tissues. Large amounts of proteinaceous connective tissue had developed (arrow, A) that contained a few small cells sparsely scattered through abundant collagenous ground substance (arrow, D). Endodermal epithelium developed within the mEB and formed internal epithelial cavities (arrows, B and E). An isolated region of cells formed a structure that resembled neuroepithelium (arrows, C and F). Scale bars represent 100 µm (A, and D), and 50 µm (B, C, E, and F). Bright-field images were taken using a Leica ICC50HD microscope and a 20x (A, and D), or 40x objective (B, C, E, and F).

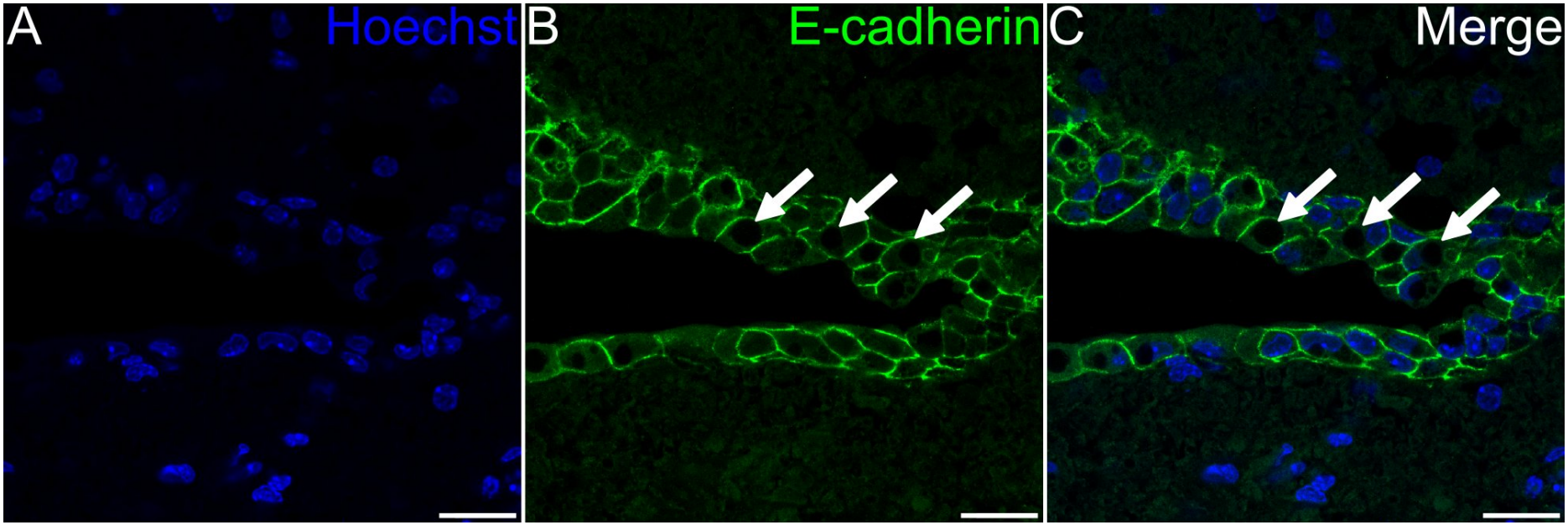

Figure 43: Immunostaining against epithelial marker E-cadherin in one p9 mEB after 32 days culture using Alvetex®Polaris.

Immunohistochemical analysis was performed on 8 µm paraffin transverse sections of one p9 mEB maintained in suspension for 5 days followed by 32 days culture using Alvetex®Polaris. E-cadherin staining identified epithelial cells within an endoderm-like epithelium. Epithelial cells contained dark regions (arrows, B and C), that may have represented granules of mucin—indicative of goblet cells—or vacuoles that are frequently observed in visceral endoderm (Wada et al., 2013). Scale bars represent 20 µm. Confocal images were taken using a Zeiss 880 CLSM and a 63x objective.

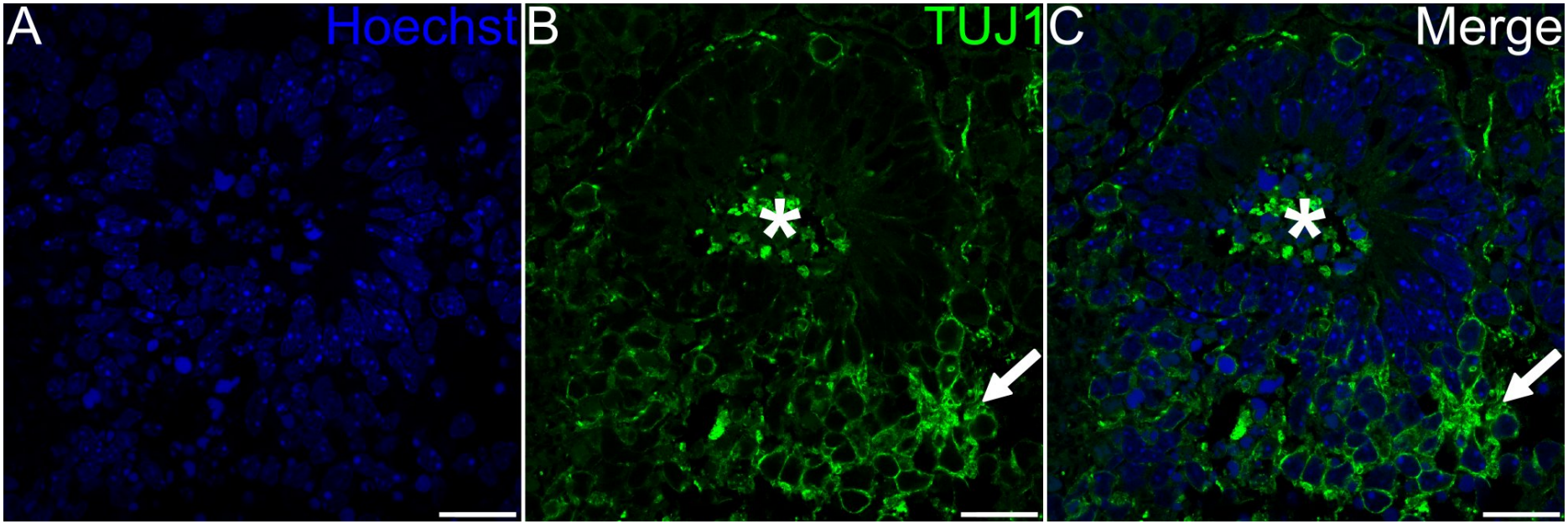

Figure 44: Immunostaining against neural marker TUJ1 in one p9 mEB after 32 days culture using Alvetex®Polaris.

Immunohistochemical analysis was performed on 8 µm paraffin transverse sections of one p9 mEB maintained in suspension for 5 days followed by 32 days culture using Alvetex®Polaris. TUJ1 staining identified neuroepithelial tissue that formed a neural rosette (asterisk, B and C) that contained $TUJ1^-$ neural progenitor cells and was surrounded by $TUJ1^+$ mature neurons (arrows, B and C). Scale bars represent 20 µm. Confocal images were taken using a Zeiss 880 CLSM and a 63x objective.

3.7 Manipulating Developmental Pathways to Direct Stem Cell Fate

A major goal in modern developmental and stem cell biology is to direct the differentiation of pluripotent stem cells to pure populations of defined somatic cell types *in vitro* that may be used for cell replacement therapies or for disease modelling and drug discovery (Murry and Keller, 2008). It was examined whether differentiation in CGR8 mEBs could be directed to specific lineages through manipulation of signalling pathways that are known to be important during embryonic development.

3.7.1 Bone Morphogenetic Protein Pathway

The BMP signalling pathway is pleiotropic during development and exhibits inductive or inhibitory effects in the specification of many somatic lineages (Li and Chen, 2013). BMP4 is indicated in the specification of the primitive streak and mesendodermal lineages and has been shown to reduce neural progenitor formation in mEBs (Finley et al., 1999). In the default model of neural plate specification, BMP inhibitors are required signals from the organiser to induce neural tissue in the embryonic ectoderm (Spemann and Mangold, 1924; Ozair et al., 2013).

To examine the effect of BMP inhibition on mESC differentiation, mEBs were maintained in suspension for 5 days with 20% FBS and in the presence of a small molecule antagonist of BMP signalling, dorsomorphin [1 µM]. Dorsomorphin elicits effects through selective inhibition of BMP type I receptors ALK2, ALK3, and ALK6 (Yu et al., 2008). Haematoxylin and eosin staining revealed stark differences between DMSO control and dorsomorphin-treated mEBs. DMSO control aggregates contained cystic cavities and mesenchymal regions that were typical of untreated mEBs (asterisks, **Figure 45C**). Dorsomophin-treated mEBs, however, were smaller than control mEBs (dorsomorphin mean diameter = 398 µm, n = 3; DMSO mean diameter = 672 µm, n = 3; unpaired *t*-test; $P = 0.011$), appeared more cell dense, and the majority failed to undergo cavitation (66%, n = 3), as has previously been reported (Coucouvanis and Martin, 1999) (**Figure 45B**). Small neuroepithelial structures were seen that resembled neural rosettes (arrows, **Figure 45D**), and immunohistochemistry was undertaken to examine the expression of neural markers.

Immunostaining revealed many small isolated regions of TUJ1 expression throughout dorsomorphin-treated aggregates that were not seen in DMSO control aggregates (arrows, **Figure 45A&B**, and data not shown). Typical neural rosettes were seen that were weakly positive for TUJ1 (asterisks, **Figure 46C&D**) and surrounded by more mature neurons that were strongly TUJ1$^+$ (arrows, **Figure 46C&D**).

These data reveal that differentiation could be directed towards neurectodermal lineages in mEBs in response to BMP inhibition. Next, dorsomorphin-treated mEBs were maintained as tissue-discs for extended periods using Alvetex®Polaris to determine the effect of prolonged culture on differentiation.

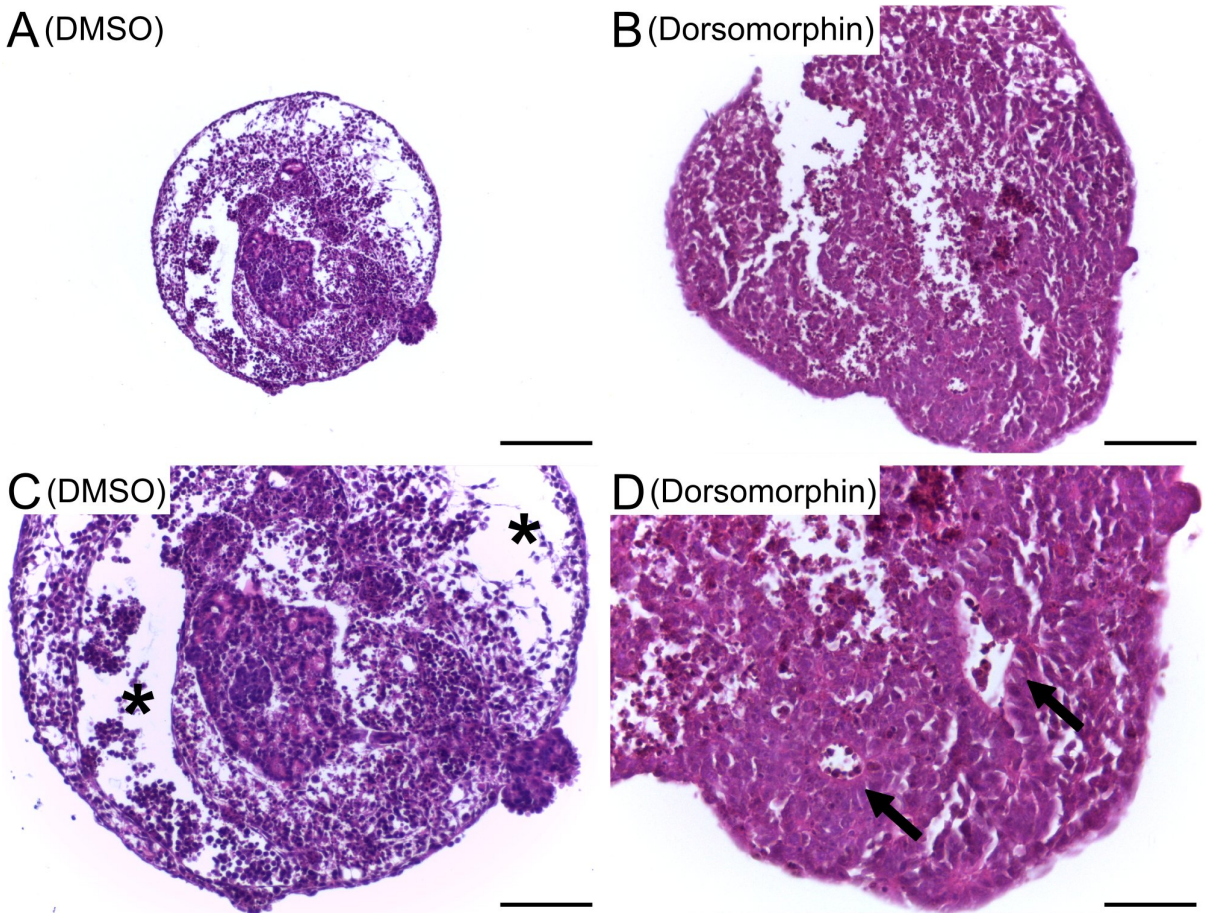

Figure 45: Histological analysis of p9 mEBs maintained in suspension for 5 days in the presence of dorsomorphin.

p9 mEBs were maintained in suspension with 20% FBS and [1 µM] dorsomorphin (or DMSO control) for 5 days and 6 µm paraffin transverse sections stained with haematoxylin and eosin. DMSO control aggregates (A, and C) underwent cavitation and developed mesenchymal regions (asterisks, C). Dorsomorphin-treated aggregates, however, failed to undergo cavitation in the majority of cases and formed smaller, more cell dense mEBs (B, and D). Neural rosette-like structures were seen, indicative of neurectodermal development (arrows, D). Scale bars represent 200 µm (A), 100 µm (B, and C), and 50 µm (D). Bright-field images were taken using a Leica ICC50HD microscope and a 10x (A), 20x (B, and C), or 40x objective (D).

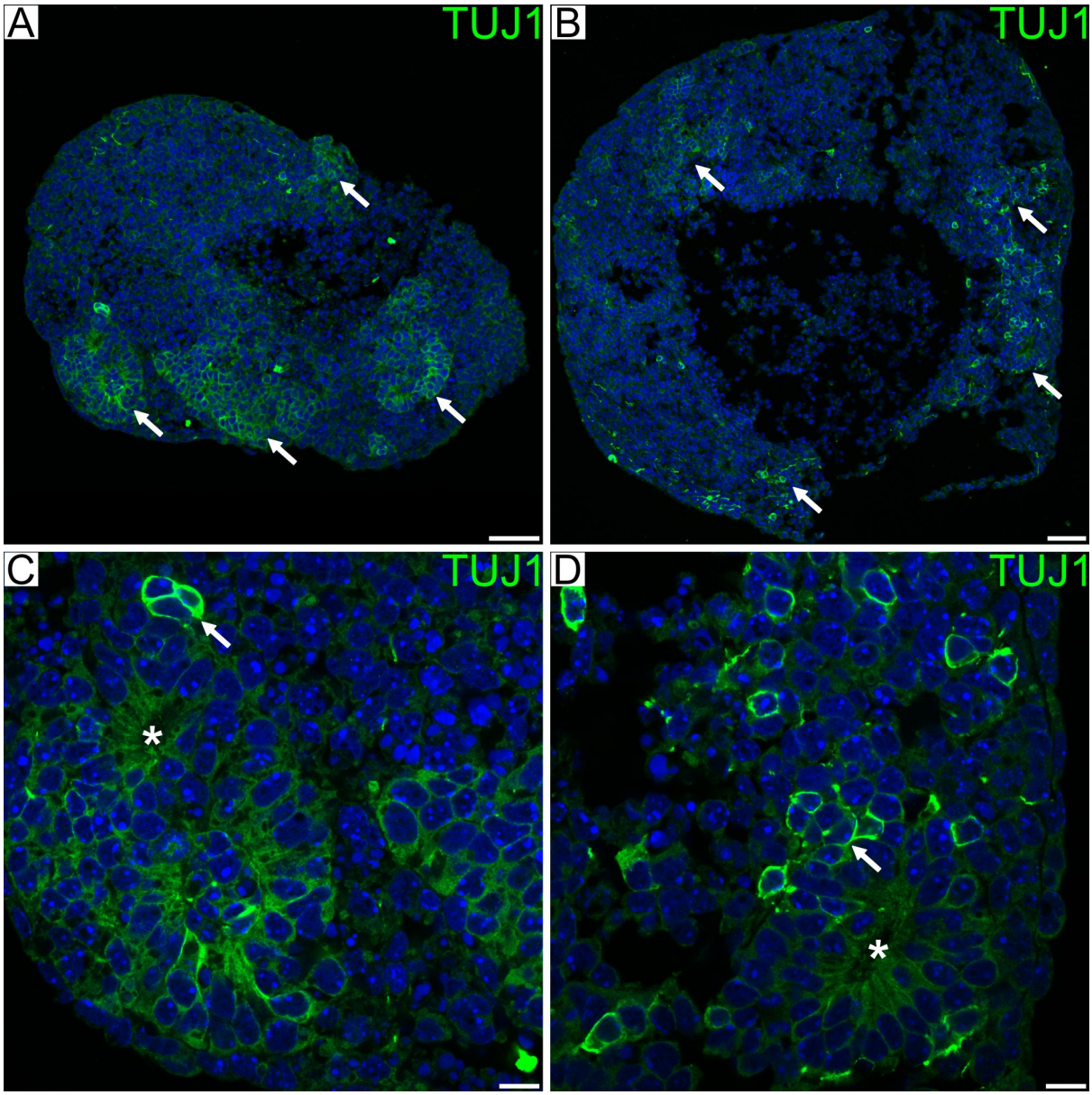

Figure 46: Immunohistochemical analysis of neural marker expression in dorsomorphin-treated mEBs after 5 days in suspension.

Immunostaining against neural marker TUJ1 was performed on 6 µm paraffin transverse sections of p9 mEBs maintained in suspension with 20% FBS in the presence of BMP antagonist dorsomorphin [1 µM]. TUJ1 expression was detected in isolated regions throughout mEBs after 5 days exposure to dorsomorphin (arrows, A and B). Typical neural rosettes were seen that were weakly positive for TUJ1 (asterisks, C and D) and surrounded by mature neurons that expressed TUJ1 strongly (arrows, C and D). Scale bars represent 50 µm (A, and B), and 10 µm (C, and D). Confocal images were taken using a Zeiss 880 CLSM and a 20x (A, and B), or 63x objective (C, and D).

p9 mEBs maintained in suspension for 5 days with 20% FBS and [1 µM] dorsomorphin were maintained using Alvetex®Polaris for 16 - 32 days. Histological analysis revealed that dorsomorphin-treated mEBs cultured as tissue-discs failed to develop endoderm-like epithelial tissues or mesodermal connective tissues that were prominent in DMSO-treated controls (**Figures 47&48**). This striking effect was seen in the majority of mEBs treated with dorsomorphin [1 µM] for 5 days followed by 16 or 32 days growth using Alvetex®Polaris (60%, n = 5).

In two mEBs examined, however, dorsomorphin appeared to have no affect on differentiation and there were no discernible differences compared to DMSO control mEBs. Large amounts of endoderm-like epithelium and mesodermal connective tissue was seen in one dorsomorphin-treated mEB maintained as a tissue-disc for 32 days (**Figure 49**). In haematoxylin and eosin stained transverse sections, eosinophilic enucleated biconcave discs were observed that resembled erythrocytes (arrows, **Figure 49C&F**) and had a mean diameter of 7.08 μm (n = 24) that is in agreement with the known diameter of erythrocytes of 7-7.2 μm (Young et al., 2000). Some of these cells were nucleated that is a feature of erythrocytes generated during yolk sac primitive haematopoiesis (**Figure 49C&F**). Interestingly, before tissue-discs were processed, a red colouration within some mEBs was observed and it was thought that media trapped within a cystic cavity could be responsible. However, the ability of mEBs to spontaneously generate blood-islands and embryonic erythrocytes is a well-known phenomenon and red colouration within mEBs has also been observed (Doetschman et al., 1985; Wang et al., 1992). This suggests that haematopoiesis occurred in mEBs cultured as tissue-discs but further analysis is required in order to confirm this.

Immunohistochemistry revealed TUJ1 expression in cells within some mEBs treated with dorsomorphin [1 µM] for 5 days and cultured for 16 days (arrow, **Figure 50A**) or 32 days using Alvetex®Polaris (arrow, **Figure 51A**), confirming that neural differentiation occurred in these mEBs. Infiltration of large numbers of $TUJ1^+$ neurites into the membrane below mEBs was observed (arrows, **Figure 50C**, and **Figure 51B**). However, many cells within mEBs did not express TUJ1 and in some cases developed into structures with non-neural morhology on the exterior of mEBs (asterisks, **Figure 51B&C**)). Further analysis of tissue-specific markers will be necessary in order to identify these non-neural cell types. Flow cytometry or other quantitative techniques should be performed to quantify the ratio of neural to non-neural cells induced in tissue-discs in response to dorsomorphin.

These data indicate that mESC differentiation can be robustly directed to neural lineages in tissue-discs through inhibition of BMP signalling by dorsomorphin. The ability of tissue-disc cultures to respond to other signalling pathways was also explored.

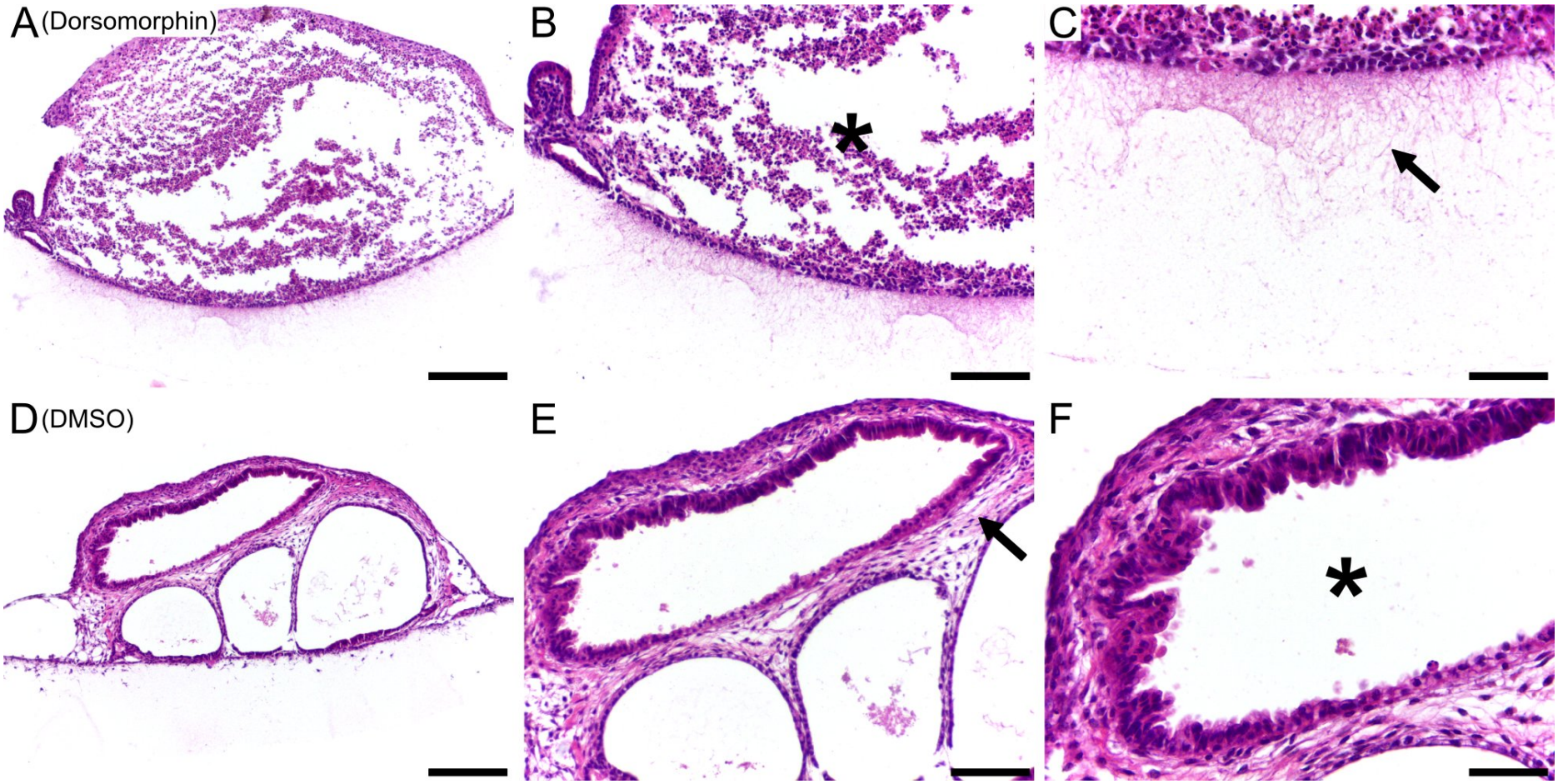

Figure 47: Histological analysis of p9 mEBs maintained in suspension with dorsomorphin for 5 days followed by 16 days culture using Alvetex®Polaris.

mEBs were maintained in suspension for 5 days in the presence of 20% FBS and [1 µM] dorsomorphin followed by 16 days maintenance using Alvetex®Polaris. Haematoxylin and eosin stained 8 µm paraffin transverse sections indicated a striking lack of endodermal epithelial cavities (asterisk, F) and mesodermal connective tissues (arrow, E) in dorsomorphin treated aggregates that were seen in DMSO controls. Instead, cells within mEBs underwent significant cell death (asterisk, B) and extended projections into the scaffold membrane below (arrow, C). Scale bars represent 200 µm (A, and D), 100 µm (B, and E), and 50 µm (C, and F). Bright-field images were taken using a Leica ICC50HD microscope and a 10x (A, and D), 20x (B, and E), or 40x objective (C, and F).

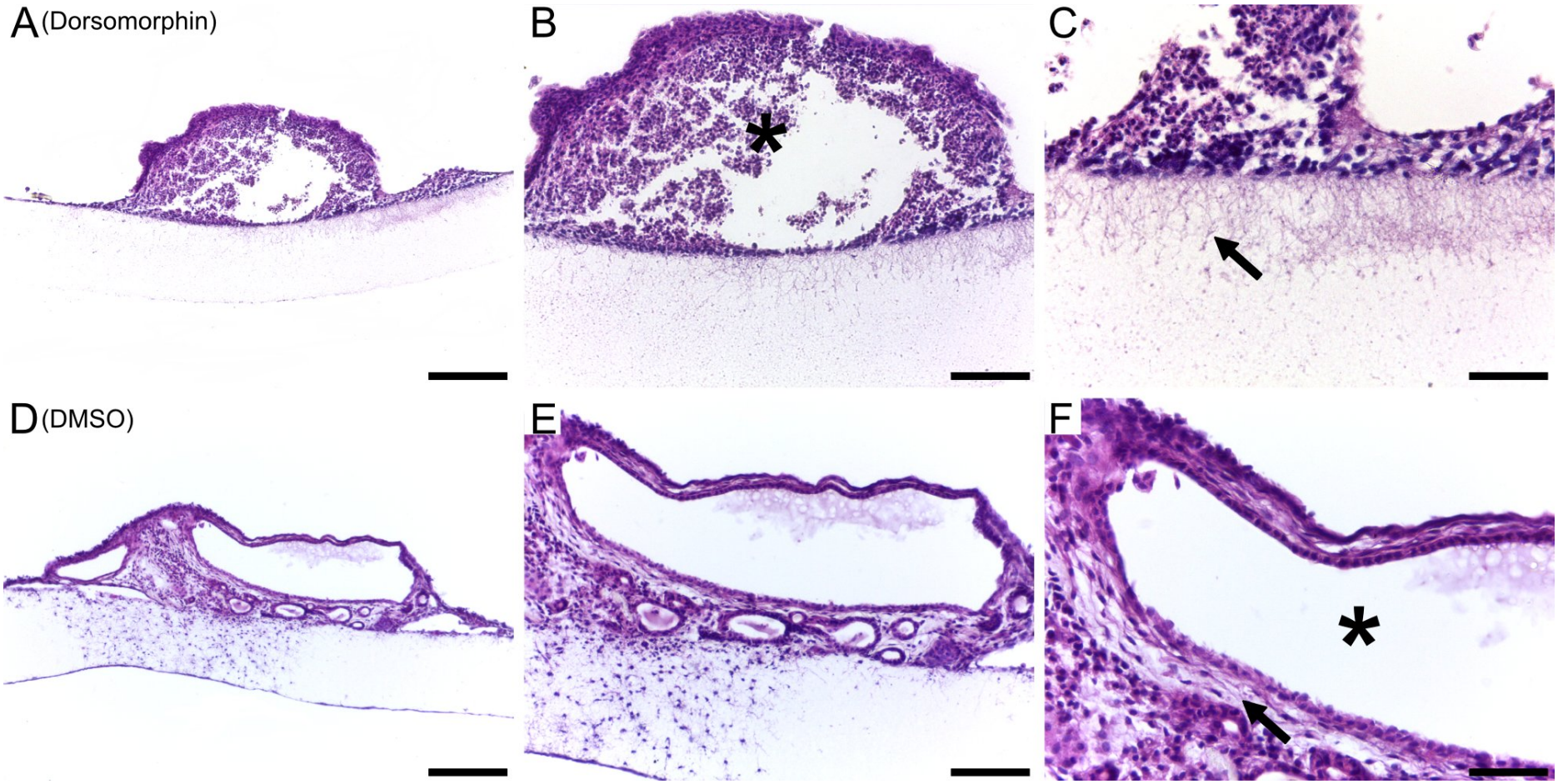

Figure 48: Histological analysis of p9 mEBs maintained in suspension with dorsomorphin for 5 days followed by 32 days culture using Alvetex®Polaris.

mEBs were maintained in suspension for 5 days in the presence of 20% FBS and [1 µM] dorsomorphin followed by 32 days maintenance using Alvetex®Polaris. Haematoxylin and eosin stained 8 µm paraffin transverse sections revealed that endodermal epithelial cavities (asterisk, F) and mesodermal connective tissues (arrow, F) had developed in DMSO control mEBs but were absent in dorsomorphin treated aggregates. Cells within dorsomorphin-treated mEBs underwent significant cell death (asterisk, B) and extended projections into the scaffold membrane below (arrow, C). Scale bars represent 200 µm (A, and D), 100 µm (B, and E), and 50 µm (C, and F). Bright-field images were taken using a Leica ICC50HD microscope and a 10x (A, and D), 20x (B, and E), or 40x objective (C, and F).

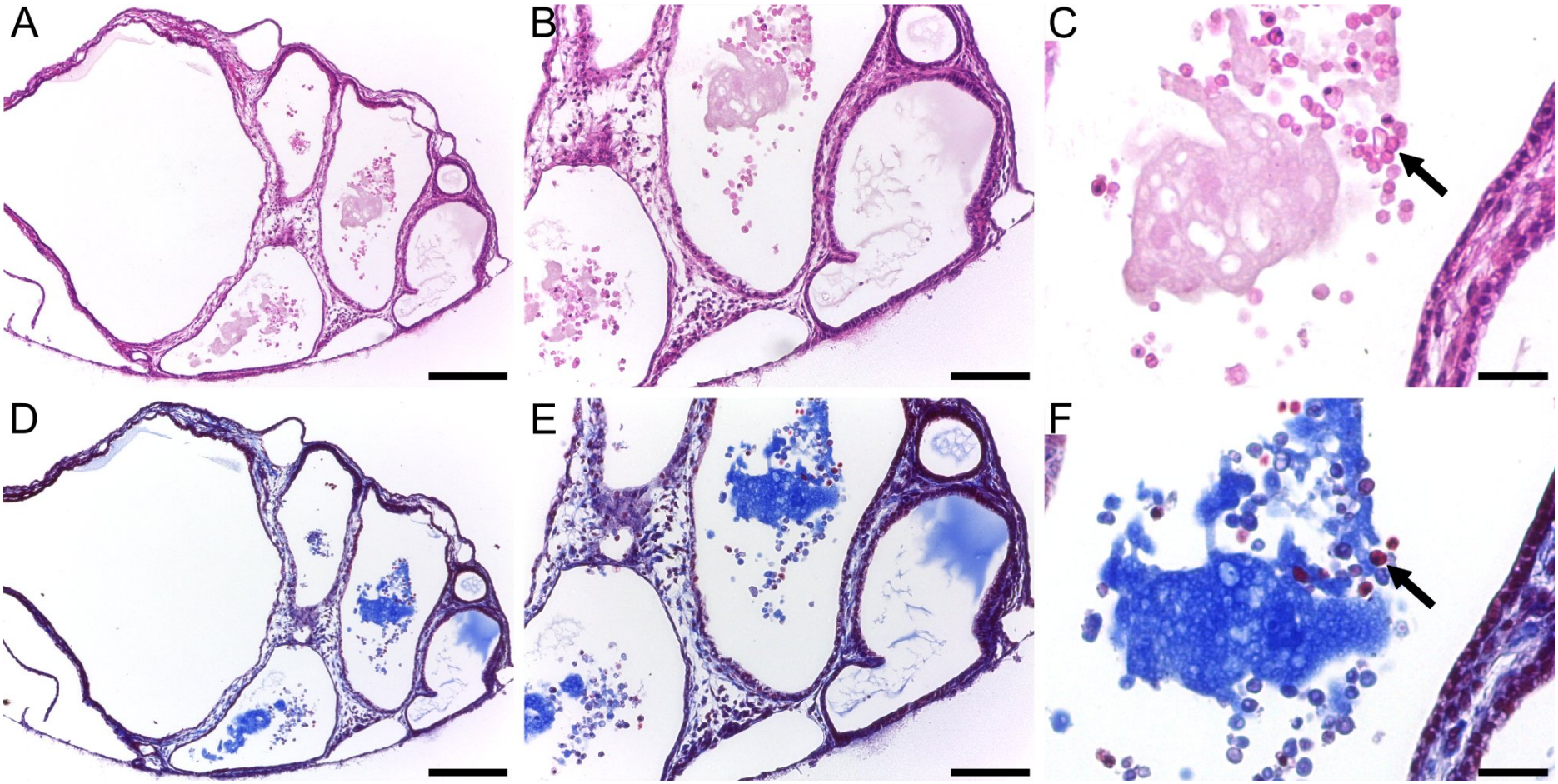

Figure 49: Histological analysis of one 32 day p9 mEB that failed to respond to dorsomorphin treatment.

Two mEBs that were maintained in suspension for 5 days in the presence of 20% FBS and [1 µm] dorsomorphin followed by 16-32 days maintenance using Alvetex®Polaris failed to respond to dorsomorphin treatment. Haematoxylin and eosin stained (A, B, and C) and Masson's trichrome stained (C, D, and E) 8 µm paraffin transverse sections of one mEB cultured for 32 days revealed large numbers of epithelial cavities lined with endoderm-like epithelial tissues and supported by collagenous mesodermal connective tissues. Interestingly, cells that resembled erythrocytes were seen (arrows, C and F), some of which stained red in Masson's trichrome stain. Scale bars represent 200 µm (A, and D), 100 µm (B, and E), and 30 µm (C, and F). Bright-field images were taken using a Leica ICC50HD microscope and a 10x (A, and D) or 20x (B, C, E, and F). Panels C and F have been digitally enlarged.

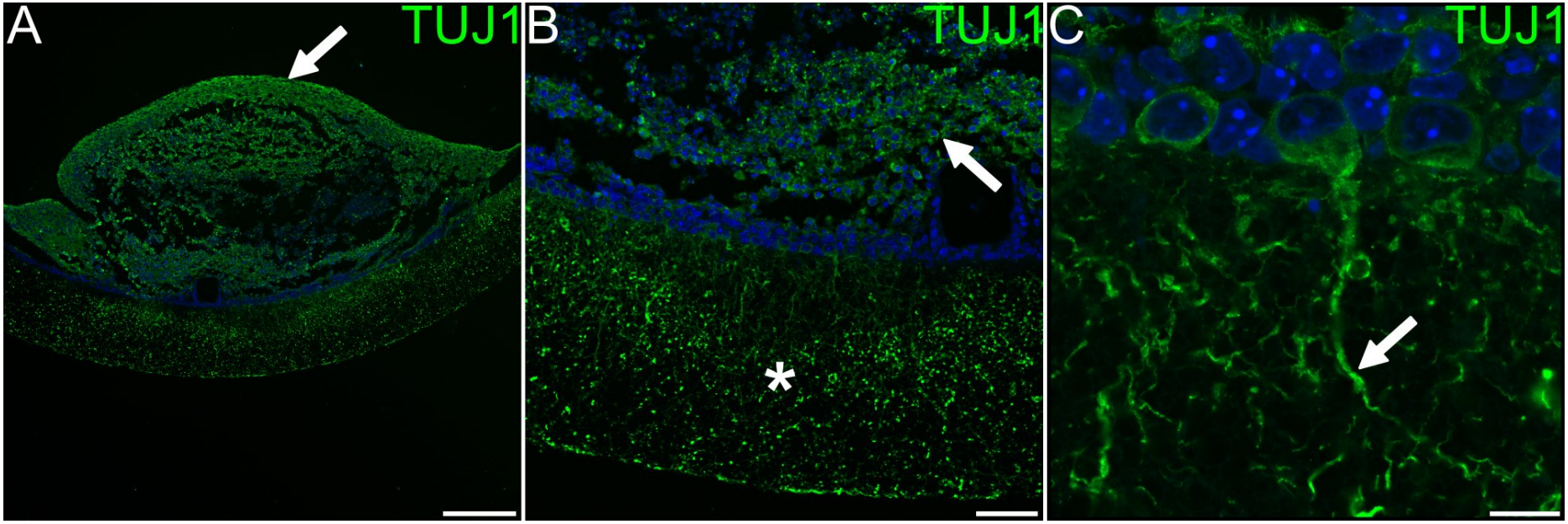

Figure 50: Immunohistochemical analysis of neural marker expression in a dorsomorphin-treated mEB maintained using Alvetex®Polaris for 16 days.

Immunostaining against TUJ1 revealed neural marker expression in 8 µm paraffin transverse sections of a dorsomorphin-treated [1 µM] p9 mEB maintained in suspension with 20% FBS for 5 days followed by 16 days growth using Alvetex®Polaris. TUJ1 was expressed in a large number of cells within the aggregate (arrows, A and B), as well as in the scaffold membrane below (asterisk, B). Confocal microscopy revealed the structure of neural cells with the cell body visible above the membrane and long $TUJ1^{+}$ neurite extensions seen protruding into the scaffold below (arrow, C). Scale bars represent 200 µm (A), 50 µm (B), and 10 µm (C). Confocal images were taken using a Zeiss 880 CLSM and a 20x (A), 40x, (B), or 63x objective (C). The resolution of the image in panel C has been enhanced using Zeiss 880 Airyscan feature.

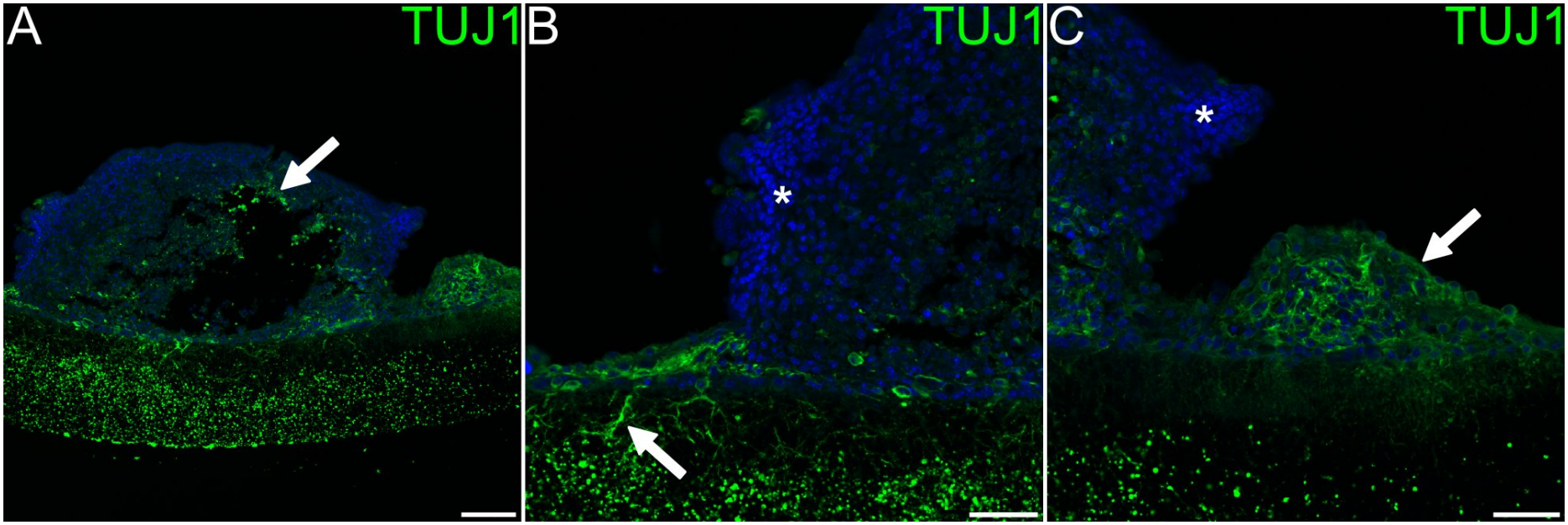

Figure 51: Immunohistochemical analysis of neural marker expression in a dorsomorphin-treated mEB maintained using Alvetex®Polaris for 32 days.

Immunostaining against TUJ1 revealed neural marker expression in 8 µm paraffin transverse sections of a dorsomorphin-treated [1 µM] p9 mEB maintained in suspension with 20% FBS for 5 days followed by 32 days growth using Alvetex®Polaris. TUJ1 was expressed in a small number of cells within the aggregate (arrows, A and B), as well as in neurites that penetrated the scaffold membrane below (arrow, B). A small group of cells that were strongly TUJ1^{+} were seen alongside the main body of the aggregate (arrow, C). Interesting structures consisting of non-neural cell types developed on the external surface of one mEB (asterisks, B and C). Scale bars represent 100 µm (A), 50 µm (B, and C). Confocal images were taken using a Zeiss 880 CLSM and a 20x (A), or 63x objective (B, and C).

3.7.2 Wnt/β-catenin Pathway

Chiron99021 (Chi) was utilised as an exogenous agonist of canonical Wnt/β-catenin signalling. Chi agonises the canonical Wnt pathway by inhibiting GSK3β and preventing the proteolytic degradation of β-catenin and allowing its nuclear translocation where it acts as a transcriptional co-regulator (Wray et al., 2011; Behrens et al., 1996).

p9 mEBs were maintained in suspension for 5 days with 20% FBS and Chi [3 µM]. Haematoxylin and eosin staining of paraffin transverse sections failed to reveal any overt differences between Chi-treated mEBs and DMSO controls (**Figure 52**). Culture time was therefore extended using Alvetex®Polaris for 16-32 days to determine if any effect on differentiation in response to Chi was apparent after a longer culture period.

After 16 days or 32 days culture using Alvetex®Polaris, a proportion of tissue-discs examined (50%, n = 4) failed to develop the large internal epithelial cavities that were typically observed in controls, and had a flatter and thinner morphology compared to control aggregates (**Figure 53**). One tissue-disc cultured for 16 days produced large amounts of connective tissue (arrow, **Figure 53C**), and also contained large regions of what appeared to be apoptotic cells (asterisk, **Figure 53C**). In contrast, connective tissue appeared absent in one mEB cultured for 32 days using Alvetex®Polaris and a layer of squamous epithelial cells or fibroblasts was seen at the exterior surface of the aggregate (arrow, **Figure 53F**).

Large internal epithelial cavities and connective tissues developed in 50% of mEBs examined that appeared similar to DMSO control mEBs (**Figure 54**). The fact that some mEBs appeared to be unaffected by Chi treatment added weight to the hypothesis that some mEBs were resistant to directed differentiation. It would be interesting to increase the number of aggregates examined and to quantify more rigorously what percentage of mEBs responded to treatment and whether this could be manipulated through altering the concentration of inducer or mEB size.

Together these data agree with what was previously observed in hEC aggregates and suggest that the canonical Wnt/β-catenin pathway inhibits the development of epithelial cavities in mEB-derived tissue discs cultured for up to 32 days.

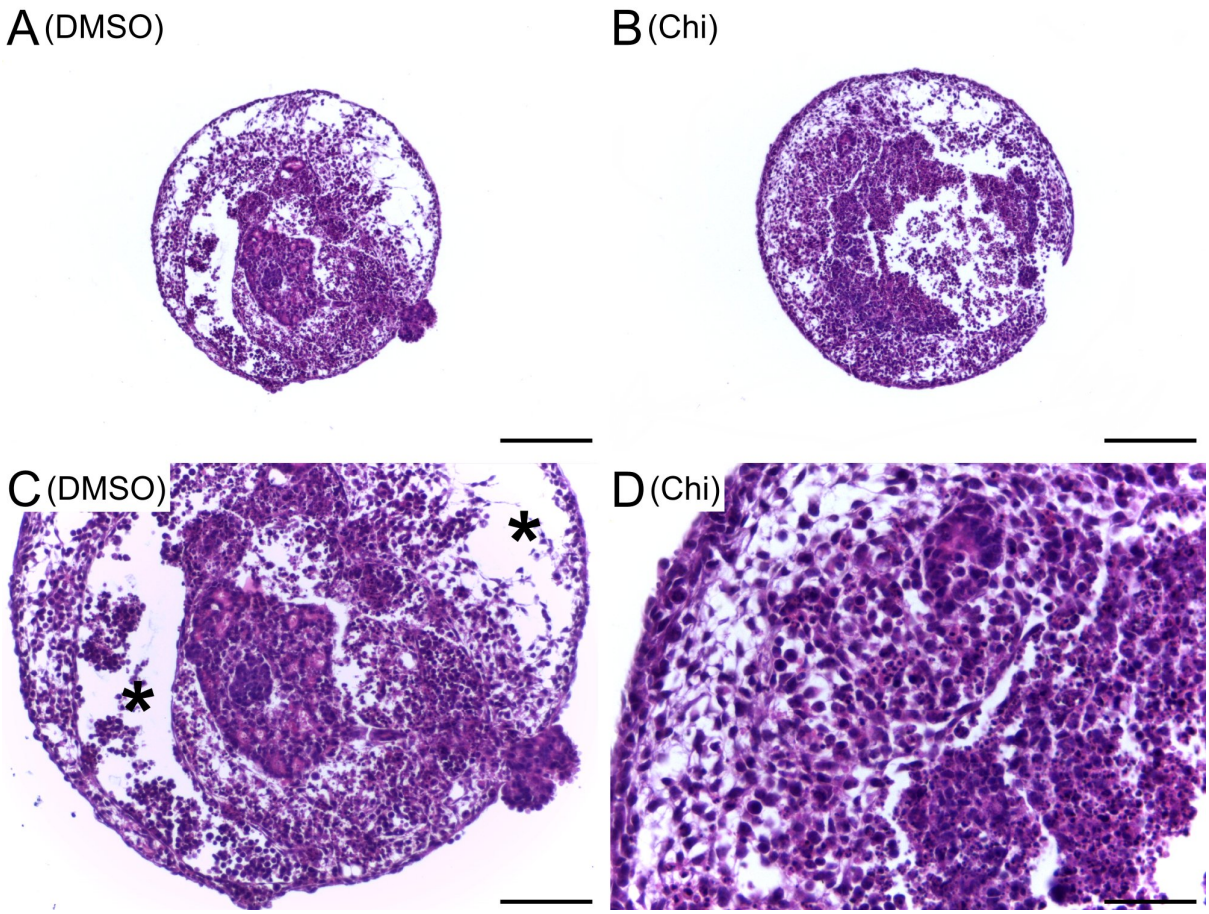

Figure 52: Histological analysis of p9 mEBs maintained in suspension for 5 days in the presence of Chiron99021.

p9 mEBs were maintained in suspension with 20% FBS and [3 µM] Chiron99021 (Chi) (or DMSO control) for 5 days and 6 µm paraffin transverse sections stained with haematoxylin and eosin. Chi-treated aggregates and DMSO controls both contained an array of differentiating cell types and developed internal cavities (asterisks, C) and mesenchymal regions. Scale bars represent 200 µm (A, and B), 100 µm (C), and 50 µm (D). Bright-field images were taken using a Leica ICC50HD microscope and a 10x (A, and B), 20x (C), or 40x objective (D).

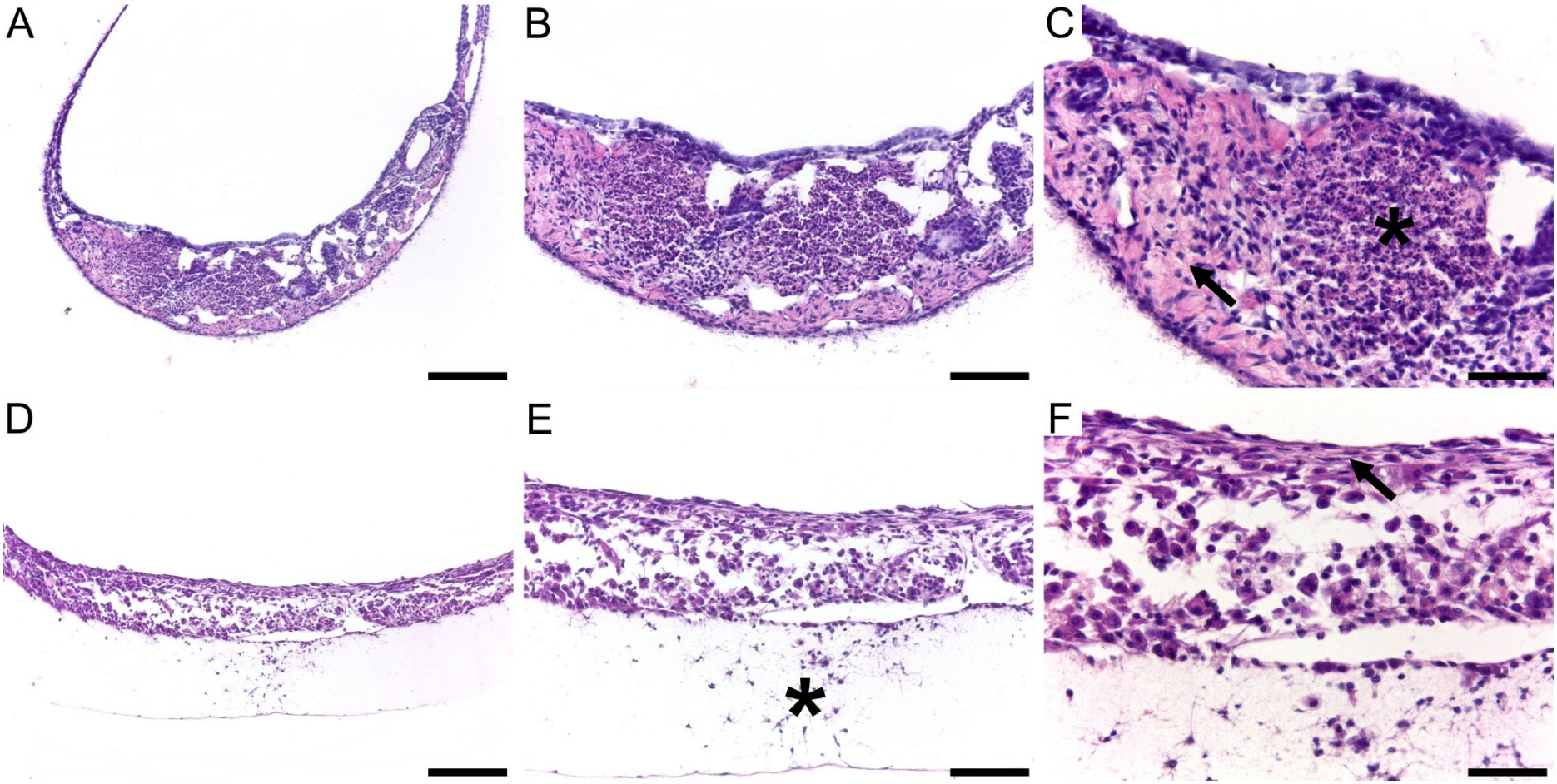

Figure 53: Histological analysis of p9 mEBs maintained in suspension with Chiron99021 for 5 days followed by 16 - 32 days culture using Alvetex®Polaris.

mEBs were maintained in suspension for 5 days in the presence of 20% FBS and [3 µM] Chiron99021 (Chi) followed by 16 days (A-C) or 32 days maintenance (D-F) using Alvetex®Polaris. Haematoxylin and eosin stained 8 µm paraffin transverse sections revealed a striking lack of endodermal epithelial cavities in Chi-treated mEBs. One mEB maintained for 16 days developed large amounts of mesodermal connective tissues (arrow, C) and regions of apparently apoptotic cells (asterisk, C). One 32 day mEB produced no connective tissues or apoptotic cells, but exhibited a layer of squamous epithelial cells or fibroblasts at the external surface of the aggregate (arrow, F). Interestingly, cells were observed to have penetrated the Alvetex®Polaris membrane (asterisk, B). Scale bars represent 200 µm (A, and D), 100 µm (B, and E), and 50 µm (C, and F). Bright-field images were taken using a Leica ICC50HD microscope and a 10x (A, and D), 20x (B, and E), or 40x objective (C, and F).

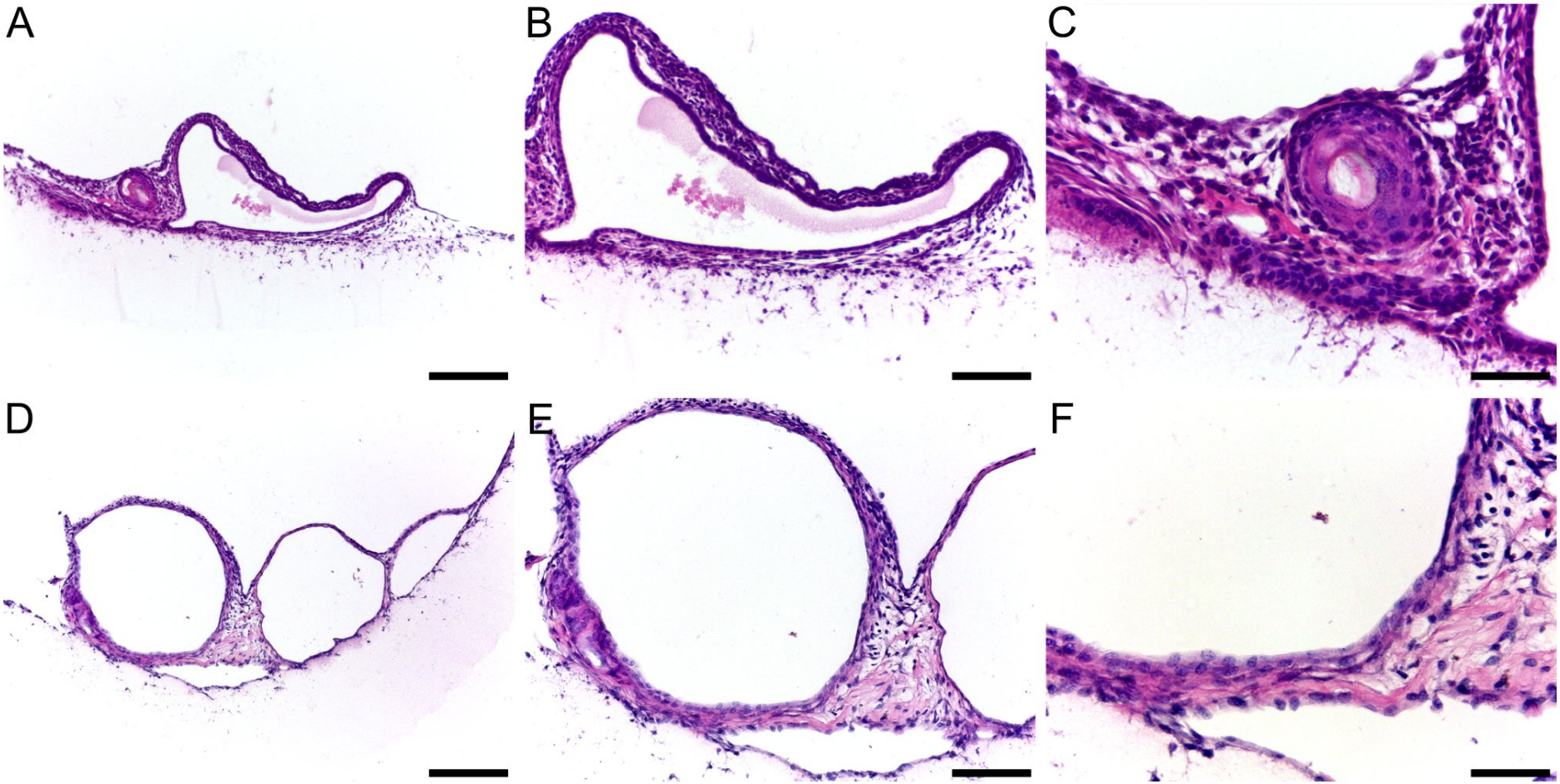

Figure 54: Histological analysis of two mEBs that failed to respond to Chiron99021 treatment.

Two mEBs that were maintained in suspension for 5 days in the presence of 20% FBS and [1 µm] Chiron99021 (Chi) followed by 16 (A-C) or 32 days (D-F) maintenance using Alvetex®Polaris failed to respond to Chi treatment. Haematoxylin and eosin staining of 8 µm paraffin transverse sections revealed large internal epithelial cavities and mesodermal connective tissues that were indistinguishable from DMSO control mEBs. Scale bars represent 200 µm (A, and D), 100 µm (B, and E), and 50 µm (C, and F). Bright-field images were taken using a Leica ICC50HD microscope and a 10x (A, and D), 20x (B, and E), or 40x objective (C, and F).

3.8 Murine Embryonic Stem Cell Teratomas

Teratoma formation from CGR8 mESCs was examined in order to compare tissues that developed *in vitro* in tissue-discs to tissues produced *in vivo* in teratomas. Teratoma samples were derived from a previous animal study that was performed as part of a collaboration between Durham University, UK, School of Biological and Biomedical Sciences, and Newcastle University, UK, Institute of Genetics, with permission from the institutions and in accordance with UK Home Office guidelines.

$1x10^6$ CGR8 mESCs were implanted subcutaneously into the flank of adult female nude (nu/nu) mice and formed teratomas over 28 days. Histological analysis was performed on paraffin transverse sections that contained an array of highly complex differentiated tissues representative of all three embryonic germ layers.

Ectodermal tissues developed including a large region of epidermal tissue that contained keratinocytes (arrow, **Figure 55B**), cornified layers of keratin (arrow, **Figure 55E**), hair follicles (asterisks, **Figure 55C&F**) with associated sebaceous glands (arrow, **Figure 55F**), and subcutaneous adipose tissue (asterisk, **Figure 55A**). Neuroepithelium also developed and typical neural rosettes were seen (arrows, **Figure 56C&F**). Mesodermal derivatives included hyaline cartilage that was identified with one or two chondrocytes that resided within lacunae (arrows, **Figure 57C&F**) and were surrounded by collagenous ground substance, as well as striated muscle and adipose tissue (data not shown). Calcium mineralisation was detected in a tissue that resembled trabecular bone (**Figure 58**). Endodermal epithelial tissue was observed that formed an internal cavity (asterisks, **Figure 59B&E**) and included columnar epithelial cells that resembled absorptive enterocytes with microvilli (arrows, **Figure 59C&F**), indicative of gastrointestinal epithelium.

It is not surprising that, comparatively speaking, the complexity and integrity of tissues seen in teratomas was greater compared to mEBs cultured as tissue-discs using Alvetex®Polaris. It is well established that the *in vivo* environment provides nutritional support through host vascularisation, supporting differentiation and facilitating the development of highly complex tissues (Przyborski, 2005). In addition, teratomas initially contained a 10-fold greater number of cells compared to mEBs and this may have provided enhanced cell interactions that are essential for tissue development. Taken together these findings confirm the pluripotency of CGR8 mESCs and indicate the ability of CGR8 mESCS to develop into complex tissues representative of all three embryonic germ layers within teratomas.

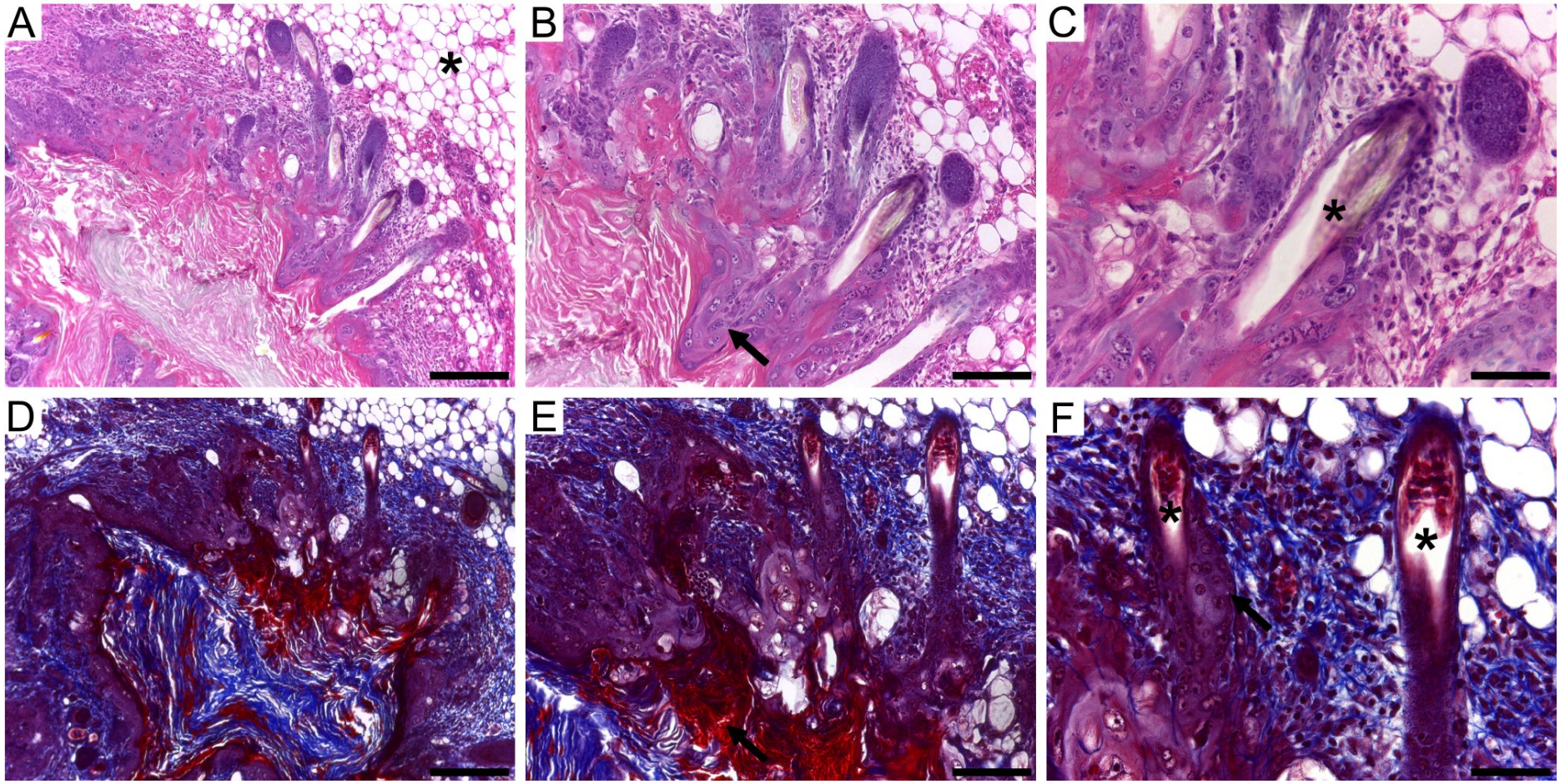

Figure 55: Identification of epidermis in CGR8 teratomas.

Haematoxylin and eosin staining (A-C) and Masson's trichrome staining (D-F) of 8 µm paraffin transverse sections of one CGR8 teratoma revealed a region of epidermal tissue that was indicative of ectodermal differentiation. Histological analysis revealed complex skin with basophilic keratinocytes (arrow, B), cornified layers of keratin (arrow, E), hair follicles (asterisks, C and F) with associated sebaceous glands (arrow, F), and subcutaneous adipose tissue (asterisk, A). Scale bars represent 200 µm (A, and D), 100 µm (B, and E), and 50 µm (C, and F). Bright-field images were taken using a Leica ICC50HD microscope and a 10x (A, and D), 20x (B, and E), or 40x objective (C, and F).

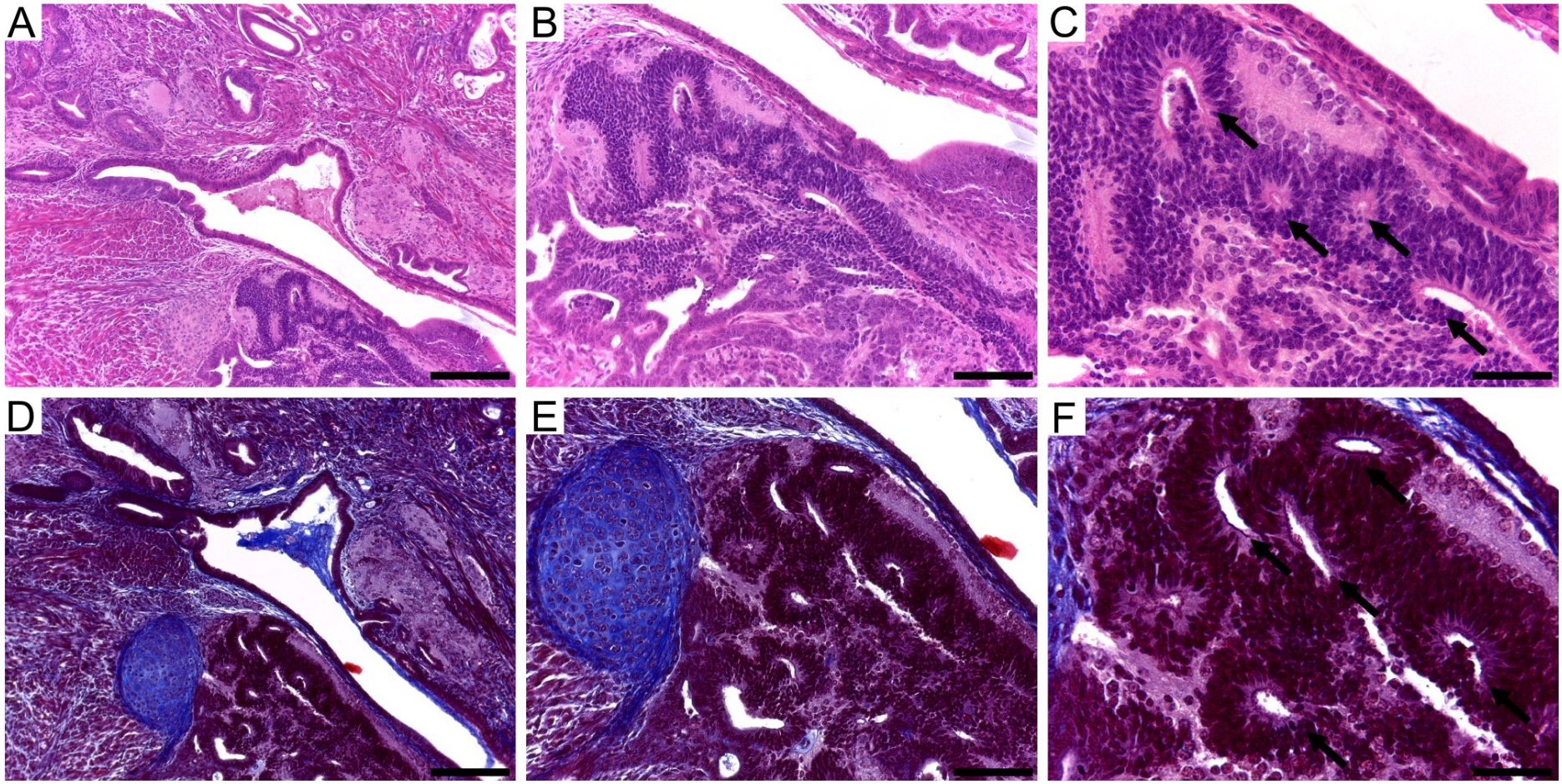

Figure 56: Identification of neuroepithelium in CGR8 teratomas.

Haematoxylin and eosin staining (A-C) and Masson's trichrome staining (D-F) of 8 µm paraffin transverse sections of one CGR8 teratoma revealed a region of neural tissue that was indicative of ectodermal differentiation. Histological analysis revealed neuroepithelial tissue that formed typical neural rosettes (arrows, C, and F). Scale bars represent 200 µm (A, and D), 100 µm (B, and E), and 50 µm (C, and F). Bright-field images were taken using a Leica ICC50HD microscope and a 10x (A, and D), 20x (B, and E), or 40x objective (C, and F).

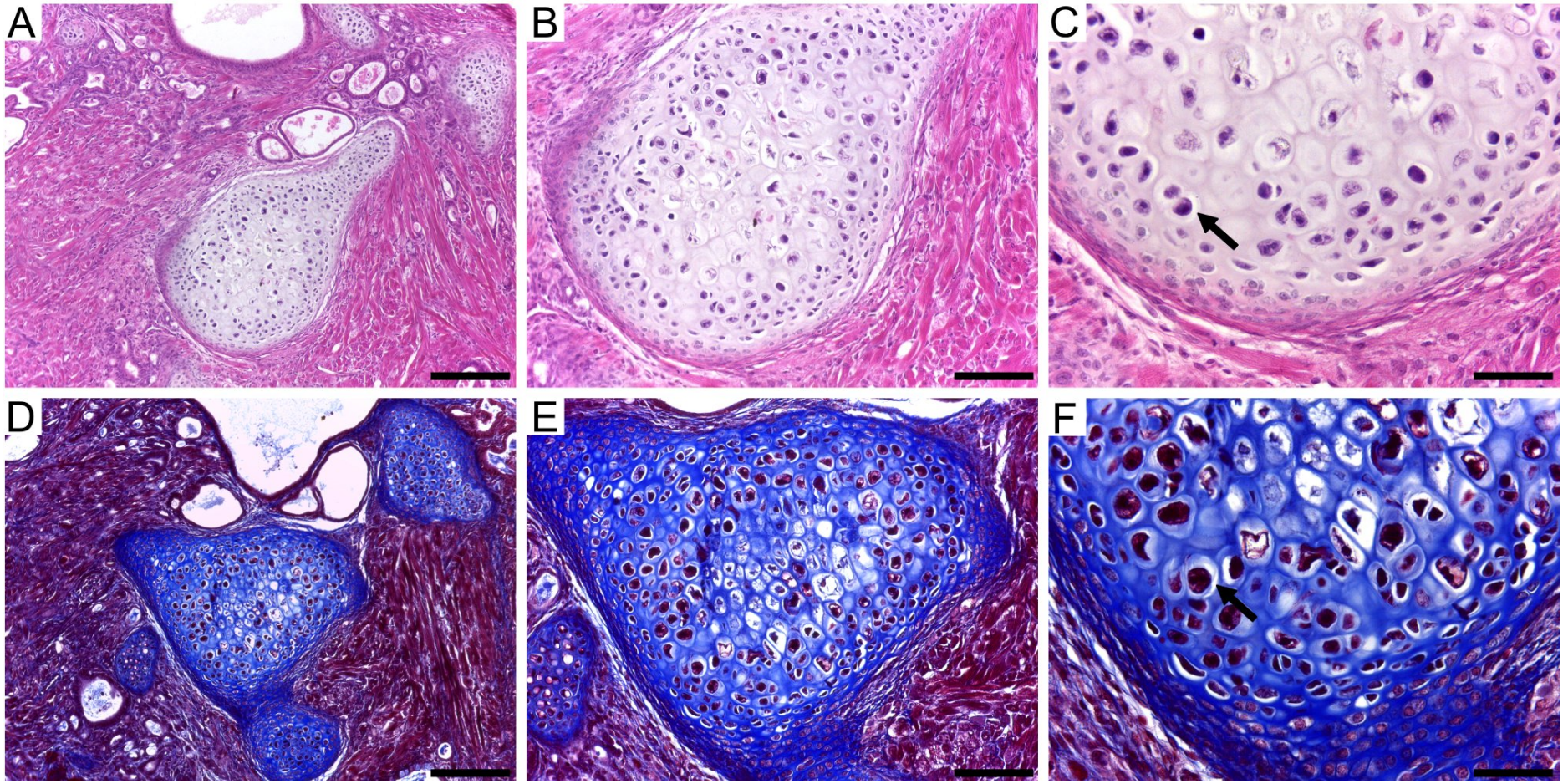

Figure 57: Identification of cartilage in CGR8 teratomas.

Haematoxylin and eosin staining (A-C) and Masson's trichrome staining (D-F) of 8 µm paraffin transverse sections of one CGR8 teratoma revealed a region of cartilage that was indicative of mesodermal differentiation. Histological analysis revealed a region of tissue that contained one or two chondrocytes within lacunae (arrows, C and F) embedded in a collagenous ground substance that stained blue in Masson's trichrome stain. Scale bars represent 200 µm (A, and D), 100 µm (B, and E), and 50 µm (C, and F). Bright-field images were taken using a Leica ICC50HD microscope and a 10x (A, and D), 20x (B, and E), or 40x objective (C, and F).

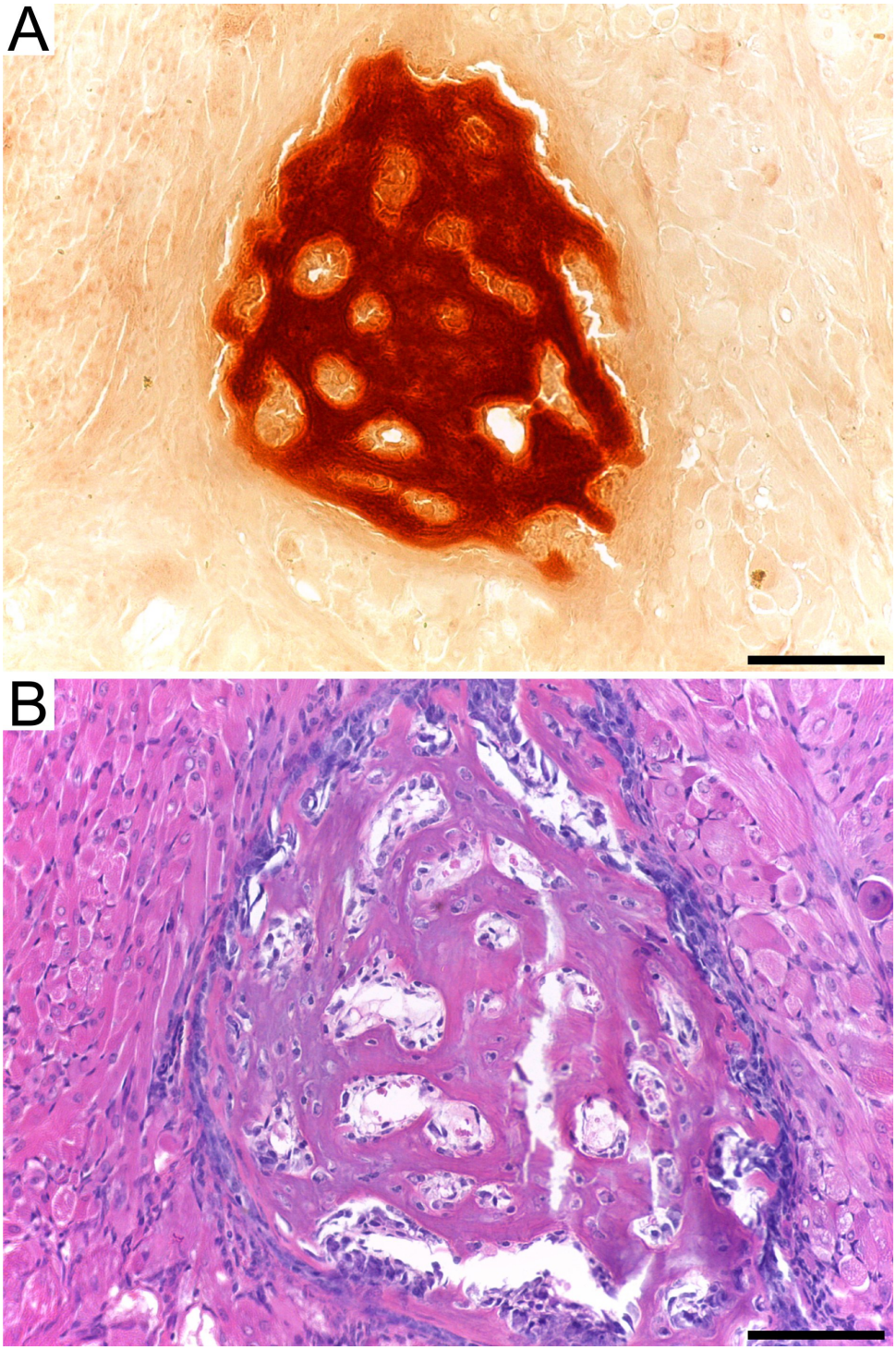

Figure 58: Identification of trabecular bone in CGR8 teratomas.

Alizarin Red staining of 8 µm paraffin transverse sections of a CGR8 teratoma revealed a region of tissue that exhibited calcium deposition, indicative of mineralisation in the tissue. Haematoxylin and eosin staining revealed the structure of the mineralised tissue was similar to trabecular bone with trabeculae containing calcium deposits. Scale bars represent 100 µm. Bright-field images were taken using a Leica ICC50HD microscope and a 20x objective.

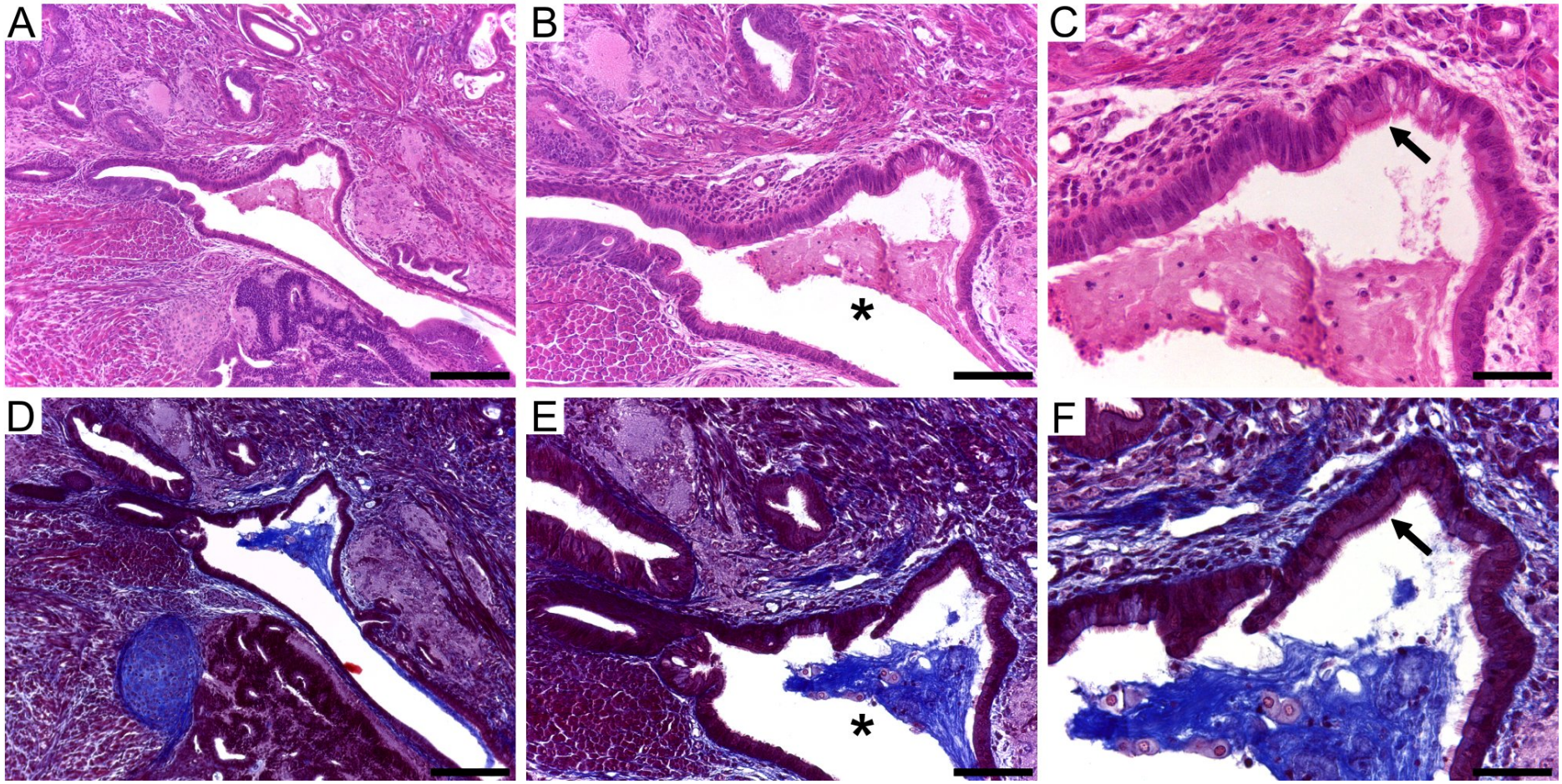

Figure 59: Identification of gastrointestinal epithelium in CGR8 teratomas.

Haematoxylin and eosin staining (A-C) and Masson's trichrome staining (D-F) of 8 µm paraffin transverse sections of one CGR8 teratoma revealed a region of endodermal epithelial tissue that formed an internal cavity (asterisks, B and E). Histological analysis identified columnar epithelial cells that resembled enterocytes with microvilli (arrows, C and F) Scale bars represent 200 µm (A, and D), 100 µm (B, and E), and 50 µm (C, and F). Bright-field images were taken using a Leica ICC50HD microscope and a 10x (A, and D), 20x (B, and E), or 40x objective (C, and F).

4 Discussion

A novel two-step culture technique of maintaining stem cell aggregates as 3D tissue-discs using Alvetex®3D polystyrene scaffolds was investigated as a means to extend the development potential of pluripotent stem cells *in vitro*.

4.1 Stem cell aggregates maintained using Alvetex®Polaris developed into flattened tissue-discs.

Aggregates of TERA2.cl.SP12 and CGR8 cells that were cultured in suspension followed by maintenance using Alvetex®Polaris developed into flattened tissue-discs. TUNEL staining indicated that some aggregates maintained for extended periods in suspension developed a necrotic core that resulted in large amounts of apoptosis and reduced cell viability (**Figure** 11). In all the tissue-discs examined, however, no necrotic core was detected and only a few scattered apoptotic cells could be identified. Tissue-disc morphology reduced the distance of cells from the media and this may have protected against the development of a necrotic core by facilitating enhanced diffusion. It has been reported that the oxygen concentration at the centre of large EBs (400 µm radius) was 50% lower than at the center of small EBs (200 µm radius), supporting the notion that flattened tissue-discs reduced apoptosis through enhanced diffusion (Van Winkle et al., 2012). Tissue-disc cultures improve cell viability over prolonged culture indicating their suitability to support long-term stem cell differentiation *in vitro*.

Although scaffolds are being used more widely in the differentiation of PSCs, most techniques involve seeding a single cell suspension into a scaffold that does not facilitate tissue-disc formation (Levenberg et al., 2003; Baharvand et al., 2006; Willerth et al., 2006; Gerecht et al., 2007). EBs have been supported using hydrogels, but this methodology also fails to support tissue-disc formation because the entire EB will be supported and may not be as suitable for long-term culture due to limited nutrient transport through the hydrogel (Kothapalli and Kamm, 2013). An alternative method used thin pre-stretched electrospun polyurethane scaffolds to maintain spheroids of adipose tissue-derived stem cells (ADSCs) (Beachley et al., 2014). Beachley *et al.* identified the ability of large tissue constructs to be assembled by joining smaller tissue spheroids together. However, differentiation of ADSCs in tissue constructs was not examined. The principle of adhering smaller aggregates together on a thin scaffold membrane to form a larger tissue construct could have uses in therapeutic tissue engineering applications (Beachley et al., 2014). Interestingly, this method could be adapted and EBs could be induced to distinct lineages and then combined in tissue-disc cultures to generate complex tissues to study tissue interactions.

One study described a more similar protocol to ours: utilising Millipore mesh well-inserts with a pore size of 0.4 µm to support hiPSC-derived serum free EBs (SFEBs) cultured under neural inductive conditions (Nestor et al., 2013). Nestor *et al.* described the ability of SFEBs maintainted in this way to flatten from 400 µm to 100 µm that facilitated live imaging and electrophysiological studies. They explained that the benefits of 3D aggregation including enhanced cell:cell and cell:matrix interactions were maintained while minimising some of the drawbacks such as the requirement for disaggregation prior to analysis. Millipore mesh well-inserts are a 2D raised platform that fa-

cilitates tissue-disc formation while allowing aggregates to contact media at both their apical and basal surfaces. Something that remains unexplored in the present study is whether attachment to a 2D surface is equivalent to attaching to a 3D scaffold, if cells are maintained within a 3D tissue-disc. Different strategies for tissue-disc maintenance may have their own relative strengths and weaknesses. For example, Millipore mesh well-inserts may be more useful for live-cell imaging studies of tissue-disc development, while Alvetex®may be better suited to histological analyses.

4.2 Tissue-disc cultures facilitate the development of complex tissues *in vitro*.

Aggregates of hEC cells and mEBs differentiated into complex tissues when maintained as tissue-discs *in vitro* for extended periods.

TERA2.cl.SP12 cells formed neuroepithelial and non-neural epithelial tissues that exhibited typical neural and epithelial marker expression when cultured as tissue-discs using Alvetex®Polaris. TERA2.cl.SP12 cells have previously been shown to produce neural and non-neural epithelial cell types upon spontaneous differentiation in 2D, as aggregates in suspension, as aggregates maintained using Alvetex®, and as teratomas (Przyborski et al., 2004; Hayman et al., 2004) and our findings confirmed their ability to do so in 3D tissue-discs.

The tissues observed in hEC aggregates cultured as tissue-discs using Alvetex®Polaris were comparable in complexity to those seen in aggregates cultured in suspension and in certain cases more *in vivo*-like. Unfortunately, histological analysis of tissue-discs was hampered by aggregates breaking up during tissue processing. A plausible explanation is that the tissues shrank during ethanol dehydration more than the polystyrene scaffold generating stress. If so, a way to overcome this problem in the future could be to use OCT embedding and cryosectioning instead of paraffin embedding and sectioning with a microtome.

Histological analysis indicated that CGR8 mESCs formed epidermis (keratin pearl), neuroepithelium, cartilage, connective tissue, and endoderm-like epithelium when cultured as 3D tissue-discs. It was challenging to identify the developmental origin of epithelial tissues because they could have represented any of several embryonic, extraembryonic or adult tissues—a challenge that has previously been reported when identifying EB-derived putative endodermal epithelial tissues (Sheridan et al., 2012). A considerable repertoire of somatic cell types and tissues have been observed in EBs previously including neurons (Bain et al., 1995), adipocytes (Dani et al., 1997), chondrocytes (Kramer et al., 2000), muscle cells (Rohwedel et al., 1994), cardiomyocytes (Hao et al., 2008), vascular endothelium (Wang et al., 1992), lymphatic endothelium (Liersch et al., 2006), kidney (Vigneau et al., 2007), and intestinal epithelium (Konuma et al., 2009). The array of cell types identified in EBs cultured as tissue-discs was not as exhaustive as this, but the small scale of this pilot study could be a primary reason for this. Moreover, some of these cell types are only generated efficiently in isolation under appropriate inductive conditions.

A number of studies have identified spontaneous development of small scale *in vivo*-like tissues including neuroepithelial tissues, connective tissues, cartilage, and gut-like epithelial tissues in EBs maintained in suspension (**Figure 60**)(Doetschman et al., 1985;

Itskovitz-Eldor et al., 2000; Sheridan et al., 2012). Tissues that developed in mEBs cultured as tissue-discs such as endoderm-like epithelial tissues, connective tissues, and neuroepithelial tissues were of a comparable complexity as tissue structures reported in previous studies. Therefore this study demonstrates proof of principal for small scale *in vivo*-like tissue development in long-term tissue-disc cultures. In further investigations it may be possible to demonstrate convincingly that the tissues produced in tissue-discs are more highly developed and *in vivo*-like in nature than those seen in suspension. This would require direct comparisons between EBs maintained in suspension and maintained as tissue-discs for an equivalent time, however, which was not investigated here.

4.3 Tissue-disc cultures can be used to study the role of developmental pathways in embryonic development.

The role of developmental pathways in embryonic development were examined in tissue-disc cultures and stem cells could be directed towards specific lineages in a predictable manner.

Despite being useful to study certain aspects of embryonic development, TERA2.cl.SP12 cells are not equivalent to hESCs or hiPSCs. Notably, expression of differentiated tissue markers TUJ1 and CK8 was detected by immunocytochemistry in undifferentiated TERA2.cl.SP12 cells in 2D culture (**Figures 6, 7, and 8**). TUJ1 was not detected in a previous study by Western blotting in undifferentiated TERA2.cl.SP12 cells in 2D (Stewart et al., 2003) and, therefore, it is possible that the expression detected here reflects the high sensitivity of immunocytochemical detection and the cells may not express these markers at biologically relevant levels. TERA2.cl.SP12 cells are a subclone of the TERA2 lineage derived from a testicular teratocarcinoma lung metastasis (Fogh and Trempe, 1975). It has been shown that TUJ1 is expressed in the testis and in highly proliferative cancer cells and, therefore, TUJ1 expression in TERA2.cl.SP12 cells could also be due to their malignant testicular tumour origin. Interestingly, CK8 is the first cytokeratin to be expressed during embryogenesis (Magin et al., 1986) and the propensity for TERA2.cl.SP12 cells to differentiate to epithelial tissues may suggest that they occupy a developmentally restricted precursor state that expresses CK8 at very low levels that is upregulated during differentiation. Despite limitations surrounding hEC cells, information about the role of signalling pathways in human embryonic development was gained.

Retinoid pathway stimulation has previously been shown to induce neural differentiation in a wide variety of PSCs including hECs and the data presented here agreed (Tonge et al., 2010; Christie et al., 2010). Interestingly, neuroepithelial tissue development was reduced in response to ec23 after 21 days suspension and 7 days culture using Alvetex®Polaris. A plausible explanation for the altered morphology of ec23 treated aggregates could be that early neuroepithelial progenitor states developed but were lost more quickly under retinoid stimulation. It seems more likely, however, that a distinct developmental pathway was being induced compared to the default neural development seen in control TERA2.cl.SP12 aggregates.

TERA2.cl.SP12 cells were directed towards a non-neural fate by treatment with BMP2. BMP2 has previously been shown to inhibit neural markers and upregulate epithe-

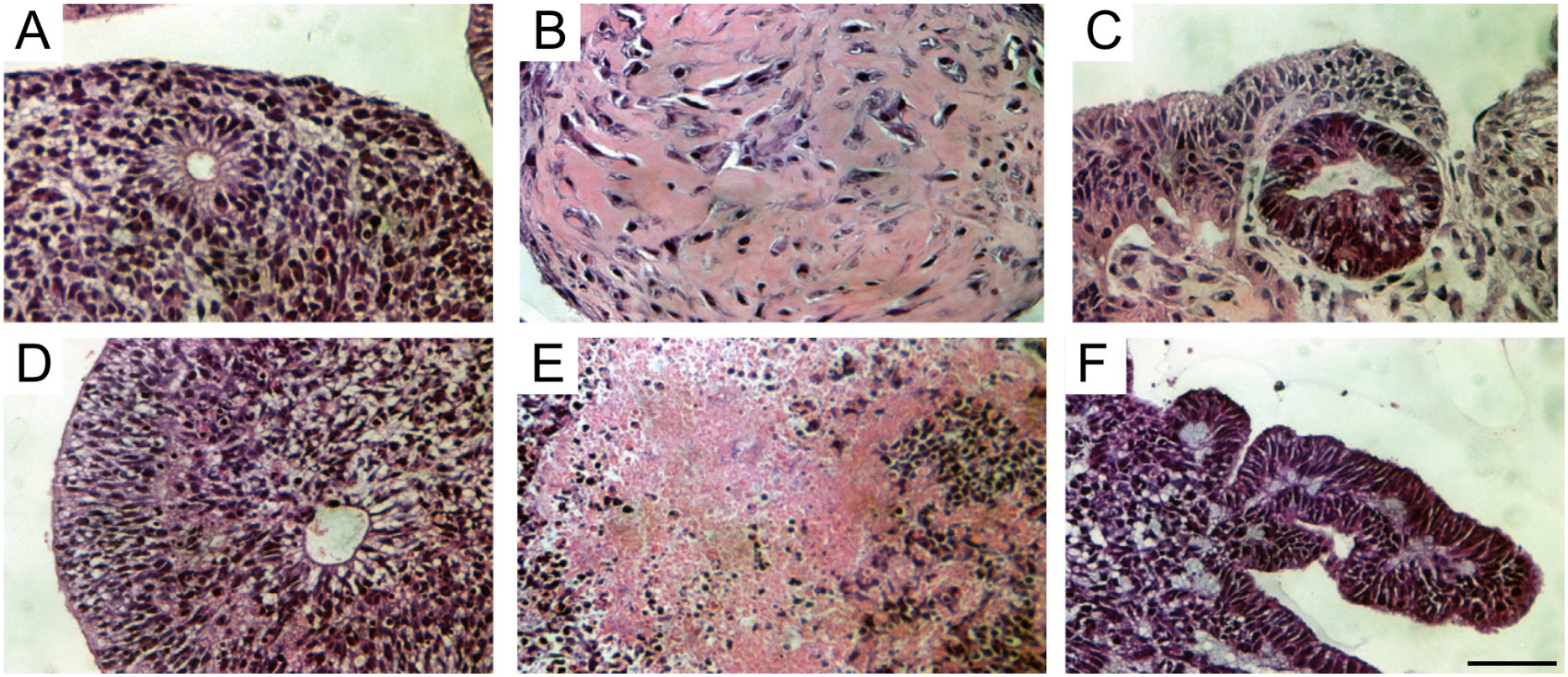

Figure 60: Histological analysis of tissues representative of all three germ layers in human embryoid bodies.

Tissues representative of all three embryonic germ layers were identified in human embryoid bodies generated from hESCs (A-C) or hiPSCs (D-F). Neuroepithelial tissues formed neural rosettes (A, and D), mesodermal derivatives formed fibrous connective tissues (B, and C), and endodermal derivatives formed gut-like epithelial tissues (C, and F). Scale bar represents 50 µm. Images were taken from Sheridan et al. (2012).

lial markers in TERA2.cl.SP12 cells in 2D and in aggregates maintained in suspension and our results reveal that tissue-discs responded in a similar manner (Horrocks et al., 2003; Christie et al., 2008). Unexpectedly, neural differentiation was not entirely blocked by BMP2 and one region of highly organised *in vivo*-like neuroepithelium developed within a large hEC aggregate after 21 days BMP2 treatment (**Figures 17&18**). It was thought that this neural tissue could have developed due to production of neural inhibitors such as noggin, but exogenous neural inhibition did not increase neuroepithelial development in hEC aggregates (**Section 3.3.3**). It is possible that because the neural tissue was surrounded by mesenchyme and excluded from the media, an hypoxic environment developed that has previously been shown to support neurogenesis (Chung et al., 2014), or that the surrounding mesenchymal tissue provided some form of nutritive support or other developmental cues that were neurogenic. Future studies should try to elucidate the role of environmental factors such as oxygen tension in neural induction in TERA2.cl.SP12 aggregates.

Unlike in hEC aggregates, in mEBs BMP inhibition promoted neurogenesis as has previously been reported (Zhou et al., 2010). This discrepancy supports the distinction of hEC cells from ESCs and indicates the use of ESCs for determining the role of signalling pathways in development. Dorsomorphin has also been shown to induce myocardial development when used at early timepoints in mESC differentiation which was not performed here (Hao et al., 2008). The fact that cardiomyocyte differentiation appeared to not occur in response to dorsomorphin reflects the stage-specific roles of signaling pathways such as the BMP pathway during development.

Both TERA2.cl.SP12 and CGR8 aggregates cultured as tissue-discs responded in a similar manner to canonical Wnt/β-catenin stimulation: Chi treatment reduced the formation of epithelial cavities. One explanation for this is that exogenous Wnt agonism by Chi was responsible for the considerable morphogenetic impacts seen in aggregates. Canonical Wnt signalling is essential for primitive streak formation and maintenance during gastrulation and induces mesodermal derivatives (Arkell et al., 2013). mEBs after 72h may have corresponded to this stage and been capable of responding to Wnt/β-catenin stimulation by increasing mesodermal differentiation. Although tentative, the results observed suggest that endodermal epithelial cavities were inhibited but mesodermal connective tissues were not, possibly adding weight to this hypothesis. In order to investigate this further, tissue-specific marker expression could be analysed in Chi-treated mEBs to determine if mesodermal markers were upregulated in response to Chi. TERA2.cl.SP12 cells are unlikely to recapitulate this developmental time frame and so would not have responded in the same manner as mESCs. Another interpretation of the data is that the Wnt/β-catenin pathway plays a role in epithelial differentiation in TERA2.cl.SP12 cells. Alternatively, the primary effect of Chi in hEC aggregates could have been to block epithelial morphogenesis through GSK3β inhibition which has previously been reported (Severson et al., 2010).

Unexpectedly, a significant proportion of mEBs failed to respond to exogenous developmental signals and developed in a similar manner to control aggregates. One possibility is that the samples were confused during processing and human error is one explanation. Similar experiments should be repeated and larger numbers of aggregates examined in order to verify whether this was a real phenomenon. Human error seems less likely an explanation, however, since similar results were found in both Chi- and

dorsomorphin-treated mEBs that were processed separately. Another explanation could be that a shell developed around those mEBs that failed to respond, preventing soluble inducers in the media from entering mEBs and affecting differentiation. It has been shown that EB morphology reduced passive diffusion of an inducer molecule by up to 80% (Sachlos and Auguste, 2008), providing a mechanism whereby the addition of soluble inducers to the media of mEBs cultured in suspension may be inefficacious. The mEBs that did respond, however, were useful to examine and allowed insight to be gained about the role of developmental pathways in murine embryonic development.

Human embryonic material has traditionally been limited by a lack of supply and ethical concerns. Before the advent of hESCs and hiPSCs, hECs offered an alternative model to study human embryonic development *in vitro* (Przyborski, 2001). In future studies the ability of human EBs (hEBs) to be cultured as tissue-discs should be examined to allow human embryonic development to be studied *in vitro*. The study of hEBs could facilitate improved directed differentiation outcomes to clinically relevant cell types such as HSCs. However, there remain ethical concerns over the prolonged maintenance of hEBs in culture. Even hiPSC-derived hEBs may fall under the remit of embryo-like structures in certain cirmumstances—such as in gastruloid cultures—and for this reason, maintaining hEBs beyond the primitive streak stage or for more than 14 days potentially constitutes an offence under current UK licensing laws (Baillie-Johnson et al., in press, Human Fertilisation and Embryology Act, 2008).

4.4 Tissue-disc cultures offer an alternative *in vitro* pluripotency assay.

Differentiation to tissues representative of all three embryonic germ layers was observed in mEBs cultured as tissue-discs for up to 32 days and, therefore, tissue-disc cultures offer a novel *in vitro* pluripotency assay.

Tissues seen in TERA2.cl.SP12 and CGR8 teratomas were larger, more complex, and more diverse than those seen in tissue-discs cultured *in vitro*. This was expected because the *in vivo* environment provides nutritional support and developmental cues facilitating the differentiation of highly complex *in vivo*-like tissues (Przyborski, 2005). Pluripotency testing, however, only requires the development of small scale tissues representative of all three embryonic germ layers and in this regard tissue-disc cultures were successful. What is not clear, however, is whether attachment to a 3D scaffold is strictly necessary for this purpose.

Development of all three embryonic germ layers has been well characterised in human (Itskovitz-Eldor et al., 2000) and murine EBs (Doetschman et al., 1985) and EBs maintained in suspension are frequently used as an *in vitro* pluripotency test that has been suggested as a replacement for the teratoma assay (Sheridan et al., 2012). The fact that tri-lineage differentiation is supported in EBs suggests that tissue-disc culturing may be unnecessary. The more *in vivo*-like the tissue produced, however, the more stringent the pluripotency test is. It is possible, therefore, that tissue-disc cultures may provide a compromise between conventional *in vitro* differentiation in EBs and *in vivo* differentiation in teratomas if long-term maintenance of EBs as tissue-discs provides an opportunity to achieve differentiation outcomes beyond what is currently possible in EBs maintained in suspension. Further work is required in order to demonstrate that

more complex and *in vivo*-like tissues can be produced in tissue-discs compared to aggregates cultured in suspension.

5 Conclusions and Future Directions

The primary aim of this thesis was to investigate whether complex tissue development is supported in 3D-cultured tissue-discs (aim 1). Neuroepithelium, epithelial cavities, and mesodermal connective tissues were seen to develop, supporting this conclusion. Flattened tissue-discs were hypothesised to increase cell viability over prolonged *in vitro* culture compared to aggregates in suspension (aim 2). While increased viability was observed, preliminary experiments must be repeated in order to validate this hypothesis. Developmental signalling pathways such as BMP and retinoic acid signalling were manipulated in aggregates and directed differentiation outcomes were achieved. These data are in support of aim 3, therefore, suggesting that 3D culturing of pluripotent stem cells can be used to study aspects of human embryogenesis.

The final aim was to investigate the utility of 3D tissue-discs as a novel *in vitro* pluripotency assay (aim 4). Good evidence for ectodermal and mesodermal differentiation was seen but endodermal tissues were not convincingly demonstrated. It seems likely that with further experiments and through the use of genetic markers, tissue-discs could be demonstrated to contain tissues representative of all three germ layers. With further investigation 3D cultured tissue-discs may therefore offer an alternative to the current gold standard teratoma assay. Further work should focus on determining the advantages or disadvantages of using different (3D) substrates for tissue-disc formation. Moreover, more cell types including EpiSCs, hESCs and hiPSCs should be investigated to demonstrate the utility of tissue-disc cultures to support complex differentiation in diverse developmental settings.

References

Amabile, G., Welner, R. S., Nombela-Arrieta, C., D'Alise, A. M., Di Ruscio, A., Ebralidze, A. K., Kraytsberg, Y., Ye, M., Kocher, O., Neuberg, D. S., Khrapko, K., Silberstein, L. E., and Tenen, D. G. (2013). In vivo generation of transplantable human hematopoietic cells from induced pluripotent stem cells. *Blood*, 121(8):1255–1264.

Amit, M. and Itskovitz-Eldor, J. (2002). Derivation and spontaneous differentiation of human embryonic stem cells. *J. Anat.*, 200(Pt 3):225–232.

Andrews, P. W. (2002). From teratocarcinomas to embryonic stem cells. *Philos. Trans. R. Soc. Lond., B, Biol. Sci.*, 357(1420):405–417.

Andrews, P. W., Matin, M. M., Bahrami, A. R., Damjanov, I., Gokhale, P., and Draper, J. S. (2005). Embryonic stem (ES) cells and embryonal carcinoma (EC) cells: opposite sides of the same coin. *Biochem. Soc. Trans.*, 33(Pt 6):1526–1530.

Andrews, P. W., Przyborski, S. A., and Thomson, J. A. (2001). Embryonal carcinoma cells as embryonic stem cells. *COLD SPRING HARBOR MONOGRAPH SERIES*, 40:231–266.

Arceci, R. J., King, A. A., Simon, M. C., Orkin, S. H., and Wilson, D. B. (1993). Mouse GATA-4: a retinoic acid-inducible GATA-binding transcription factor expressed in endodermally derived tissues and heart. *Mol. Cell. Biol.*, 13(4):2235–2246.

Arkell, R. M., Fossat, N., and Tam, P. P. (2013). Wnt signalling in mouse gastrulation and anterior development: new players in the pathway and signal output. *Curr. Opin. Genet. Dev.*, 23(4):454–460.

Awad, H. A., Wickham, M. Q., Leddy, H. A., Gimble, J. M., and Guilak, F. (2004). Chondrogenic differentiation of adipose-derived adult stem cells in agarose, alginate, and gelatin scaffolds. *Biomaterials*, 25(16):3211–3222.

Baharvand, H., Hashemi, S. M., Kazemi Ashtiani, S., and Farrokhi, A. (2006). Differentiation of human embryonic stem cells into hepatocytes in 2D and 3D culture systems in vitro. *Int. J. Dev. Biol.*, 50(7):645–652.

Baillie-Johnson, P., van den Brink, S. C., Balayo, T., Turner, D. A., and Martinez Arias, A. (in press). Generation of aggregates of mouse embryonic stem cells that show symmetry breaking, polarization and emergent collective behaviour in vitro. *JOVE*.

Bain, G., Kitchens, D., Yao, M., Huettner, J. E., and Gottlieb, D. I. (1995). Embryonic stem cells express neuronal properties in vitro. *Dev. Biol.*, 168(2):342–357.

Beachley, V., Kasyanov, V., Nagy-Mehesz, A., Norris, R., Ozolanta, I., Kalejs, M., Stradins, P., Baptista, L., da Silva, K., Grainjero, J., Wen, X., and Mironov, V. (2014). The fusion of tissue spheroids attached to pre-stretched electrospun polyurethane scaffolds. *J Tissue Eng*, 5:2041731414556561.

Behrens, J., von Kries, J. P., Kuhl, M., Bruhn, L., Wedlich, D., Grosschedl, R., and Birchmeier, W. (1996). Functional interaction of beta-catenin with the transcription factor LEF-1. *Nature*, 382(6592):638–642.

Bibel, M., Richter, J., Schrenk, K., Tucker, K. L., Staiger, V., Korte, M., Goetz, M., and Barde, Y.-A. (2004). Differentiation of mouse embryonic stem cells into a defined neuronal lineage. *Nature neuroscience*, 7(9):1003–1009.

Bokhari, M., Carnachan, R. J., Cameron, N. R., and Przyborski, S. A. (2007). Novel cell culture device enabling three-dimensional cell growth and improved cell function. *Biochem. Biophys. Res. Commun.*, 354(4):1095–1100.

Bosse, T., Piaseckyj, C. M., Burghard, E., Fialkovich, J. J., Rajagopal, S., Pu, W. T., and Krasinski, S. D. (2006). Gata4 is essential for the maintenance of jejunal-ileal identities in the adult mouse small intestine. *Mol. Cell. Biol.*, 26(23):9060–9070.

Bradley, A., Evans, M., Kaufman, M. H., and Robertson, E. (1984). Formation of germ-line chimaeras from embryo-derived teratocarcinoma cell lines. *Nature*, 309(5965):255–256.

Brons, I. G., Smithers, L. E., Trotter, M. W., Rugg-Gunn, P., Sun, B., Chuva de Sousa Lopes, S. M., Howlett, S. K., Clarkson, A., Ahrlund-Richter, L., Pedersen, R. A., and Vallier, L. (2007). Derivation of pluripotent epiblast stem cells from mammalian embryos. *Nature*, 448(7150):191–195.

Buta, C., David, R., Dressel, R., Emgard, M., Fuchs, C., Gross, U., Healy, L., Hescheler, J., Kolar, R., Martin, U., Mikkers, H., Muller, F. J., Schneider, R. K., Seiler, A. E., Spielmann, H., and Weitzer, G. (2013). Reconsidering pluripotency tests: do we still need teratoma assays? *Stem Cell Res*, 11(1):552–562.

Cai, J., Yang, M., Poremsky, E., Kidd, S., Schneider, J. S., and Iacovitti, L. (2010). Dopaminergic neurons derived from human induced pluripotent stem cells survive and integrate into 6-OHDA-lesioned rats. *Stem Cells Dev.*, 19(7):1017–1023.

Chambers, I., Colby, D., Robertson, M., Nichols, J., Lee, S., Tweedie, S., and Smith, A. (2003). Functional expression cloning of Nanog, a pluripotency sustaining factor in embryonic stem cells. *Cell*, 113(5):643–655.

Chen, C., Uluda?, H., Wang, Z., and Jiang, H. (2012). Noggin suppression decreases BMP-2-induced osteogenesis of human bone marrow-derived mesenchymal stem cells in vitro. *J. Cell. Biochem.*, 113(12):3672–3680.

Chen, U. (2014). Do we have a workable clinical protocol for differentiating lympho-hematopoietic stem cells from the source of embryonic stem cells and induced pluripotent stem cells in culture? *Scand. J. Immunol.*, 80(4):247–249.

Christie, V. B., Barnard, J. H., Batsanov, A. S., Bridgens, C. E., Cartmell, E. B., Collings, J. C., Maltman, D. J., Redfern, C. P., Marder, T. B., Przyborski, S., et al. (2008). Synthesis and evaluation of synthetic retinoid derivatives as inducers of stem cell differentiation. *Organic & biomolecular chemistry*, 6(19):3497–3507.

Christie, V. B., Maltman, D. J., Henderson, A. P., Whiting, A., Marder, T. B., Lako, M., and Przyborski, S. A. (2010). Retinoid supplementation of differentiating human neural progenitors and embryonic stem cells leads to enhanced neurogenesis in vitro. *Journal of Neuroscience Methods*, 193(2):239 – 245.

Chua, S. J., Bielecki, R., Wong, C. J., Yamanaka, N., Rogers, I. M., and Casper, R. F. (2009). Neural progenitors, neurons and oligodendrocytes from human umbilical cord blood cells in a serum-free, feeder-free cell culture. *Biochem. Biophys. Res. Commun.*, 379(2):217–221.

Chung, D. J., Wong, A., Hayashi, K., and Yellowley, C. E. (2014). Effect of hypoxia on generation of neurospheres from adipose tissue-derived canine mesenchymal stromal cells. *Vet. J.*, 199(1):123–130.

Clarke, K. E., Whiting, A., and Przyborski, S. A. (2014). Optimisation of a novel neurite outgrowth model to study the role of neurite inhibition in human stem cell derived neurons. *European Cells and Materials*, 28:49. Supplement 4.

Cooke, M. J., Stojkovic, M., and Przyborski, S. A. (2006). Growth of teratomas derived from human pluripotent stem cells is influenced by the graft site. *Stem Cells Dev.*, 15(2):254–259.

Coucouvanis, E. and Martin, G. R. (1999). BMP signaling plays a role in visceral endoderm differentiation and cavitation in the early mouse embryo. *Development*, 126(3):535–546.

Dani, C., Smith, A. G., Dessolin, S., Leroy, P., Staccini, L., Villageois, P., Darimont, C., and Ailhaud, G. (1997). Differentiation of embryonic stem cells into adipocytes in vitro. *J. Cell. Sci.*, 110 (Pt 11):1279–1285.

De Gendt, K., Denolet, E., Willems, A., Daniels, V. W., Clinckemalie, L., Denayer, S., Wilkinson, M. F., Claessens, F., Swinnen, J. V., and Verhoeven, G. (2011). Expression of tubb3, a beta-tubulin isotype, is regulated by androgens in mouse and rat sertoli cells. *Biology of reproduction*, 85(5):934–945.

Diaspro, A., Bianchini, P., Vicidomini, G., Faretta, M., Ramoino, P., and Usai, C. (2006). Multi-photon excitation microscopy. *Biomed Eng Online*, 5:36.

Doetschman, T. C., Eistetter, H., Katz, M., Schmidt, W., and Kemler, R. (1985). The in vitro development of blastocyst-derived embryonic stem cell lines: formation of visceral yolk sac, blood islands and myocardium. *J Embryol Exp Morphol*, 87:27–45.

Doevendans, P. A., Kubalak, S. W., An, R. H., Becker, D. K., Chien, K. R., and Kass, R. S. (2000). Differentiation of cardiomyocytes in floating embryoid bodies is comparable to fetal cardiomyocytes. *J. Mol. Cell. Cardiol.*, 32(5):839–851.

Duarte, A. R. C., Mano, J. F., and Reis, R. L. (2009). Preparation of chitosan scaffolds loaded with dexamethasone for tissue engineering applications using supercritical fluid technology. *European Polymer Journal*, 45(1):141 – 148.

Durston, A. J., Timmermans, J. P., Hage, W. J., Hendriks, H. F., de Vries, N. J., Heideveld, M., and Nieuwkoop, P. D. (1989). Retinoic acid causes an anteroposterior transformation in the developing central nervous system. *Nature*, 340(6229):140–144.

Evans, M. J., Kaufman, M. H., et al. (1981). Establishment in culture of pluripotential cells from mouse embryos. *nature*, 292(5819):154–156.

Ferrandina, G., Zannoni, G. F., Martinelli, E., Paglia, A., Gallotta, V., Mozzetti, S., Scambia, G., and Ferlini, C. (2006). Class III beta-tubulin overexpression is a marker of poor clinical outcome in advanced ovarian cancer patients. *Clin. Cancer Res.*, 12(9):2774–2779.

Finley, M. F., Devata, S., and Huettner, J. E. (1999). BMP-4 inhibits neural differentiation of murine embryonic stem cells. *J. Neurobiol.*, 40(3):271–287.

Fogh, J. and Trempe, G. (1975). New human tumor cell lines. In *Human tumor cells in vitro*, pages 115–159. Springer.

Funa, N. S., Schachter, K. A., Lerdrup, M., Ekberg, J., Hess, K., Dietrich, N., Honore, C., Hansen, K., and Semb, H. (2015). -Catenin Regulates Primitive Streak Induction through Collaborative Interactions with SMAD2/SMAD3 and OCT4. *Cell Stem Cell*, 16(6):639–652.

Gadue, P., Huber, T. L., Paddison, P. J., and Keller, G. M. (2006). Wnt and TGF-beta signaling are required for the induction of an in vitro model of primitive streak formation using embryonic stem cells. *Proc. Natl. Acad. Sci. U.S.A.*, 103(45):16806–16811.

Gerecht, S., Burdick, J. A., Ferreira, L. S., Townsend, S. A., Langer, R., and Vunjak-Novakovic, G. (2007). Hyaluronic acid hydrogel for controlled self-renewal and differentiation of human embryonic stem cells. *Proc. Natl. Acad. Sci. U.S.A.*, 104(27):11298–11303.

Gotz, M. and Huttner, W. B. (2005). The cell biology of neurogenesis. *Nat. Rev. Mol. Cell Biol.*, 6(10):777–788.

Greep, R. and Weiss, L. (1977). *Histology, Fourth Edition*. McGraw-Hill Book Company.

Gropp, M., Shilo, V., Vainer, G., Gov, M., Gil, Y., Khaner, H., Matzrafi, L., Idelson, M., Kopolovic, J., Zak, N. B., and Reubinoff, B. E. (2012). Standardization of the teratoma assay for analysis of pluripotency of human ES cells and biosafety of their differentiated progeny. *PLoS ONE*, 7(9):e45532.

Groppe, J., Greenwald, J., Wiater, E., Rodriguez-Leon, J., Economides, A. N., Kwiatkowski, W., Affolter, M., Vale, W. W., Izpisua Belmonte, J. C., and Choe, S. (2002). Structural basis of BMP signalling inhibition by the cystine knot protein Noggin. *Nature*, 420(6916):636–642.

Hall, B., Limaye, A., and Kulkarni, A. B. (2009). Overview: generation of gene knockout mice. *Current protocols in cell biology*, pages 19–12.

Hao, J., Daleo, M. A., Murphy, C. K., Yu, P. B., Ho, J. N., Hu, J., Peterson, R. T., Hatzopoulos, A. K., and Hong, C. C. (2008). Dorsomorphin, a selective small molecule inhibitor of BMP signaling, promotes cardiomyogenesis in embryonic stem cells. *PLoS ONE*, 3(8):e2904.

Hayman, M. W., Smith, K. H., Cameron, N. R., and Przyborski, S. A. (2004). Enhanced neurite outgrowth by human neurons grown on solid three-dimensional scaffolds. *Biochem. Biophys. Res. Commun.*, 314(2):483–488.

Horrocks, G. M., Lauder, L., Stewart, R., and Przyborski, S. (2003). Formation of neurospheres from human embryonal carcinoma stem cells. *Biochemical and Biophysical Research Communications*, 304(2):411 – 416.

II, E. (2008). Human fertilisation and embryology act. *Department of Health*.

Itskovitz-Eldor, J., Schuldiner, M., Karsenti, D., Eden, A., Yanuka, O., Amit, M., Soreq, H., and Benvenisty, N. (2000). Differentiation of human embryonic stem cells into embryoid bodies compromising the three embryonic germ layers. *Mol. Med.*, 6(2):88–95.

Jones-Villeneuve, E. M., McBurney, M. W., Rogers, K. A., and Kalnins, V. I. (1982). Retinoic acid induces embryonal carcinoma cells to differentiate into neurons and glial cells. *J. Cell Biol.*, 94(2):253–262.

Jongpaiboonkit, L., King, W. J., Lyons, G. E., Paguirigan, A. L., Warrick, J. W., Beebe, D. J., and Murphy, W. L. (2008). An adaptable hydrogel array format for 3-dimensional cell culture and analysis. *Biomaterials*, 29(23):3346–3356.

Katsetos, C. D., Legido, A., Perentes, E., and Mork, S. J. (2003). Class III beta-tubulin isotype: a key cytoskeletal protein at the crossroads of developmental neurobiology and tumor neuropathology. *J. Child Neurol.*, 18(12):851–866.

Kimbrel, E. A. and Lanza, R. (2015). Current status of pluripotent stem cells: moving the first therapies to the clinic. *Nat Rev Drug Discov*.

Kleinsmith, L. J. and Pierce, G. B. (1964). Multipotentiality of single embryonal carcinoma cells. *Cancer research*, 24(9):1544–1551.

Knight, E., Murray, B., Carnachan, R., and Przyborski, S. (2011). Alvetex: polystyrene scaffold technology for routine three dimensional cell culture. *Methods Mol. Biol.*, 695:323–340.

Knight, E. and Przyborski, S. (2014). Advances in 3d cell culture technologies enabling tissue-like structures to be created in vitro. *Journal of anatomy*.

Konuma, N., Wakabayashi, K., Matsumoto, T., Kusumi, Y., Masuko, T., Iribe, Y., Mitsumata, M., Okano, H., Kusafuka, T., and Mugishima, H. (2009). Mouse embryonic stem cells give rise to gut-like morphogenesis, including intestinal stem cells, in the embryoid body model. *Stem Cells Dev.*, 18(1):113–126.

Kothapalli, C. R. and Kamm, R. D. (2013). 3D matrix microenvironment for targeted differentiation of embryonic stem cells into neural and glial lineages. *Biomaterials*, 34(25):5995–6007.

Kramer, J., Hegert, C., Guan, K., Wobus, A. M., Muller, P. K., and Rohwedel, J. (2000). Embryonic stem cell-derived chondrogenic differentiation in vitro: activation by BMP-2 and BMP-4. *Mech. Dev.*, 92(2):193–205.

Lamb, T. M., Knecht, A. K., Smith, W. C., Stachel, S. E., Economides, A. N., Stahl, N., Yancopolous, G. D., and Harland, R. M. (1993). Neural induction by the secreted polypeptide noggin. *Science*, 262(5134):713–718.

Levenberg, S., Huang, N. F., Lavik, E., Rogers, A. B., Itskovitz-Eldor, J., and Langer, R. (2003). Differentiation of human embryonic stem cells on three-dimensional polymer scaffolds. *Proc. Natl. Acad. Sci. U.S.A.*, 100(22):12741–12746.

Levenstein, M. E., Ludwig, T. E., Xu, R. H., Llanas, R. A., VanDenHeuvel-Kramer, K., Manning, D., and Thomson, J. A. (2006). Basic fibroblast growth factor support of human embryonic stem cell self-renewal. *Stem Cells*, 24(3):568–574.

Li, Z. and Chen, Y. G. (2013). Functions of BMP signaling in embryonic stem cell fate determination. *Exp. Cell Res.*, 319(2):113–119.

Li, Z., Leung, M., Hopper, R., Ellenbogen, R., and Zhang, M. (2010). Feeder-free self-renewal of human embryonic stem cells in 3D porous natural polymer scaffolds. *Biomaterials*, 31(3):404–412.

Liersch, R., Nay, F., Lu, L., and Detmar, M. (2006). Induction of lymphatic endothelial cell differentiation in embryoid bodies. *Blood*, 107(3):1214–1216.

Linker, C. and Stern, C. D. (2004). Neural induction requires BMP inhibition only as a late step, and involves signals other than FGF and Wnt antagonists. *Development*, 131(22):5671–5681.

MacDonald, B. T., Tamai, K., and He, X. (2009). Wnt/beta-catenin signaling: components, mechanisms, and diseases. *Dev. Cell*, 17(1):9–26.

Magin, T. M., Jorcano, J. L., and Franke, W. W. (1986). Cytokeratin expression in simple epithelia. II. cDNA cloning and sequence characteristics of bovine cytokeratin A (no. 8). *Differentiation*, 30(3):254–264.

Mark, M., Ghyselinck, N. B., and Chambon, P. (2009). Function of retinoic acid receptors during embryonic development. *Nucl Recept Signal*, 7:e002.

Martí, M., Mulero, L., Pardo, C., Morera, C., Carrió, M., Laricchia-Robbio, L., Esteban, C. R., and Belmonte, J. C. I. (2013). Characterization of pluripotent stem cells. *Nature protocols*, 8(2):223–253.

Martin, G. R. (1981). Isolation of a pluripotent cell line from early mouse embryos cultured in medium conditioned by teratocarcinoma stem cells. *Proceedings of the National Academy of Sciences*, 78(12):7634–7638.

Mauney, J. R., Nguyen, T., Gillen, K., Kirker-Head, C., Gimble, J. M., and Kaplan, D. L. (2007). Engineering adipose-like tissue in vitro and in vivo utilizing human bone marrow and adipose-derived mesenchymal stem cells with silk fibroin 3D scaffolds. *Biomaterials*, 28(35):5280–5290.

Mic, F. A., Molotkov, A., Molotkova, N., and Duester, G. (2004). Raldh2 expression in optic vesicle generates a retinoic acid signal needed for invagination of retina during optic cup formation. *Dev. Dyn.*, 231(2):270–277.

Micallef, S. J., Janes, M. E., Knezevic, K., Davis, R. P., Elefanty, A. G., and Stanley, E. G. (2005). Retinoic acid induces Pdx1-positive endoderm in differentiating mouse embryonic stem cells. *Diabetes*, 54(2):301–305.

Muller, F. J., Goldmann, J., Loser, P., and Loring, J. F. (2010). A call to standardize teratoma assays used to define human pluripotent cell lines. *Cell Stem Cell*, 6(5):412–414.

Murry, C. E. and Keller, G. (2008). Differentiation of embryonic stem cells to clinically relevant populations: lessons from embryonic development. *Cell*, 132(4):661–680.

Myers, F. B., Silver, J. S., Zhuge, Y., Beygui, R. E., Zarins, C. K., Lee, L. P., and Abilez, O. J. (2013). Robust pluripotent stem cell expansion and cardiomyocyte differentiation via geometric patterning. *Integr Biol (Camb)*, 5(12):1495–1506.

Nagy, A., Rossant, J., Nagy, R., Abramow-Newerly, W., and Roder, J. C. (1993). Derivation of completely cell culture-derived mice from early-passage embryonic stem cells. *Proc. Natl. Acad. Sci. U.S.A.*, 90(18):8424–8428.

Najm, F. J., Zaremba, A., Caprariello, A. V., Nayak, S., Freundt, E. C., Scacheri, P. C., Miller, R. H., and Tesar, P. J. (2011). Rapid and robust generation of functional oligodendrocyte progenitor cells from epiblast stem cells. *Nat. Methods*, 8(11):957–962.

Nestor, M. W., Paull, D., Jacob, S., Sproul, A. A., Alsaffar, A., Campos, B. A., and Noggle, S. A. (2013). Differentiation of serum-free embryoid bodies from human induced pluripotent stem cells into networks. *Stem Cell Res*, 10(3):454–463.

Obokata, H., Wakayama, T., Sasai, Y., Kojima, K., Vacanti, M. P., Niwa, H., Yamato, M., and Vacanti, C. A. (2014). Stimulus-triggered fate conversion of somatic cells into pluripotency. *Nature*, 505(7485):641–647.

Ozair, M. Z., Kintner, C., and Brivanlou, A. H. (2013). Neural induction and early patterning in vertebrates. *Wiley Interdiscip Rev Dev Biol*, 2(4):479–498.

Przyborski, S. A. (2001). Isolation of human embryonal carcinoma stem cells by immunomagnetic sorting. *Stem Cells*, 19(6):500–504.

Przyborski, S. A. (2005). Differentiation of human embryonic stem cells after transplantation in immune-deficient mice. *Stem Cells*, 23(9):1242–1250.

Przyborski, S. A., Christie, V. B., Hayman, M. W., Stewart, R., and Horrocks, G. M. (2004). Human embryonal carcinoma stem cells: models of embryonic development in humans. *Stem Cells Dev.*, 13(4):400–408.

Rhinn, M. and Dolle, P. (2012). Retinoic acid signalling during development. *Development*, 139(5):843–858.

Roelandt, P., Vanhove, J., and Verfaillie, C. (2013). Directed differentiation of pluripotent stem cells to functional hepatocytes. *Methods Mol. Biol.*, 997:141–147.

Rohwedel, J., Maltsev, V., Bober, E., Arnold, H. H., Hescheler, J., and Wobus, A. M. (1994). Muscle cell differentiation of embryonic stem cells reflects myogenesis in vivo: developmentally regulated expression of myogenic determination genes and functional expression of ionic currents. *Dev. Biol.*, 164(1):87–101.

Rojas, A., Schachterle, W., Xu, S. M., Martin, F., and Black, B. L. (2010). Direct transcriptional regulation of Gata4 during early endoderm specification is controlled by FoxA2 binding to an intronic enhancer. *Dev. Biol.*, 346(2):346–355.

Sachlos, E. and Auguste, D. T. (2008). Embryoid body morphology influences diffusive transport of inductive biochemicals: a strategy for stem cell differentiation. *Biomaterials*, 29(34):4471–4480.

Scholer, H. R., Balling, R., Hatzopoulos, A. K., Suzuki, N., and Gruss, P. (1989). Octamer binding proteins confer transcriptional activity in early mouse embryogenesis. *EMBO J.*, 8(9):2551–2557.

Severson, E. A., Kwon, M., Hilgarth, R. S., Parkos, C. A., and Nusrat, A. (2010). Glycogen Synthase Kinase 3 (GSK-3) influences epithelial barrier function by regulating occludin, claudin-1 and E-cadherin expression. *Biochem. Biophys. Res. Commun.*, 397(3):592–597.

Sheridan, S. D., Surampudi, V., and Rao, R. R. (2012). Analysis of embryoid bodies derived from human induced pluripotent stem cells as a means to assess pluripotency. *Stem Cells Int*, 2012:738910.

Smith, A. G. (2001). Embryo-derived stem cells: of mice and men. *Annu. Rev. Cell Dev. Biol.*, 17:435–462.

Solter, D. and Knowles, B. B. (1978). Monoclonal antibody defining a stage-specific mouse embryonic antigen (SSEA-1). *Proc. Natl. Acad. Sci. U.S.A.*, 75(11):5565–5569.

Spemann, H. and Mangold, H. (1924). Über induktion von embryonalanlagen durch implantation artfremder organisatoren. *Development Genes and Evolution*, 100(3):599–638.

Stewart, R., Christie, V. B., and Przyborski, S. A. (2003). Manipulation of human pluripotent embryonal carcinoma stem cells and the development of neural subtypes. *STEM CELLS*, 21(3):248–256.

Storch, K. N., Taatjes, D. J., Bouffard, N. A., Locknar, S., Bishop, N. M., and Langevin, H. M. (2007). Alpha smooth muscle actin distribution in cytoplasm and nuclear invaginations of connective tissue fibroblasts. *Histochem. Cell Biol.*, 127(5):523–530.

Takahashi, K., Tanabe, K., Ohnuki, M., Narita, M., Ichisaka, T., Tomoda, K., and Yamanaka, S. (2007). Induction of pluripotent stem cells from adult human fibroblasts by defined factors. *cell*, 131(5):861–872.

Takahashi, K. and Yamanaka, S. (2006). Induction of pluripotent stem cells from mouse embryonic and adult fibroblast cultures by defined factors. *cell*, 126(4):663–676.

Tam, P. P. and Behringer, R. R. (1997). Mouse gastrulation: the formation of a mammalian body plan. *Mechanisms of development*, 68(1):3–25.

ten Berge, D., Koole, W., Fuerer, C., Fish, M., Eroglu, E., and Nusse, R. (2008). Wnt signaling mediates self-organization and axis formation in embryoid bodies. *Cell Stem Cell*, 3(5):508–518.

Tesar, P. J., Chenoweth, J. G., Brook, F. A., Davies, T. J., Evans, E. P., Mack, D. L., Gardner, R. L., and McKay, R. D. (2007). New cell lines from mouse epiblast share defining features with human embryonic stem cells. *Nature*, 448(7150):196–199.

Thatava, T., Nelson, T. J., Edukulla, R., Sakuma, T., Ohmine, S., Tonne, J. M., Yamada, S., Kudva, Y., Terzic, A., and Ikeda, Y. (2011). Indolactam V/GLP-1-mediated differentiation of human iPS cells into glucose-responsive insulin-secreting progeny. *Gene Ther.*, 18(3):283–293.

Thomson, J. A., Itskovitz-Eldor, J., Shapiro, S. S., Waknitz, M. A., Swiergiel, J. J., Marshall, V. S., and Jones, J. M. (1998). Embryonic stem cell lines derived from human blastocysts. *science*, 282(5391):1145–1147.

Tonge, P. D., Olariu, V., Coca, D., Kadirkamanathan, V., Burrell, K. E., Billings, S. A., and Andrews, P. W. (2010). Prepatterning in the stem cell compartment. *PLoS ONE*, 5(5):e10901.

Turner, D. A., Rue, P., Mackenzie, J. P., Davies, E., and Martinez Arias, A. (2014). Brachyury cooperates with Wnt/-catenin signalling to elicit primitive-streak-like behaviour in differentiating mouse embryonic stem cells. *BMC Biol.*, 12:63.

Urist, M. R. and Strates, B. S. (1971). Bone morphogenetic protein. *J. Dent. Res.*, 50(6):1392–1406.

van den Brink, S. C., Baillie-Johnson, P., Balayo, T., Hadjantonakis, A. K., Nowotschin, S., Turner, D. A., and Martinez Arias, A. (2014). Symmetry breaking, germ layer specification and axial organisation in aggregates of mouse embryonic stem cells. *Development*, 141(22):4231–4242.

Van Winkle, A. P., Gates, I. D., and Kallos, M. S. (2012). Mass transfer limitations in embryoid bodies during human embryonic stem cell differentiation. *Cells Tissues Organs (Print)*, 196(1):34–47.

Vigneau, C., Polgar, K., Striker, G., Elliott, J., Hyink, D., Weber, O., Fehling, H. J., Keller, G., Burrow, C., and Wilson, P. (2007). Mouse embryonic stem cell-derived embryoid bodies generate progenitors that integrate long term into renal proximal tubules in vivo. *J. Am. Soc. Nephrol.*, 18(6):1709–1720.

Wada, Y., Sun-Wada, G. H., and Kawamura, N. (2013). Microautophagy in the visceral endoderm is essential for mouse early development. *Autophagy*, 9(2):252–254.

Wang, R., Clark, R., and Bautch, V. L. (1992). Embryonic stem cell-derived cystic embryoid bodies form vascular channels: an in vitro model of blood vessel development. *Development*, 114(2):303–316.

Wang, R. N., Green, J., Wang, Z., Deng, Y., Qiao, M., Peabody, M., Zhang, Q., Ye, J., Yan, Z., Denduluri, S., Idowu, O., Li, M., Shen, C., Hu, A., Haydon, R. C., Kang, R., Mok, J., Lee, M. J., Luu, H. L., and Shi, L. L. (2014). Bone Morphogenetic Protein (BMP) signaling in development and human diseases. *Genes Dis*, 1(1):87–105.

Wang, S., Bates, J., Li, X., Schanz, S., Chandler-Militello, D., Levine, C., Maherali, N., Studer, L., Hochedlinger, K., Windrem, M., and Goldman, S. A. (2013). Human iPSC-derived oligodendrocyte progenitor cells can myelinate and rescue a mouse model of congenital hypomyelination. *Cell Stem Cell*, 12(2):252–264.

Weissbein, U. and Benvenisty, N. (2015). rsPSCs: A new type of pluripotent stem cells. *Cell Res.*, 25(8):889–890.

Weitzer, G. (2006). Embryonic stem cell-derived embryoid bodies: an in vitro model of eutherian pregastrulation development and early gastrulation. *Handb Exp Pharmacol*, (174):21–51.

Willerth, S. M., Arendas, K. J., Gottlieb, D. I., and Sakiyama-Elbert, S. E. (2006). Optimization of fibrin scaffolds for differentiation of murine embryonic stem cells into neural lineage cells. *Biomaterials*, 27(36):5990–6003.

Williams, R. L., Hilton, D. J., Pease, S., Willson, T. A., Stewart, C. L., Gearing, D. P., Wagner, E. F., Metcalf, D., Nicola, N. A., and Gough, N. M. (1988). Myeloid leukaemia inhibitory factor maintains the developmental potential of embryonic stem cells. *Nature*, 336(6200):684–687.

Wilson, P. A. and Hemmati-Brivanlou, A. (1995). Induction of epidermis and inhibition of neural fate by Bmp-4. *Nature*, 376(6538):331–333.

Wray, J., Kalkan, T., Gomez-Lopez, S., Eckardt, D., Cook, A., Kemler, R., and Smith, A. (2011). Inhibition of glycogen synthase kinase-3 alleviates Tcf3 repression of the pluripotency network and increases embryonic stem cell resistance to differentiation. *Nat. Cell Biol.*, 13(7):838–845.

Wu, J., Okamura, D., Li, M., Suzuki, K., Luo, C., Ma, L., He, Y., Li, Z., Benner, C., Tamura, I., Krause, M. N., Nery, J. R., Du, T., Zhang, Z., Hishida, T., Takahashi, Y., Aizawa, E., Kim, N. Y., Lajara, J., Guillen, P., Campistol, J. M., Esteban, C. R., Ross, P. J., Saghatelian, A., Ren, B., Ecker, J. R., and Izpisua Belmonte, J. C. (2015). An alternative pluripotent state confers interspecies chimaeric competency. *Nature*, 521(7552):316–321.

Ying, Q.-L., Nichols, J., Chambers, I., and Smith, A. (2003). {BMP} induction of id proteins suppresses differentiation and sustains embryonic stem cell self-renewal in collaboration with {STAT3}. *Cell*, 115(3):281 – 292.

Ying, Q.-L., Wray, J., Nichols, J., Batlle-Morera, L., Doble, B., Woodgett, J., Cohen, P., and Smith, A. (2008). The ground state of embryonic stem cell self-renewal. *Nature*, 453(7194):519–523.

Young, B., Heath, J., Stevens, A., Wheater, P., Lowe, J., and Burkitt, H. (2000). *Wheater's functional histology: a text and colour atlas*. Number v. 1 in Functional Histology. Churchill Livingstone.

Yu, P. B., Hong, C. C., Sachidanandan, C., Babitt, J. L., Deng, D. Y., Hoyng, S. A., Lin, H. Y., Bloch, K. D., and Peterson, R. T. (2008). Dorsomorphin inhibits BMP signals required for embryogenesis and iron metabolism. *Nat. Chem. Biol.*, 4(1):33–41.

Yuan, H., Corbi, N., Basilico, C., and Dailey, L. (1995). Developmental-specific activity of the FGF-4 enhancer requires the synergistic action of Sox2 and Oct-3. *Genes Dev.*, 9(21):2635–2645.

Zhao, X. Y., Li, W., Lv, Z., Liu, L., Tong, M., Hai, T., Hao, J., Guo, C. L., Ma, Q. W., Wang, L., Zeng, F., and Zhou, Q. (2009). iPS cells produce viable mice through tetraploid complementation. *Nature*, 461(7260):86–90.

Zhou, J., Su, P., Li, D., Tsang, S., Duan, E., and Wang, F. (2010). High-efficiency induction of neural conversion in human ESCs and human induced pluripotent stem cells with a single chemical inhibitor of transforming growth factor beta superfamily receptors. *Stem Cells*, 28(10):1741–1750.